Machine Learning Algorithms for Cognitive Radio Wireless Networks

by

Olusegun Peter Awe

A Doctoral Thesis submitted in partial fulfilment of the requirements for the award of the degree of Doctor of Philosophy (PhD)

November 2015

Signal Processing and Networks Research Group,
Wolfson School of Mechanical, Manufacturing and Electrical Engineering,
Loughborough University, Loughborough,
Leicestershire, UK, LE11 3TU

CERTIFICATE OF ORIGINALITY

This is to certify that I am responsible for the work submitted in this thesis, that the original work is my own except as specified in acknowledgements or in footnotes, and that neither the thesis nor the original work contained therein has been submitted to this or any other institution for a degree.

..... (Signed)

.....Olusegun..Peter..Awe..... (candidate)

I dedicate this thesis to my wife, Oluwakemi Awe, my son, Ifemayowa Awe, my daughter, Ifemayokun Awe and the memory of my late father, Olayiwola Awe.

Abstract

In this thesis new methods are presented for achieving spectrum sensing in cognitive radio wireless networks. In particular, supervised, semi-supervised and unsupervised machine learning based spectrum sensing algorithms are developed and various techniques to improve their performance are described.

Spectrum sensing problem in multi-antenna cognitive radio networks is considered and a novel eigenvalue based feature is proposed which has the capability to enhance the performance of support vector machines algorithms for signal classification. Furthermore, spectrum sensing under multiple primary users condition is studied and a new re-formulation of the sensing task as a multiple class signal detection problem where each class embeds one or more states is presented. Moreover, the error correcting output codes based multi-class support vector machines algorithms is proposed and investigated for solving the multiple class signal detection problem using two different coding strategies.

In addition, the performance of parametric classifiers for spectrum sensing under slow fading channel is studied. To address the attendant performance degradation problem, a Kalman filter based channel estimation technique is proposed for tracking the temporally correlated slow fading channel and updating the decision boundary of the classifiers in real time. Simulation studies are included to assess the performance of the proposed schemes.

Finally, techniques for improving the quality of the learning features and improving the detection accuracy of sensing algorithms are studied and a novel beamforming based pre-processing technique is presented for feature realization in multi-antenna cognitive radio systems. Furthermore, using the beamformer derived features, new algorithms are developed for multiple

hypothesis testing facilitating joint spatio-temporal spectrum sensing. The key performance metrics of the classifiers are evaluated to demonstrate the superiority of the proposed methods in comparison with previously proposed alternatives.

Contents

Statement of Originality

The contribution of this thesis is mainly on the development of machine learning algorithms for cognitive radio wireless networks. The novelty of the contributions is supported by the following international journal, book chapter and conference papers:

In Chapter 3, a novel eigenvalue feature is proposed for improving the classification performance of SVM classifiers. Multi-class error correcting output codes based algorithms are also proposed for spatio-temporal spectrum sensing in cognitive radio networks. The results have been published/ accepted for publication in:

1. O.P. Awe, Z. Zhu and S. Lambotharan, "Eigenvalue and support vector machine techniques for spectrum sensing in cognitive radio networks", In: proc. Conference on Technologies and Application of Artificial Intelligence (TAAI), Taipei, Taiwan, Dec. 6-8, 2013, pp. 223–227.

2. O.P. Awe and S. Lambotharan, "Cooperative spectrum sensing in cognitive radio networks using multi-class support vector machine algorithms", *to appear in* proc. IEEE 9th International Conference on Signal Processing and Communication Systems (ICSPCS), Cairns, Australia, Dec. 2015.

The contribution of Chapter 4 is the proposition of a novel method that involves using the Kalman filter tracker for estimating the temporally correlated, dynamic channel gain under flat fading channel conditions to enable mobile SU's update decision boundary in real time towards enhancing the sensing performance. This work has been published in:

3. O.P. Awe, S.N.R. Naqvi and S. Lambotharan, "Kalman filter enhanced parametric classifiers for spectrum sensing under flat fading channels", In: Weichold, M., Hamdi, M., Shakir, M.Z., Abdallah, M., Ismail, M.

(Eds.), Cognitive Radio Oriented Wireless Networks, Springer International Publishing (2015), pp. 235–247.

In Chapter 5, unsupervised variational Bayesian learning algorithm is presented for autonomous spectrum sensing. The novelty of this work is supported by the following publication:

4. O.P. Awe, S.N.R. Naqvi, and S. Lambotharan, "Variational Bayesian learning technique for spectrum sensing in cognitive radio networks," In: proc. IEEE Global Conference on Signal and Information Processing (GlobalSIP), Atlanta, Georgia, USA, Dec. 3-5, 2014, pp.1353–1357.

In Chapter 6, a novel beamforming based pre-processing technique to enhance the quality of the feature vectors for learning algorithms is proposed. The novelty of this work is supported by the following article which is under review:

5. O.P. Awe, and S. Lambotharan, "Beamformer-Aided SVM Algorithms for Spatio-Temporal Spectrum Sensing in Cognitive Radio Networks,", *submitted* to IEEE Trans. on Wireless Communications, Sept. 2015.

Acknowledgements

I AM DEEPLY INDEBTED to my supervisor Professor Sangarapillai Lambotharan for his kind interest, generous support and constant advice throughout the past three years. I have benefited tremendously from his rare insight, his ample intuition and his exceptional knowledge. This thesis would never have been a reality without his tireless and patient mentoring. I consider it a great privilege to have been one of his research students. I wish that I will have more opportunities to work with him in the future.

I am extremely thankful to Professor Jonathon A. Chambers and Dr. Mohsen Naqvi for their support and encouragement.

I am also grateful to all my colleagues in the Signal Processing and Networks Research Group Bokamoso, Tian, Dr. Ye, Abdullahi, Ramaddan, Funmi, Dr. Ivan, Isaac, Gaia, Tasos, Dr. Ousama, Yu, Partheepan, Dr. Anastasia and Dr. Miao for providing a friendly, stable and cooperative environment within the research group.

I really can not find appropriate words or suitable phrases to express my deepest and sincere heartfelt thanks, appreciations and gratefulness to my mother, my brothers, my sisters and all my friends in Loughborough for their constant encouragement, attention, prayers and their support in innumerable ways both before and throughout my PhD. I can not thank you all enough.

Above all, I give all thanks to Jehovah, my God, the giver of life and custodian of all knowledge for making this work a success. To him be praise, honor and glory forever and ever.

Olusegun Peter Awe

October, 2015

List of Acronyms

AOA	Angle of Arrival
ANN	Artificial Neural Networks
AuC	Area Under ROC Curve
AWGN	Additive White Gaussian Noise
AR	Auto Regressive
BPSK	Binary Phase Shift Key-in
BFSVM	Beamformer Support Vector Machine
CSN	Collaborating Sensor Node
CR	Cognitive Radio
CD	Cyclostationary Detection
CAF	Cyclic Autocorrelation Function
CD	Cyclostationary Detection
CAF	Cyclic Autocorrelation Function
CWT	Continuous Wavelet Transform
DOA	Direction of Arrival
DPC	Dirty Paper Coding

dB	Decibel
DWV	Distance Weighted Voting
DAG	Decision Acyclic Graph
ETSI	European Telecommunications Standards Institute
EM	Expectation Maximization
ED	Energy Detection
EME	Energy and Minimum Eigenvalue
ECOC	Error Correcting Output Codes
FCC	Federal Communications Commissions
FDA	Fisher's Discriminant Analysis
GHz	Gigahertz
GMM	Gaussian Mixture Model
kHz	kilohertz
KL	Kullback Leibler
KKT	Karush-Kuhn-Tucker
LDA	Linear Discriminant Analysis
LOS	Line of Sight
ML	Maximum Likelihood
MSE	Mean Square Error
MIM	Multiple Independent Model
MHz	Megahertz

MAC	Media Access Control
MME	Maximum and Minimum Eigenvalue
MC	Multi Cycle
MAP	Maximum a Posteriori
MV	Majority Voting
NB	Naive Bayes
NN	Nearest Neighbor
MSVM	Multi-class Support Vector Machines
NBFSVM	Non Beamformer Support Vector Machine
PU	Primary User
Pfa	Probability of False Alarm
PHD	Probability Hypothesis Density
PDF	Probability Density Function
PHY	Physical
PSD	Power Spectral Density
Pd	Probability of Detection
QoS	Quality of Service
QDA	Quadratic Discriminant Analysis
RF	Radio Frequency
SU	Secondary User
SVM	Support Vector Machine

SNR	Signal-to-Noise Ratio
SCF	Spectrum Correlation Function
SC	Single Cycle
SBS	Secondary Base Station
OVO	One Versus One
OVA	One Versus All
ROC	Receiver Operating Characteristics
R.H.S	Right Hand Side
ULA	Uniform Linear Array
VB	variational Bayesian

List of Symbols

Scalar variables are denoted by plain lower-case letters, (e.g., x), vectors by bold-face lower-case letters, (e.g., $\mathbf{x}$), and matrices by upper-case bold-face letters, (e.g., $\mathbf{X}$). Some frequently used notations are as follows:

$\|.\|$	Absolute value
$\bigcup$	AND operation
ω	Angular frequency
$\phi(.)$	Channel gain coefficient
Σ	Covariance matrix
$(\cdot)^*$	Complex conjugate
$\int$	Continuous summation
Card	Cardinality of set
$\digamma(.)$	Digamma function
$\sum$	Discrete summation
$\exp(.)$	Exponential function
$\|\|.\|\|_2$	Euclidean norm
$\Gamma(\cdot)$	Gamma function
$\mathcal{N}(.)$	Gaussian / Normal distribution

$(\cdot)^H$	Hermitian transpose
$\mathbf{I}$	Identity matrix
$I(.)$	Indicator function
$Q^{-1}(.)$	Inverse Q function
i	Imaginary part
$K(.,.)$	Kernel function
$\max(\cdot)$	Maximum value
$\min(\cdot)$	Minimum value
$\|.\|$	Modulus of a complex number
$\boldsymbol{\mu}$	Mean vector
$log(.)$	Natural logarithm function
P	Number of PUs
N_s	Number of samples
η	Noise
$\bigcap$	OR operation
$\prod$	Product
$p(.)$	Probability of a function
$\mathbf{\Lambda}$	Precision Matrix
$\mathcal{P}$	Power set
$Q(.)$	Q function / Gaussian probability tail function
r	Real part

x	Received signal
$\mathrm{E}(\cdot)$	Statistical expectation
$sgn(.)$	Signum function
T_s	Symbol duration
f_s	Sampling Rate
$(\cdot)^T$	Transpose
$\mathrm{Tr}(\cdot)$	Trace
argmax	The argument which maximizes the expression
argmin	The argument which minimizes the expression
s	Transmit signal
$\mathcal{S}$	Training set
σ^2	Variance
$\mathcal{W}(.)$	Wishart distribution

List of Figures

Chapter 1

INTRODUCTION

1.1 Basic Problem

In many countries around the globe, the electromagnetic spectrum assigned to wireless networks and services is managed by governmental regulatory bodies. For example, there is the European Telecommunications Standards Institute in Europe (ETSI) and the Federal Communications Commissions (FCC) in United States. These governing bodies are saddled with the responsibility of allocating spectral frequency blocks to specific groups or companies. More often than not, the allocation process involves (*i*) partitioning of the spectrum into distinct bands, with each band spanning across a range of frequencies; (*ii*) assigning specific communication services to specific bands, and (*iii*) deciding the licensee for each band who usually is given the exclusive right over the use of the allocated frequency band. Since the licensee reserves the right over the assigned spectrum, it can easily manage interference and the quality of service (QoS) among its users [3].

In the last one decade, there has been unprecedented concern over the static manner in which the natural frequency spectrum is being allocated. This concern is further being heightened by the ever increasing demand for higher data rates as wireless communication technology advances from voice only communications to data intensive multimedia and interactive services now being ubiquitously deployed [4]. In order to meet the challenge of spectrum crisis thus created, a paradigm shift from the hitherto, command and

control manner of frequency allocation to dynamic spectrum access has become imperative. Interestingly, going by the current allocation technique, spectrum occupancy measurements have shown that most of the allocated spectral bands are often underutilized. For example, studies conducted in the United States have revealed that in most locations, only 15% of spectrum is used. More specifically, a field spectrum measurement taken in New York City showed that the maximum total spectrum occupancy for bands from 30MHz to 3GHz is only 13.1 % [4], [5]. Similar result was also obtained in the most crowded area of downtown Washington, D.C., where occupancy of less than 35 % is recorded for the radio spectrum below 3 GHz [4]. In addition, it is a well known fact that spectrum usage also varies significantly at various time, frequency and geographic locations [6].

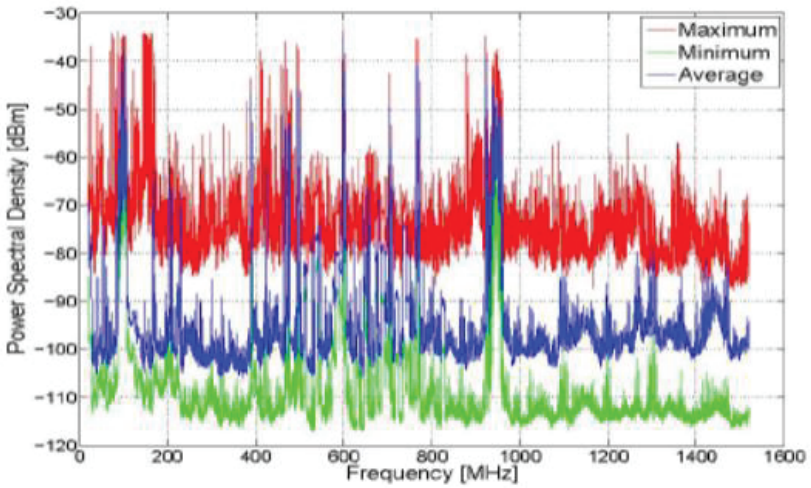

Figure 1.1. Maximum, minimum, and average received power spectral density in the frequency band 20 - 1,520 MHz with a 200-kHz resolution bandwidth of the receiver. Outdoor location: on top of 10 - storey building in Aachen, Germany [1].

Figure 1.1 shows the maximum, minimum and average spectrum usage in an outdoor environment at a typical location in Aachen, Germany, demonstrating enormous variations of interference power. In Figure 1.2, it is further shown that in an indoor environment, the spectrum usage is even

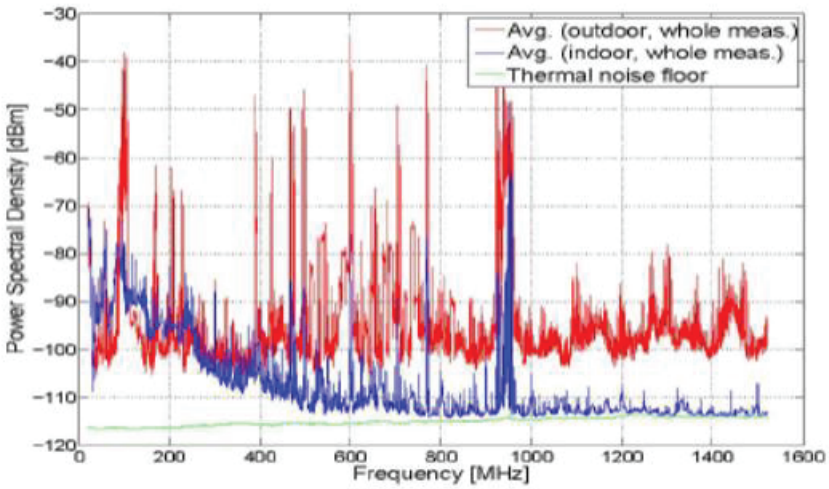

Figure 1.2. Average received power spectral density in the frequency band 20 - 1,520 MHz with a 200-kHz resolution bandwidth of the receiver. Indoor location: inside an office building in Aachen, Germany [1].

smaller, and on average, mostly thermal noise is present. From the foregoing, it is very clear that radically new approaches are required for better utilization of spectrum, especially in the face of the current unprecedented level of demand for spectrum access.

1.2 Cognitive Radio Technology

Cognitive radio (CR) is an emerging technology that can successfully deal with the growing demand and scarcity of the wireless spectrum [7–11]. It is a paradigm of wireless communication in which an intelligent wireless system utilizes information about the radio environment to adapt its operating characteristics in order to ensure reliable communication and efficient spectrum utilization. Recently, several IEEE 802 standards for wireless systems have considered cognitive radio systems such as IEEE 802.22 standard [12] and IEEE 802.18 standard [13].

To exploit limited bandwidth efficiently, CR technology allows unlicensed

users popularly referred to as the secondary users (SUs) to access licensed spectrum bands without causing harmful interference to the service of the licensed users otherwise referred to as primary users (PUs) [8]. In the following sub-section, the basic approaches that facilitate the implementation of dynamic spectrum access in CR networks will be described.

1.2.1 Cognitive Radio Network Paradigms

There are three main techniques that are being considered for cognitive spectrum sharing. These are the overlay, underlay and interweave techniques [3]. In the overlay approach, the SUs coexist with PUs based on the assumption that the knowledge of the PU's codebook and message is available to the SUs. This knowledge can be used to either cancel or reduce the interference caused by the PUs' transmission to the SUs thorough sophisticated signal processing techniques such as dirty paper coding (DPC) [3]. In order to offset the interference caused by the SUs' transmissions to the PUs, the SUs can split up their transmission power and use part of it to relay the PUs' signals to the intended primary receiver. This will ensure that the PUs' signal is received with desired signal-to-noise ratio (SNR). At the same time, the SUs can use the remaining transmit power for their own communication. Hence, both the PUs and the SUs benefit by allowing SUs spectrum access.

In the underlay approach, the SUs access the licensed spectrum without causing harmful interference to PUs' communications. This requires the SUs to ensure that interference leakage to the primary users is below an acceptable threshold. One way the SUs can meet the interference constraint is by employing multiple antennas to steer their beams away from the PUs. Alternatively, the SUs may employ spread spectrum technique whereby the transmitted signal is spread across a wide bandwidth such that the power level is below the noise floor. At the SU receivers, the signals may then be recovered through de-spreading. It should be noted that since the constraint

on the interference is somewhat restrictive under the underlay method, the transmissions by the SUs may be limited to short range communications. The underlay approach is illustrated in Fig. 1.3.

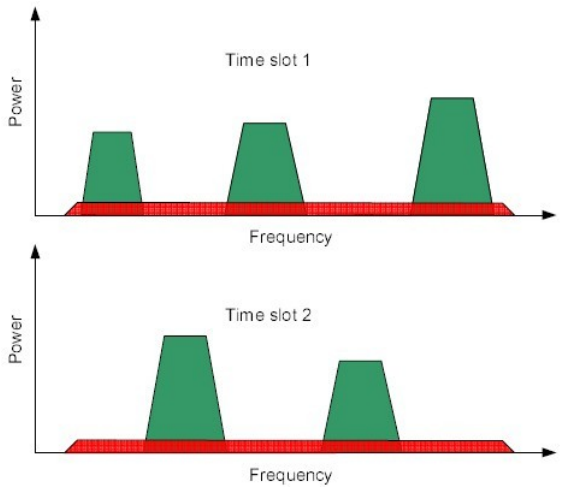

Figure 1.3. Underlay spectrum paradigm. Green and red represent the spectrum occupied by the primary users and the secondary users respectively.

The third cognitive technique for spectrum sharing is the interweave method shown in Fig. 1.4, in which case the SUs are permitted to access the licensed band in an opportunistic manner, i.e. only *when* and *where* it is not being used. The absence of an active PU in a band indicates that its allocated channel is idle and available for use by SUs while the PU's presence indicates otherwise. An idle or unused channel is often described as a spectrum hole or white space [3], [8]. However, since the PUs have priorities to use the bands, the SUs need to continuously monitor the activities of the PU to avoid causing intolerable interference to the PU's service. To meet this requirement, once granted permission to utilize unused spectrum, the SU must be alert to detect the reappearance of the PU and once detected, it should vacate the spectrum within the shortest possible, permissible time to minimize the interference caused to the licensed user.

In view of the above consideration, it can be understood that a funda-

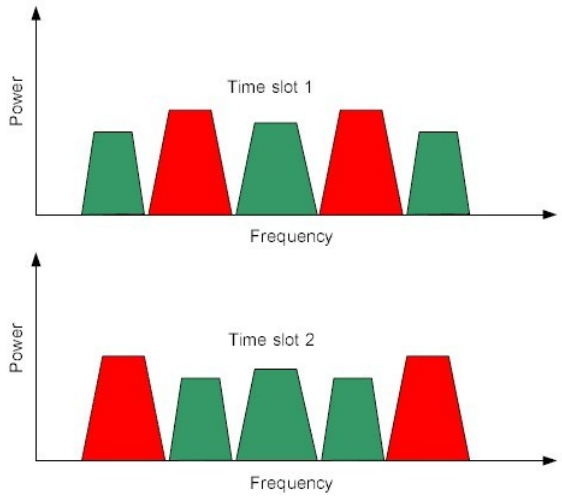

Figure 1.4. Interweave spectrum scheme. Green and red represent the spectrum occupied by the primary users and secondary users respectively.

mental task that is crucial to the successful implementation of the interweave cognitive radio system is detecting the presence or absence of the PU. This is usually referred to as spectrum sensing [4]. Put in another way, without spectrum sensing, no opportunistic use of the spectrum hole by SUs can take place. To summarize, the interweave cognitive radio can be described as an intelligent wireless communication system which requires the SUs to continuously monitor the activities of the PUs and intelligently detect availability of spectrum holes in order to take advantage of idle band towards achieving efficient utilization of radio spectrum resources.

There is no gainsaying that identifying spectrum holes in the absence of cooperation between primary and secondary networks is a very challenging task [14]. Nevertheless, unlike in overlay and underlay methods, the interweave scheme is non-invasive and there is no restriction in terms of transmit power and coverage, thus offering tremendous advantages in terms of high data rate and achievable QoS for the SUs, especially so in the event that the licensed band is idle for a reasonably prolonged period of time. Hence, the rest of this thesis is aimed at developing intelligent sensing techniques for

opportunistic spectrum access.

1.3 Motivation for Machine Learning Techniques

In order for cognitive devices to be really cognizant of the changes in the activities taking place in their radio frequency (RF) environment, it is imperative that they be equipped with both learning and reasoning functionalities. Little wonder then, that Simon Haykin in [8] envisioned CRs to be brain-empowered wireless devices that are specifically deigned to improve the utilization of the electromagnetic spectrum. These capabilities can easily be embedded in a cognitive engine which coordinates the actions of the CR by making use of machine learning * algorithms. In wireless communication and dynamic spectrum access in particular, several parameters and policies need to be adjusted simultaneously; these include transmit power, coding scheme, modulation scheme, sensing algorithm, communication protocol, sensing policy, etc. No simple formula may be able to determine these parameters simultaneously due to the complex interactions among these factors and their impact on the RF environment. Learning methods can be successfully applied to allow efficient adaption of the CRs to their environment, yet without the complete knowledge of the dependence among these parameters [16].

In general, learning methods can be classified as supervised, semi-supervised and unsupervised [17]. Supervised algorithms require training and creating decision models using labeled data. On the other hand, semi supervised techniques do not require labeled data, however, the knowledge of the statistical characteristics of the distribution which the training data follows may be required. The unsupervised classification algorithms do not require labeled training data and can be classified as either parametric or non-parametric.

*Machine learning is a bio-inspired field of study which can be described as "the science of getting computers to act without being explicitly programmed" [15].

While the supervised and semi-supervised techniques can generally be used in familiar or known environments with prior knowledge about the characteristics of the environment, these knowledge may not be required for the implementation of unsupervised learning, thus lending itself readily to autonomous signal detection in alien radio environments. It is particularly of interest to know that these learning techniques have been applied in solving many data mining problems involving classification. It is opined that they can equally be successfully developed into algorithms for proffering solution to our spectrum sensing problem.

1.4 Structure of Thesis and Contributions

To facilitate the understanding of this thesis and its contributions, the structure is summarized as follows:

In Chapter 1, the current frequency allocation method as well as the spectrum scarcity and under-utilization problems is first introduced. This is followed by a general description of the CR technology as a widely acceptable panacea. Further, the various possible approaches for implementing CR systems are described and spectrum sensing is highlighted as a fundamental process crucial to the successful implementation of CR. In addition, the motivation for choosing machine learning techniques as the basis for the various solutions that are proposed in this thesis is provided. The chapter concludes with an outline of the thesis structure and its contributions.

In Chapter 2, a brief introduction of the spectrum sensing problem formulation is presented. This is followed by a consideration of the existing local techniques for spectrum sensing that have been proposed for use by stand alone sensor nodes. The techniques described cover both blind and semi blind methods such as the matched filtering method, energy detection based methods and the hybrid schemes. The cooperative sensing method

for mitigating the effects of channel imperfections and improving detection performance is also briefly described.

In Chapter 3, supervised classifiers based algorithms are presented and the performance is evaluated in terms of spectrum sensing capability using the energy based features. Next, a novel eigenvalue based feature is proposed and its capability to improve the performance of the support vector machine (SVM) algorithms under multi-antenna considerations is demonstrated. Furthermore, spectrum sensing under multiple PU scenarios is considered and to facilitate spatio-temporal spectrum hole detection, the conventional, binary hypothesis spectrum sensing problem is re-formulated as a multiple signal detection problem comprising multiple system states. In addition, the performance evaluation of the multi-class error correcting output codes (ECOC) based SVM algorithms is presented using both the energy and eigenvalue based features. The simulation results indicate that the proposed detectors are robust to both temporal and joint spatio-temporal spectrum hole detection.

In Chapter 4, two semi-supervised parametric classifier algorithms are presented for use in sensing scenarios where only partial information about the PUs' network is available to the SUs. With these algorithms in mind, the problem of spectrum sensing in mobile SUs is further considered and a technique for enhancing the classifiers' performance is proposed. In particular, spectrum sensing under slow fading Rayleigh channel conditions due to the mobility of SUs in the presence of scatterers and the resulting performance degradation is of concern. To address this problem, the use of Kalman filter based channel estimation technique for tracking the temporally correlated slow fading channel is proposed to aid the classifiers to update the decision boundary in real time.

In Chapter 5, a fully Bayesian, soft assignment unsupervised classification algorithms based on the variational learning framework is presented.

This technique overcomes some of the limitations of supervised and semi-supervised algorithms in terms of the amount of information about the PU network that is required for optimal performance. In particular, the problem of blindly estimating the number of active transmitters and the statistical parameters that characterize the distribution of the signals from the unknown number of transmitters is considered. The inference problem is approached as a blind source separation problem. The proposed algorithm is shown to be useful for simultaneously monitoring the activities of multiple PU across multiple sub-bands and for autonomous spectrum sensing in alien radio environments where the prior knowledge of the exact number of sources is not available at the SU.

The performance of classification algorithms depends to a large extent on the quality of the training and prediction data used. In harmony with this thought, in Chapter 6 a novel, beamformer based pre-processing technique for feature realization is proposed towards improving the quality of our features and hence, the performance of our classifier based sensing algorithms particularly in multi-antenna CR networks. Using this novel feature technique, the ECOC based multi-class SVM algorithms is re-investigated and a multiple independent model (MIM) alternative is provided for solving the multi-class spectrum sensing problem. Simulation results are provided to demonstrate the superiority of the proposed methods over previously proposed alternatives.

Finally, in Chapter 7 this thesis is concluded with a summary of its contributions and suggestions for possible future research directions.

Chapter 2

REVIEW OF RELEVANT LITERATURE

2.1 Introduction

Spectrum sensing problem is usually approached in one of two ways. These are the physical layer (PHY) and the media access control layer (MAC) approaches [18]. The PHY layer based spectrum sensing is the most common and typically focuses on the detection of instantaneous primary user signals. The MAC layer approach on the other hand is essentially a resource allocation issue, where the concern is how to handle the problem of scheduling when the channel of interest is best sensed. It also involves addressing estimation problem where the desire is to extract the statistical properties of the randomly varying PU-SU channel based on the assumption that the physical layer sensing provides sufficiently accurate results on instantaneous channel availability [18]. In this chapter, attention is focused primarily on the physical layer approach and a review of the most common and relevant methods is presented.

2.2 Local Spectrum Sensing Techniques

As highlighted in the opening chapter of this thesis, the goal in performing spectrum sensing is to identify the availability of spectrum holes while also

protecting the PU terminals from harmful interference. In general, from the perspective of local spectrum sensing involving individual SUs, if the instantaneous signal received at the SU terminal is represented as $x(n)$, the spectrum sensing problem can be formulated as a binary hypothesis testing of the form

$$x(n) = \begin{cases} \eta(n), & \text{under } H_0 \\ \phi(n)s(n) + \eta(n), & \text{under } H_1 \end{cases} \tag{2.2.1}$$

where H_0 denotes the hypothesis that the PU is absent and H_1 denotes the hypothesis that the PU signal is present in the band of interest. Furthermore, $\eta(n)$ is the additive white Gaussian noise (AWGN), $\phi(n)$ is the gain coefficient of the channel between the PU and the SU and $s(n)$ is the transmitted primary signal. To solve the signal detection problem in (2.2.1), different techniques have been proposed which are described as follows.

2.2.1 Matched Filtering Detection Method

The match filtering (MF) technique also known as coherent detection is a method that requires the SU to have perfect knowledge of the PU signal and the channel between PU and SU so that with accurate synchronization, the received signal can be correlated with the known signal to determine the presence or absence of the PU [19]. The MF method has been described as the optimal detection method because it maximizes the SNR in the presence of additive noise and also minimizes the decision errors [10], [20]. If the primary transmitted signal, $s(n)$, is deterministic and known a priori, the matched filter correlates the known signal $s(n)$ with the received, unknown signal $x(n)$, and the decision is made using the expression [21], [22]

$$\Upsilon(x) \triangleq \sum_{n=1}^{N_s} x(n)s^*(n) \underset{H_0}{\overset{H_1}{\gtrless}} \theta_t \tag{2.2.2}$$

where $\Upsilon(x)$ is the test statistic which is assumed to be normally distributed under both hypotheses H_0 and H_1, i.e.,

$$\Upsilon(x) \sim \begin{cases} \mathcal{N}(0, N_s\sigma_s^2\sigma_\eta^2), & \text{under } H_0 \\ \mathcal{N}(N_s\sigma_s^2, N_s\sigma_s^2\sigma_\eta^2), & \text{under } H_1 \end{cases} \tag{2.2.3}$$

$\sigma_s^2 = \|s\|^2/N_s$, represents the average primary signal power while θ_t is the decision threshold and N_s is the number of samples used to perform correlation. The probability of false alarm (Pfa) and probability of detection (Pd) are given by

$$P_{fa} = Q\big(\frac{\theta_t}{\sigma_\eta\sigma_s\sqrt{N_s}}\big) \tag{2.2.4}$$

and

$$P_d = Q\big(\frac{\theta_t - N_s\sigma_s^2}{\sigma_\eta\sigma_s\sqrt{N_s}}\big) \tag{2.2.5}$$

where $Q(z) = \frac{1}{\sqrt{2\pi}}\int_z^{+\infty} e^{-\frac{\tau^2}{2}}\, d\tau$ is the tail probability of a zero-mean unit variance Gaussian random variable, also known as Q-function. If we let $SNR \triangleq \frac{\sigma_s^2}{\sigma_\eta^2} = \frac{\|s\|^2}{N_s\sigma_\eta^2}$, then the required number of samples, N_s, to achieve an operating point in terms of P_{fa} and P_d can be determined by combining (2.2.4) and (2.2.5), as

$$N_s = [Q^{-1}(P_{fa}) - Q^{-1}(P_d)]^2 SNR^{-1} \tag{2.2.6}$$

The main advantage of MFs is that within a short time, a certain Pd or Pfa is achievable compared to the other proposed methods [4]. However, in a situation where the signal transmitted by the PU is unknown to the SU, the MF technique cannot be used. Also, it is not very useful when synchronization becomes very difficult especially at low SNR. Furthermore, owing to the fact that the CR needs receiver for all types of signal, the implementation complexity of the sensing unit would be impractically large. Moreover, the power consumption of the MF is also considerably high since for detection,

various receiver algorithms need to be executed [4]. Nevertheless, the MF can be very useful in applications where the pilot signal of the primary signal is known [23].

2.2.2 Cyclostationary Feature Detection Method

The cyclostationary detector (CD) is one of the feature detectors that take the advantage of the fact that unique patterns that are peculiar to a specific signal can be used to detect its presence or absence. Most primary signals are modulated sinusoidal carriers, have certain symbol periods, or have cyclic prefixes which constitute built in periodicity. Such periodicity can distinguish the PU signal from other modulated signals and background noise, even at a very low SNR [21, 23, 24]. Mathematically, cyclostationary detection can be realized by analyzing the cyclic autocorrelation function (CAF) of the received signal or its two-dimensional spectrum correlation function (SCF) [23]. The modulated signal $s(n)$, can be characterized as a wide sense second order cyclostationary process because both its mean and autocorrelation exhibit periodicity [21]. If we let $\mu_s = \mathbb{E}[s(n)]$ and $R_s(n_1, n_2)$ $= \mathbb{E}[s(n_1)s^*(n_2)]$, then, $\forall$ n, n_1 and n_2, it holds that $\mu_s(n) = \mu_s(n+T_0)$ and $R_s(n_1, n_2) = R_s(n_1 + T_0, n_2 + T_0)$, where $T_0 > 0$ is a fundamental period. For a wide-sense second order cyclo-stationary process, having a non-zero cyclic frequency ($\omega \neq 0$), the cyclic autocorrelation function is defined as

$$R_s^{\omega}(l) \triangleq \mathbb{E}[s(n)s^*(n+l)e^{-2\pi\omega n}]. \tag{2.2.7}$$

Equation (2.2.7) can be described as

$$R_s^{\omega}(l) = \begin{cases} \text{finite}, & \text{if } \omega = \frac{m}{T_0} \\ 0, & \text{otherwise} \end{cases} \tag{2.2.8}$$

for any non-zero integer m. Thus, for a cyclostationary process $\{s(n)\}$, $\exists\omega \neq 0$ such that $R_s^{\omega}(l) \neq 0$ for some value of l. In the frequency domain, the corresponding representation of $R_s^{\omega}(l)$, known as the spectral correlation function can be obtained by using the discrete time Fourier transformation. This can be expressed as

$$\mathbf{s}_s^{\omega}(e^{i\varsigma}) = \sum_{l=-\infty}^{+\infty} R_s^{\omega}(l)e^{-i\varsigma l}, \tag{2.2.9}$$

where $\varsigma \in [-\pi, \pi]$ is the digital frequency corresponding to the sampling rate, f_s. The binary hypotheses test for the cyclostationary detection can then be written as

$$\mathbf{s}_x^{\omega}(e^{i\varsigma}) = \begin{cases} \mathbf{s}_{\eta}^{\omega}(e^{i\varsigma}), & \text{under} \quad H_0 \\ \mathbf{s}_s^{\omega}(e^{i\varsigma}) + \mathbf{s}_{\eta}^{\omega}(e^{i\varsigma}), & \text{under} \quad H_1. \end{cases} \tag{2.2.10}$$

Unlike the transmitted primary signal, the noise $\eta(n)$ is in general *not periodic* such that $\mathbf{s}_{\eta}^{\omega}(e^{i\varsigma}) = 0$, $\forall\omega \neq 0$. For N_s available measurements of the received signal, at $\varsigma = \frac{2\pi g}{D}$, the spectral correlation function can be obtained as

$$\hat{\mathbf{s}}_x^{\omega}(g) = \frac{1}{N_s}\sum_{n=1}^{N_s} \mathbf{x}_D(n, g + \frac{g_\omega}{2})\mathbf{x}_D^*(n, g - \frac{g_\omega}{2}), \tag{2.2.11}$$

where

$$\mathbf{x}_D(n, g) = \frac{1}{\sqrt{D}} \sum_{d=n-\frac{D}{2}}^{n+\frac{D}{2}-1} x(d)e^{-\frac{i2\pi gd}{D}} \tag{2.2.12}$$

is the D-point discrete Fourier transform around the n-th sample of the received signal, and $g_\omega = \frac{\omega D}{f_s}$ is known as the index of the frequency bin corresponding to the cyclic frequency, ω. Suppose that for a single cycle (sc) the ideal spectral correlation function, $\mathbf{s}_s^{\omega}(g)$, is known a priori, the test

statistic for the cyclostationary detection is given by [21]

$$\Upsilon_{sc}(\mathbf{x}) = \sum_{g=0}^{D-1} \left[\hat{\mathbf{s}}_x^{\omega}(g)\right] \left[\mathbf{s}_s^{\omega}(g)\right]^* \underset{H_0}{\overset{H_1}{\gtrless}} \theta_t, \tag{2.2.13}$$

and for a multicycle (mc) detector, the test statistics is

$$\Upsilon_{sc}(\mathbf{x}) = \sum_{\omega} \sum_{g=0}^{D-1} \left[\hat{\mathbf{s}}_x^{\omega}(g)\right] \left[\mathbf{s}_s^{\omega}(g)\right]^* \underset{H_0}{\overset{H_1}{\gtrless}} \theta_t. \tag{2.2.14}$$

where the sum is taken over all ω's for which $\mathbf{s}_s^{\omega}(g)$ is not identically zero and the vectors, $\mathbf{x}$ and $\mathbf{s}$ can be defined as: $\mathbf{x} \triangleq [x(1), \cdots, x(N_s)]^T$ and $\mathbf{s} \triangleq [s(1), \cdots, s(N_s)]^T$. While the CD is well coveted for its robustness in the presence of noise uncertainty and low SNR, its drawbacks include the requirement of having a priori knowledge of the PU signal characteristics which may not be practical for many frequency reuse applications, long sensing time and high computational complexity [10], [18]. The detector is suitable when the period, T_0 of the primary signal is known [23].

2.2.3 Energy Detection Method

The energy detection (ED), also known as radiometry or periodogram is the most common and most investigated spectrum sensing method because of its low computational and implementation complexity [4, 19, 25–28]. In the ED method, the a priori knowledge of the characteristics of the PU signal is not required and as such, it is a non-coherent technique that can be used to detect the presence or absence of the primary signal based on the sensed energy. The decision is made by comparing the mean squared accumulation of the received signal strength in a certain time interval to a pre-determined threshold [29]. Like the other spectrum sensing techniques, the goal is to decide between the two hypotheses, H_0 and H_1. The decision rule in this

case is given by

$$\Upsilon(\mathbf{x}) = \sum_{n=1}^{N_s} |x(n)|^2 \underset{H_0}{\overset{H_1}{\gtrless}} \theta_t, \tag{2.2.15}$$

where $\Upsilon(\mathbf{x})$ is the test statistics and θ_t is the corresponding decision threshold. When the PU is absent, $\Upsilon(\mathbf{x})$ obeys a central Chi-square distribution with N_s degrees of freedom; otherwise, $\Upsilon(\mathbf{x})$ obeys a non-central Chi-distribution with N_s degrees of freedom and a non-centrality parameter $\lambda = \sigma_s^2 N_s$ [27]. If N_s is large enough ($N_s > 20$) [30], due to central limit theorem, $\Upsilon(\mathbf{x})$ is asymptotically normally distributed, hence the statistics can be modeled as

$$\Upsilon(x) \sim \begin{cases} \mathcal{N}(N_s\sigma_\eta^2, 2N_s\sigma_\eta^4), & H_0 \\ \mathcal{N}(N_s\sigma_\eta^2 + N_s\sigma_s^2, 2N_s\sigma_\eta^4 + 4N_s\sigma_\eta^2\sigma_s^2), & H_1. \end{cases} \tag{2.2.16}$$

The P_{fa}, and the P_d, can be approximated as [21]

$$P_{fa} = Q\big(\frac{\theta_t - N_s\sigma_\eta^2}{\sigma_\eta^2\sqrt{2N_s}}\big) \tag{2.2.17}$$

and

$$P_d = Q\big(\frac{\theta_t - N_s\sigma_\eta^2 - N_s\sigma_s^2}{\sigma_\eta\sqrt{2N_s\sigma_\eta^2 + 4N_s\sigma_s^2}}\big) \tag{2.2.18}$$

respectively. Using (2.2.17) and (2.2.18), the number of samples, N_s required to attain desired values of P_{fa} and P_d is given by

$$N_s = 2[Q^{-1}(P_{fa}) - Q^{-1}(P_d)\sqrt{1 + 2SNR}]^2 SNR^{-2}. \tag{2.2.19}$$

The ED is very practical since no information about the primary user is required. However, the uncertainty of noise degrades its performance [20]. Besides, below an SNR threshold referred to as the SNR wall, a reliable detection cannot be achieved by increasing the sensing duration [19], [31]. Moreover, the energy detector cannot distinguish the PU signal from the

noise and other interference signals, which may lead to a high false alarm probability.

2.2.4 Eigenvalue Based Detection Methods

The eigenvalue-based detection has been proposed for use in spectrum sensing in a multi-antenna system [19]. The technique is found to achieve both high P_d and low P_{fa} without requiring much information about the PU signal and noise power. In the existing methods, the expression for the decision threshold, P_d and P_{fa} are calculated based on the asymptotical distributions of the eigenvalues [32]. The eigenvalue of the signal received at the SU during the sensing interval is derived as follows. Let us suppose that the SU is equipped with M antennas and that the PU is transmitting, the $M \times 1$ observation vector at the receiver can be defined as

$$\mathbf{x}(n) \triangleq [x_1(n), x_2(n), ..., x_M(n)]^T \tag{2.2.20}$$

$$\mathbf{h}_p(n) \triangleq [h_{1,p}(n), h_{2,p}(n), ..., h_{M,p}(n)]^T \tag{2.2.21}$$

$$\boldsymbol{\eta}(n) \triangleq [\eta_1(n), \eta_2(n), ..., \eta_M(n)]^T \ . \tag{2.2.22}$$

If we assume that there are P transmitting PUs, the received signal vector can be expressed as

$$\mathbf{x}(n) = \sum_{p=1}^{P} \sum_{k=0}^{K_p} \mathbf{h}_p(k) s_p(n-k) + \boldsymbol{\eta}(n), n = 0, 1, 2 \cdots \tag{2.2.23}$$

where the vector $\mathbf{h}_p(n)$ represents the channel gain between PU_p and all the antennas of the SU while K_p is the order of the channel between PU_p and each antenna of the SU. Assuming we also consider N consecutive samples of the transmitted PU signal, the corresponding signal and noise vectors can

be defined as

$$\begin{aligned}\mathbf{x}_N(n) &\triangleq [\mathbf{x}^T(n), \mathbf{x}^T(n-1), ..., \mathbf{x}^T(n-N+1)]^T \\ \mathbf{s}_N(n) &\triangleq [\mathbf{s}_1^T(n), \mathbf{s}_2^T(n), ..., \mathbf{s}_P^T(n)]^T \\ \boldsymbol{\eta}_N(n) &\triangleq [\boldsymbol{\eta}^T(n), \boldsymbol{\eta}^T(n-1), ..., \boldsymbol{\eta}^T(n-N+1)]^T\end{aligned} \tag{2.2.24}$$

where $\mathbf{s}_p^T(n) \triangleq [s_p(n), s_p(n-1), \cdots, s_p(n-K_p-N+1)]$ and N is known as the smoothing factor [32], [33]. In matrix form, the received signal model can be expressed as

$$\mathbf{x}_N(n) = \mathbf{H}\mathbf{s}_N(n) + \boldsymbol{\eta}_N(n) \tag{2.2.25}$$

where the matrix $\mathbf{H}$, of order $MN \times (K + NP)$, $K = \sum_{p=1}^{P} K_p$ is defined as

$$\mathbf{H} \triangleq [\mathbf{H}_1, \mathbf{H}_2, \cdots, \mathbf{H}_P] \ , \tag{2.2.26}$$

where

$$\mathbf{H}_p \triangleq \begin{bmatrix} \mathbf{h}_p(0) & \cdots & \cdots & \mathbf{h}_p(K_p) & \cdots & 0 \\ & \ddots & & & \ddots & \\ 0 & \cdots & \mathbf{h}_p(0) & \cdots & \cdots & \mathbf{h}_p(K_p) \end{bmatrix}, \tag{2.2.27}$$

and $\mathbf{H}_p$ is a $MN \times (K_p + N)$ matrix. The statistical covariance matrix of the received signals can then be written as

$$\mathbf{R}_x = \mathbf{H}\mathbf{R}_s\mathbf{H}^{\mathbf{H}} + \sigma_n^2\mathbf{I}_{MN}, \tag{2.2.28}$$

where $\mathbf{R}_s = \mathbf{E}[\mathbf{S}_N(n)\mathbf{S}_N^{\mathbf{H}}(n)]$, $\mathbf{I}_{MN}$ is the identity matrix of order MN and $(.)^{\mathbf{H}}$ denotes Hermitian transpose. However, in practice, we have only finite number of samples, denoted as N_s. This means that instead of the statistical covariance matrix in (2.2.28), we can only obtain the sample covariance

matrix which can be written as [32]

$$\mathbf{R}_s(N_s) \triangleq \frac{1}{N_s} \sum_{n=L-1}^{L-2+N_s} \mathbf{x}(n)\mathbf{x}^{\dagger}(n). \tag{2.2.29}$$

Based on the matrix in (2.2.29), two blind spectrum sensing algorithms have been proposed [32]. The first one is called the maximum-minimum eigenvalue (MME) detection algorithm where as the name suggests, the maximum and minimum eigenvalue of the matrix denoted as λ_{max} and λ_{min} are computed and the test statistics for deciding the presence or absence of the PU is the ratio λ_{max} to λ_{min}. The decision rule is given as

$$\Upsilon(\mathbf{R}_s(N_s)) = \frac{\lambda_{max}}{\lambda_{min}} \underset{H_0}{\overset{H_1}{\gtrless}} \theta_t \tag{2.2.30}$$

where $\theta_t > 1$ is a threshold. The second sensing algorithm is known as the energy with minimum eigenvalue (EME) detection method. In this case, test statistics for detection is the ratio of energy to minimum eigenvalue, i.e. $\frac{T(N_s)}{\lambda_{min}}$ where the energy, $T(N_s)$, of the received signals in this instance is computed as [32]

$$T(N_s) = \frac{1}{MN_s} \sum_{m=1}^{M} \sum_{n=0}^{N_s-1} |x_m(n)|^2. \tag{2.2.31}$$

The decision rule is therefore given as

$$\Upsilon(\mathbf{R}_s(N_s)) = \frac{T(N_s)}{\lambda_{min}} \underset{H_0}{\overset{H_1}{\gtrless}} \theta_t \tag{2.2.32}$$

where θ_t is as defined for the MME method.

2.2.5 Covariance Based Method

In general, the statistical covariance matrices or autocorrelations of signal and noise are different. Using sample covariance matrix computed over N_s,

Zeng and Liang [34], proposed to use the difference to perform spectrum sensing under the assumption that the PU's signal is correlated. If we denote the statistical covariance matrix as $\mathbf{R}_x$, and the sample autocorrelations of the received signal is computed as

$$r(l) = \frac{1}{N_s} \sum_{n=0}^{N_s-1} x(n)x(n-l), \quad l = 0, 1, ..., N-1, \tag{2.2.33}$$

where N is known as the smoothing factor. The sample covariance matrix, $\hat{\mathbf{R}}_x(N_s)$, which approximates the statistical covariance matrix can be defined as

$$\hat{\mathbf{R}}_x(N_s) \triangleq \begin{bmatrix} r(0) & r(1) & \cdots & r(N-1) \\ r(1) & r(0) & \cdots & r(N-2) \\ \vdots & \vdots & \ddots & \vdots \\ r(N-1) & r(N-2) & \cdots & r(0) \end{bmatrix}. \tag{2.2.34}$$

Under H_0, the off-diagonal elements of $\hat{\mathbf{R}}_x(N_s)$ are theoretically zero since the noise is usually assumed to be uncorrelated. The diagonal elements also contain the noise power. On the other hand, under H_1, the off-diagonal elements should be non-zeros due to the correlatedness of the primary signal. In this case, there are two terms of interest and they are computed as

$$T_1(N_s) = \frac{1}{N} \sum_{i}^{L} \sum_{j}^{N} |r_{ij}(N_s)| \tag{2.2.35}$$

and

$$T_2(N_s) = \frac{1}{N} \sum_{i}^{N} |r_{ii}(N_s)| \tag{2.2.36}$$

where $r_{ij}(N_s)$ are the elements of the matrix in (2.2.34). The test statistics for determining the presence or absence of PU is given by

$$\Upsilon(\hat{\mathbf{R}}_x(N_s)) = \frac{T_1(N_s)}{T_2(N_s)} \underset{H_0}{\overset{H_1}{\gtrless}} \theta_t \tag{2.2.37}$$

where θ_t is an appropriate threshold.

2.2.6 Wavelet Method

The wavelet transform is a powerful mathematical tool for analyzing singularities and edges [35]. In wavelet method based spectrum sensing schemes, the spectrum of interest is usually decomposed as a train of consecutive frequency sub-bands and wavelet transform is then used to detect irregularities in these bands. An important characteristic of the power spectral density (PSD) is that it is relatively smooth within the sub-bands and possesses irregularities at the edges between two neighboring sub-bands. So, wavelet transform carries information about the locations of these frequencies and the PSD of the sub-bands. Vacant frequency bands can be obtained through the detection of the *singularities* in the PSD of the signal observed, by performing the wavelet transform of its PSD [20].

The process for the wavelet detection methods can be described as follows [35]. First, let us assume that we have a total of B Hz spread across the frequency range $[f_0, f_N]$ for a wideband wireless system. Further, we assume that the entire band is divided into N sub-bands where each sub-band is occupied by individual PU and all sub-bands are being simultaneously monitored. The sensing task involves detecting the locations and PSD within each sub-band. Let us suppose that the sub-bands lie consecutively within $[f_0, f_N]$, such that there are frequency boundaries located at $f_0 < f_1 < \cdots f_N$. The n-th band may thus be defined by $B_n : \{f \in B_n : f_{n-1} \leq f < f_n\}, n = 1, 2, \cdots, N$. Under H_1, the normalized, unknown power shape within each band, B_n is denoted by $S_n(f)$ and satisfies the conditions [35]

$$S_n(f) = 0, \ \forall f \notin B_n; \tag{2.2.38}$$

$$\int_{f_{n-1}}^{f_n} S_n(f) df = f_n - f_{n-1}. \tag{2.2.39}$$

If it is assumed that the PSD within each band, B_n is smooth and almost flat but exhibits discontinuities from its neighboring bands B_{n-1} and B_{n+1}, such that irregularities in PSD appears only at the edges of the bands, $S_n(f)$ may be approximated as

$$S_n(f) = \begin{cases} 1, & \forall f \in B_n. \\ 0, & \forall f \notin B_n. \end{cases} \tag{2.2.40}$$

The PSD of the observed time domain signal, $x(t)$, can then be written as

$$S_x(f) = \sum_{n=1}^{N} \bar{\alpha}_n^2 S_n(f) + S_w(f), f \in [f_0, f_N] \tag{2.2.41}$$

where it is assumed that the noise is additive and white with two sided PSD, $S_w(f) = \frac{N_0}{2}$, $\forall f$, and $\bar{\alpha}_n^2$ indicates the n-th band signal power density. Furthermore, the corresponding time domain equivalent of (2.2.41) can be written as

$$x(t) = \sum_{n=1}^{N} \bar{\alpha}_n p_n(t) + w(t) \tag{2.2.42}$$

where $S_n(f)$ is the signal spectrum of $p_n(t)$ and $w(t)$ is the additive noise whose PSD is $S_w(f)$. Furthermore, if we assume a pulse shaper, h_t of bandwidth $f_n - f_{n-1}$, and the center frequency is denoted by $f_{c,n} = \frac{f_{n-1}+f_n}{2}$, the spectral shape, $S_n(f)$ is proportional to $|\mathcal{F}\{h_t\}|^2$, where $\mathcal{F}\{.\}$ denotes the Fourier transform (FT). It is desired that $x(t)$ with PSD $S_x(f)$ be used to estimate $\{f_n\}_{n=1}^{N-1}$ and $\{\bar{\alpha}_n^2\}_{n=1}^{N}$, which characterize the wideband spectral environment under consideration. If we let $\kappa(f)$ be a wavelet smoothing function, for example, the Gaussian function with a compact support, g vanishing moments and g times continuously differentiable, the dilation of $\kappa(f)$ by a scale factor s is given by [35]

$$\kappa_s(f) = \frac{1}{s}\kappa(\frac{f}{s}) \tag{2.2.43}$$

where for dyadic scales, s takes values from powers of 2, i.e. $s = 2^j$, $j = 1, \cdots, J$. The continuous wavelet transform (CWT) of $S_x(f)$ in (2.2.41) is given by

$$\mathcal{W}_s S_x(f) = S_x * \kappa_s(f) \tag{2.2.44}$$

where $*$ denotes the convolution operation. It is worth noting here that CWT in (2.2.44) is implemented in the frequency domain and $S_x(f)$ is related to $x(t)$ via the FT. For the $S_x(f)$ under consideration, the edges and irregularities at scale s are defined as local sharp variations points of $S_x(f)$ smoothed by $\kappa(f)$. Furthermore, since the edges of a function are often indicated in the shapes of its derivatives, by using the CWT, the first and second order derivatives of $S_x(f)$ smoothed by the scaled wavelet, $\kappa(f)$, can be written as [35]

$$\begin{aligned} \mathcal{W}'_s S_x(f) &= s\frac{d}{df}(S_x * \kappa_s)(f) \\ &= S_x * (s\frac{d\kappa_s}{df})(f) \end{aligned} \tag{2.2.45}$$

and

$$\begin{aligned} \mathcal{W}''_s S_x(f) &= s^2\frac{d^2}{df^2}(S_x * \kappa_s)(f) \\ &= S_x * (s^2\frac{d^2\kappa_s}{df^2})(f) \end{aligned} \tag{2.2.46}$$

respectively. According to [36], the signal irregularities is characterized by the local extrema of the first derivative and the zero crossings of the second derivative. However, for spectrum purposes, the local maxima of the wavelet modulus are sharp variation points which yields better detection accuracy than local minima points. Therefore, the edges or boundaries corresponding to the spectral content, $\{f_n\}_{n=1}^{N-1}$, in the received signal, $x(t)$, of interest can be obtained in terms of the local maxima of the wavelet modulus in (2.2.45)

with respect to f as

$$\hat{f}_n = maxima_f\{|\mathcal{W}'_s S_x(f)|\}, \quad f \in [f_0, f_N] \tag{2.2.47}$$

or from the zero crossing points of (2.2.46) as

$$\hat{f}_n = zeros_f\{\mathcal{W}''_s S_x(f)\}, \ subject\ to \quad \mathcal{W}''_s S_x(\hat{f}_n) = 0. \tag{2.2.48}$$

In searching for the presence of frequency, $\hat{f}_n$, only those modulus maxima or zero crossings that propagate to large dyadic scale, s are retained while others are simply regarded and removed as noise [36].

After determining the frequencies present in $x(t)$, i.e. $\{f_n\}_{n=1}^{N-1}$, the next task is to estimate the PSD level, $\{\bar{\alpha}_n^2\}_{n=1}^{N}$. The average PSD within the band B_n, $\forall n$ can be computed as

$$\beta_n = \frac{1}{f_n - f_{n-1}} \int_{f_{n-1}}^{f_n} S_x(f) df. \tag{2.2.49}$$

Based on the earlier assumption that the PSD within each band is smooth and almost flat, but exhibiting discontinuities from the neighboring band, β_n is related to the required $\bar{\alpha}_n^2$ according to $\beta_n \approx \bar{\alpha}_n^2 + N_0/2$. However, in an empty band, i.e. where the PU is absent, say the n'-th band, $\bar{\alpha}_{n'}^2 = 0$ so that $\beta_{n'} = N_0/2$ for $f \in B_{n'}$. Therefore, the estimate of spectral density, $\bar{\alpha}_n^2$ denoted as $\hat{\alpha}_{n'}^2$ can be obtained from S_x as [35]

$$\hat{\alpha}_{n'}^2 = \beta_n - \min_{n'} \beta_{n'}, \ n = 1, \cdots, N \tag{2.2.50}$$

where $\{f_n\}$ used for computing $\{\beta_n\}$ in (2.2.49) can be replaced by their estimates derived via the wavelet method.

2.2.7 Moment Based Detection

The moment-based spectrum sensing is a blind technique that has been found to be useful when accurate noise variance and PU signal power are unknown. These unknown parameters are often estimated from the constellation of the PU signal [37]. In the event the SU does not have knowledge of the PU constellation, an approach had been developed that approximates a finite quadrature amplitude modulation constellation by a continuous uniform distribution [38].

2.2.8 Hybrid Methods

Apart from the stand alone schemes described in the preceding subsections, research efforts have also been geared towards developing systems that exploit the advantages offered by combining two or more sensing schemes, although, in most cases such systems are complicated for most practical realizations. These kinds of systems are known as the hybrid systems. Dhope et al in [20] considered a hybrid detection method that combines the ED and the covariance based detection methods. The proposed system utilized the ED in low correlation and covariance method in high correlation. In [39], a two stage spectrum sensing technique based on combining the ED and first order CD was proposed. These are referred to as coarse and fine detection stages respectively, in the ensuing hybrid system. The energy based coarse detection stage is first used to search the band of interest for the presence of the PU signal. The cyclostationary feature sensing is then performed to identify the type of the incoming signal. Another form of the latter sensing scheme was also introduced in [40] which utilized two levels of threshold. In the first stage and for a given channel, ED is performed and the channel is declared occupied if the energy received is above a certain threshold, θ_t. If the energy received is below the threshold, however, CD is performed in the second stage. If the test statistics in this stage exceeds a certain threshold,

θ_t', the channel is declared occupied, else, the presence of a spectrum hole is declared. It should be noted that in all cases of hybrid systems reviewed, the proposed systems are reported to outperform systems where stand alone detection methods are employed.

2.3 Cooperative Spectrum Sensing

Fading and shadowing are inherent characteristics of the wireless channels and can significantly affect the performance of local sensors (stand alone system). One very viable solution to this challenge is collaboration among users through cooperative spectrum sensing (CSS). It has been established that CSS can also decrease sensing time and solve the hidden node problem, where the PU signal experiences deep fading or is blocked by obstacles such that the power of the PU signal received at the SU may be too weak to be detected [4], [41], [42]. With the collaboration of several SU's for spectrum sensing, the detection performance of a sensing system can be improved by taking advantage of spatial diversity [19].

2.4 Summary

In this chapter, an overview of the various spectrum sensing methods for cognitive radio wireless networks that are of interest to this thesis was presented. From this consideration, it can be noted that different detector can be applied under different scenarios, depending on the amount of information about the PU that is available to the SU. In the succeeding four chapters, the focus will be on machine learning algorithms based solutions to spectrum sensing problem. In particular, supervised, semi supervised and unsupervised techniques are investigated and their performance is demonstrated by simulations.

Chapter 3

SUPERVISED LEARNING ALGORITHMS FOR SPECTRUM SENSING IN COGNITIVE RADIO NETWORKS

3.1 Introduction

Supervised learning is one of the fundamental machine learning approaches that has been successfully applied in solving many pattern recognition and classification problems in the field of data mining [17]. Essentially, it is the task of inferring a decision function from labeled data which usually consist of a set of training examples known as the training features [43]. In supervised learning, more often than not, each training example is a pair (typically a vector) consisting of an input object and a desired output value (label) which plays the role of supervisory signal. A supervised learning algorithm is required to analyze the training data and generate an inferred function for the purpose of classifying new examples. The ultimate goal is to produce an optimal algorithm which minimizes the training and generalization errors

[44].

In this chapter, five prominent supervised learning algorithms are considered, namely; artificial neural network (ANN) algorithm, the naive Bayes (NB) algorithm, Fisher's discriminant analysis (FDA) methods, the K-nearest neighbor (KNN) algorithm and the SVM algorithm. However, without loss of generality, to demonstrate how these learning methods can be used to solve the CR spectrum sensing problem at hand and the associated benefits, the SVM technique is used as an example.

3.2 Artificial Neural Networks

The concept of ANN is borne from attempts to replicate the biological neural systems, particularly, the structure of the human brain which consists of nerve cells commonly referred to as neurons [45]. In humans, neurons are connected together by means of axons which can be compared to strands of fiber. When a neuron receives sufficient stimulation, it transmits impulses to other neurons via axons. The axons of a neuron are connected to other neurons through dendrites which essentially are extensions from the cell body of a neuron. The point of contact between an axon and a dendrite is known as synapse. It is of interest to know that the human brain *learns* by adjusting the strength of the synaptic connection between neurons when acted upon repeatedly by the same impulse. Similarly, the ANN is comprised of an assembly of nodes that are interconnected by directed links. A simple example of the ANN based learning algorithms is the perceptron which will be described in the next sub-section to illustrate how the ANN technique can be applied to solve our signal detection problem.

3.2.1 The Perceptron Learning Algorithm

The perceptron is a single layer, feed-forward ANN network whose architecture consists of two types of nodes as shown in Fig. 3.1. These are the

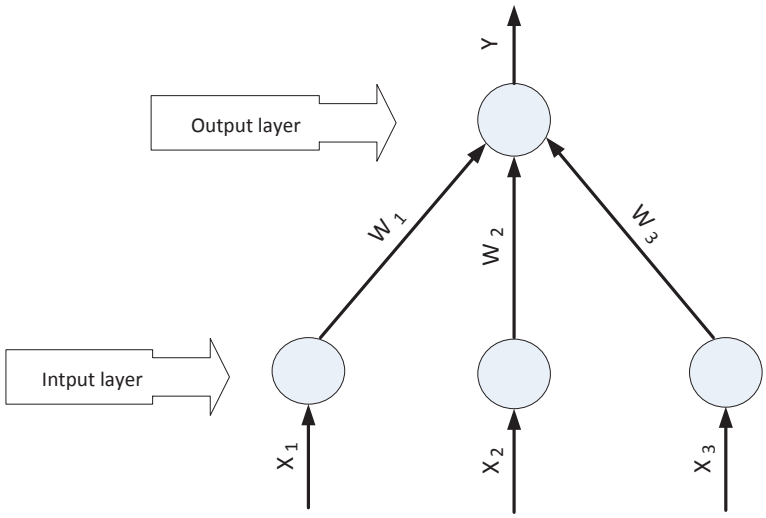

Figure 3.1. A three input single layer perceptron

input nodes through which the training examples are fed into the learning machine and an output node which performs necessary mathematical operations and from where the model output (decision) is obtained. The input nodes and the output node are connected by weighted links that represents the synaptic connections strength. The main goal of the perceptron model is to determine the set of weight that minimizes the total sum of square of the error, i.e., the difference between the desired output and the actual prediction made by the model. During the training process, this is accomplished by adapting the synaptic weight until the input-output relationship of the underlying data is matched. For example, given a set of labeled data, $\mathcal{S} = \{(\mathbf{x}_i, y_i)\}_{i=1}^{N} \in \{H_0, H_1\}$, where $\mathbf{x}_i \in R^K$ is the i-th training feature vector, y_i is the corresponding supervisory signal or the actual class label for $\mathbf{x}_i$ and K is the number of input nodes, the perceptron output, $\hat{y}$ for the i-th training example is computed as

$$\hat{y} = sgn(\mathbf{w}^T\mathbf{x} - t) \tag{3.2.1}$$

where $\mathbf{w} = [w_1, \cdots, w_K]$ is the vector of synaptic weight parameters, t is the bias factor which is more or less a decision threshold, $\hat{y}$ is the output value computed as the difference between the weighted sum of the input training data and the bias factor and sgn is the signum function which acts as an activation function for the output neuron.

By learning the perceptron model, the desire is to minimize the total sum of squared prediction errors over all training data, $e(\mathbf{w})$, given by

$$e(\mathbf{w}) = \frac{1}{N}\sum_{i=1}^{N}(y_i - \hat{y}_i)^2 \tag{3.2.2}$$

which is accomplished by adjusting $\mathbf{w}$ iteratively using the expression

$$w_k^{j+1} = w_k^j + \rho(y_i - \hat{y}_i^j)x_{i,k} \tag{3.2.3}$$

where w_k^j is the weight parameter for the k-th input link after the j-th iteration, $\rho \in \{0, 1\}$ is the learning rate parameter used to control the amount of adjustment per iteration and $x_{i,k}$ is the k-th component of the i-th training vector, $\mathbf{x}_i$. To predict the class of a new feature vector, $\mathbf{x}'$ the set of optimal weight parameters, $\mathbf{w}_{opt}$, obtained through the training are used in the decision function similar to (3.2.1) defined as

$$\hat{y} = sgn(\mathbf{w}_{opt}^T\mathbf{x}' - t)\ . \tag{3.2.4}$$

It should be noted that in the case of a linearly separable training set, the perceptron algorithm is guaranteed to converge on some solution. However, it is possible for the algorithm to pick any solution and as a result, the learning algorithm may admit many solutions of varying quality [46]. In Algorithm 3.1, an algorithm that summarizes the perceptron learning and classification process for a simple, single layer network is presented.

Algorithm 3.1: Perceptron ANN learning spectrum sensing algorithm

i. Given the training set $\mathcal{S} = \{\mathbf{x}_i, y_i\}_{i=1}^{N} \in \{H_0, H_1\}$, where $\mathbf{x}_i \in R^K$,

ii. Initialize the weight vector, $\mathbf{w}^0 = [w_1^0, \cdots, w_K^0]$ with random values

iii. **do repeat**

iv. **for** each training example $(\mathbf{x}_i, y_i) \in \mathcal{S}$

v. Compute the predicted output $\hat{y}_i^j$

vi. **for** each weight, w_k **do**

vii. Update the weight, w_k^{j+1} in (3.2.3)

viii. **end for**

ix. **end for**

x. **until** convergence or stopping criterion is met

xi. Classify each new data point, $\mathbf{x}'$ to decide the corresponding PU status, H_0 or H_1.

3.3 The Naive Bayes Classifier

Naive Bayes (NB) is a probabilistic method for constructing models that can be used for classification purpose [47]. It is a learning technique that has been demonstrated to be very useful in solving many complex, real world problems such as text categorization, document classification (for example as authorized or spam) and automatic medical diagnosis [48]. Unlike other conventional classifiers, though, the NB is built on the assumption that different value of the attributes (elements) constituting a feature vector are independent of one another regardless of whether they are correlated or not. As such, NB relies on the assumption that each attribute contributes independently to the probability that a given feature belongs to a particular class where each class is a member of a finite set of classes. A very interesting

characteristic of the NB method is that only a small amount of training data is required to obtain an estimate of the model parameters needed for classification.

3.3.1 Naive Bayes Classifier Model Realization

Suppose $\mathbf{x} = [x_1, \cdots, x_K]$ is a feature vector that is to be classified into one out of J classes, where $x_k, x_l \ \forall k, l \in K$ is assumed to be independent continuous random variable, the conditional probability, $p(C_j|x_1, \cdots, x_K)$, is evaluated for all J classes using the Bayes' theorem which is described by [48]

$$p(C_j|\mathbf{x}) = \frac{p(C_j)\ p(\mathbf{x}|C_j)}{p(\mathbf{x})} \tag{3.3.1}$$

where $p(C_j|\mathbf{x})$ is the posterior probability, $p(C_j)$ is the prior, $p(\mathbf{x}|C_j)$ is the likelihood and $p(\mathbf{x})$ is the model evidence. Since $p(\mathbf{x})$ is independent of class, C_j, and the values of each attribute $x_k \in \mathbf{x}$ is known, the model evidence is effectively a constant so that it is fixed for all classes. It follows therefore, that essentially the concern is to evaluate the numerator of (3.3.1) which is equivalent to the joint probability model over all attributes and the class of interest, $p(C_j, x_1, \cdots, x_K)$. By applying the chain rule of probability described by

$$p(\bigcap_{k=1}^{K} x_k) = \prod_{k=1}^{K} p(x_k|\bigcap_{q=1}^{k-1} x_q)\ , \tag{3.3.2}$$

$p(C_j, x_1, \cdots, x_K)$ may be re-written as

$$\begin{aligned} p(C_j, x_1, \cdots, x_K) &= p(x_1, \cdots, x_K|C_j)\ p(C_j) \\ &= p(x_K|x_{K-1}, \cdots, x_1, C_j)\ \cdots\ p(x_2|x_1, C_j)\ p(x_1|C_j)\ p(C_j). \end{aligned} \tag{3.3.3}$$

Furthermore, following from the conditional independence assumption adopted in NB where it is *naively* assumed that x_k is conditionally independent of

x_l, $k \neq l$ $\forall k, l \in K$, we can infer that

$$p(x_k|x_l, C_j) = p(x_k|C_j) \tag{3.3.4}$$

for $k \neq l$ where the influence of the independent attribute, x_l is subsumed by the presence of the class identifier, C_j. Therefore, (3.3.3) may be re-expressed as

$$\begin{aligned} p(C_j, x_1, \cdots, x_K) &\equiv p(x_1, \cdots, x_K|C_j) \\ &\equiv p(x_1|C_j)\ p(x_2|C_j)\ \cdots\ p(x_K|C_j)\ p(C_j) \\ &\equiv p(C_j) \prod_{k=1}^{K} p(x_k|C_j) \end{aligned} \tag{3.3.5}$$

and from (3.3.1)

$$\begin{aligned} p(C_j|\mathbf{x}) &= \frac{p(C_j)\ p(\mathbf{x}|C_j)}{p(\mathbf{x})} \\ &= \frac{p(C_j)}{p(\mathbf{x})} \prod_{k=1}^{K} p(x_k|C_j). \end{aligned} \tag{3.3.6}$$

In the spectrum sensing problem, if we assume that each attribute of the feature vector is a continuous random variable as it is in the case of energy values computed at the SUs terminals (sensor nodes), in sub-section 3.3.2, how the probability model given in (3.3.6) can be used to solve the sensing problem under this scenario is described.

3.3.2 Naive Bayes Classifier for Gaussian Model

To derive the NB classifier for solving the sensing problem, the probability model in (3.3.6) is combined with an appropriate decision rule such as the one based on maximum a posteriori (MAP). In this case, the predicted class for a feature vector, $\mathbf{x}'$, depends on the most probable hypothesis, i.e., the class $j \in \{1, \cdots, J\}$ that maximizes the posterior probability in (3.3.6). The

decision function of the NB classifier based on the MAP can be derived as

$$\hat{j} = \underset{j \in \{1,\cdots,J\}}{\operatorname{argmax}} \; p(C_j) \prod_{k=1}^{K} p(x'_k|C_j) \tag{3.3.7}$$

where $\hat{j}$ is the predicted class of the feature vector, $\mathbf{x}'$, and the prior, $p(C_j)$, may be assumed to be equiprobable for a two-hypothesis spectrum sensing problem where for example, $p(H_0)$ may be set equals to $p(H_1) = 0.5$ or may be determined from the prior knowledge of the number of training examples belonging to a particular class. Finally, the remaining term in (3.3.7) is the likelihood function, $p(x'_k|C_j)$, which for a Gaussian random variable is expressed as

$$p(x'_k|C_j) = \frac{1}{\sigma_j^2\sqrt{2\pi}} \; exp(-\frac{(x'_k - \mu_j)^2}{2\sigma_j^2}) \tag{3.3.8}$$

where the mean, μ_j, and variance, σ_j^2, $\forall \; j \in \{1, \cdots, J\}$, can be obtained from the labeled training examples.

3.4 Nearest Neighbors Classification Technique

Nearest neighbor classification technique is an instance-based learning method which does not require maintaining an abstraction or building a model from training data. It uses specific training instances or examples to predict the class of a test instance based on a chosen proximity measure [49]. The assumption here is that if we are able to find all the training examples in the neighborhood (*nearest neighbors*) of a test example, whose attributes are relatively similar to that of the test instance, these nearest neighbors can be used to predict the class to which the test example belongs. The justification for the assumption is illustrated by the saying that [43] "*if it walks like a duck, quacks like a duck, and looks like a duck, then it is probably a duck.*"

Given a test instance, x, which is assumed to be a continuous random

variable, its proximity to other training data points is computed by using proximity measures such as the Mahalanobis or Euclidean distance. The k nearest neighbors are the k training examples that are closest to x in the feature space whose class labels are used to classify x. However, if the neighbors have more than one label such as could occur when spectrum sensing data are obtained under low SNR regime, the test point is assigned to the class of the majority of the nearest neighbors. In the situation where there is a tie between classes, the test instance is randomly assigned to one of the classes.

3.4.1 Nearest Neighbors Classifier Algorithm

In Algorithm 3.4, the summary of the nearest neighbor classifier is presented whereby the distance between a test example, $x = (\tilde{\mathbf{z}}, \tilde{y})$, that belongs to an unknown class, $\tilde{y}$ and all training examples, $(\mathbf{z}_i, y_i), \forall i \in \mathcal{S}$, with respective class label, y_i are first computed to obtain a list of its nearest neighbors, $\mathcal{S}_x$. After generating the list of the nearest-neighbors, the test example will be classified using the majority voting (MV) rule described by [43]

$$MV : \tilde{y} = \underset{j}{\operatorname{argmax}} \sum_{(\mathbf{z}_i, y_i) \in \mathcal{S}_x} I(j = y_i) \ , \tag{3.4.1}$$

where $j = \{1, \cdots, J\}$ is a class label and $I(.)$ is an indicator function defined as

$$I(.) = \begin{cases} 1, \text{ if } j = y_i \\ 0, \text{ otherwise } . \end{cases}$$

It should be noted that the majority voting based k-NN algorithm is sensitive to the choice of k due to the fact that every neighbor is allowed to have the same influence on classification decision regardless of how close or far they may be to the test example. To reduce the impact of k, one approach is to assign appropriate weight to the influence of each nearest neighbor, $\mathbf{z}_i$

such that training examples that are far away from x have weaker impact on classification compared to those that are close to x. The weighting factor for each neighbor is determined as $w_i = \frac{1}{d(\tilde{\mathbf{z}},\mathbf{z}_i)^2}$, where $d(.,.)$ is the distance between $\tilde{\mathbf{z}}$ and $\mathbf{z}_i$ as computed by a metric of choice. Subsequently, the class label for $\tilde{\mathbf{z}}$ using the distance-weighted voting (DWV) approach can be derived by using

$$DWV : \tilde{y} = \underset{j}{\operatorname{argmax}} \sum_{(\mathbf{z}_i,y_i)\in\mathcal{S}_x} w_i \times I(j = y_i) \ . \tag{3.4.2}$$

Algorithm 3.4: Weighted k-NN classification based spectrum sensing algorithm

i. Given the training set $\mathcal{S} = \{\mathbf{z}_i, y_i\}_{i=1}^{N} \in \{H_0, H_1\}$, where $\mathbf{z}_i \in R^K$, let k be the number of nearest neighbors.

ii. **for** each test example, $x = (\tilde{\mathbf{z}}, \tilde{y})$ **do**

iii. Compute $d(\tilde{\mathbf{z}}, \mathbf{z}_i)^2$, the distance between x and every training example, $(\mathbf{z}, y) \in \mathcal{S}$.

iv. Choose $\mathcal{S}_x \subseteq \mathcal{S}$, the set of k training examples closest to x.

v. Calculate the weights, $w_i = \frac{1}{d(\tilde{\mathbf{z}},\mathbf{z}_i)^2}$, $\forall \mathbf{z}_i \in \mathcal{S}_x$.

vi. Evaluate $\tilde{y} = \underset{j}{\operatorname{argmax}} \sum_{(\mathbf{z}_i,y_i)\in\mathcal{S}_x} w_i \times I(j = y_i)$.

vii. Infer PU's status, H_0 or H_1 from $\tilde{y}$.

viii. **end for**

3.5 Fisher's Discriminant Analysis Techniques

Fisher's discriminant analysis (FDA) is a machine learning technique used to find combination of features that characterizes or separates two or more classes of object [50], [51]. There are two closely related forms of FDA, namely; the linear and quadratic discriminant analysis. The linear dis-

criminant analysis (LDA) attempts to find linear combination of features that models the difference between classes of data [49]. To describe how the LDA is implemented, let us consider that we have a training data set, $\mathcal{S} = \{\mathbf{x}_i, y_i\}_{i=1}^{L}$, $\mathbf{x}_i \in R^d$. Let us also assume that $\mathcal{S} \in \{H_0, H_1\}$ so that there are two classes of data, C_k and C_l in $\mathcal{S}$ that we wish to be able to discriminate. Suppose we further assume that $p(\mathbf{x}|C_k)$ is the class-conditional density of $\mathbf{x}$ in class k, and also let the prior probability of C_k be represented by π_k where $\sum_{k=1}^{K} \pi_k = 1$. By applying the Bayes theorem, we simply obtain

$$p(C_k|\mathbf{x}) = \frac{p(\mathbf{x}|C_k)\ p(C_k)}{\sum_{l=1}^{K} p(\mathbf{x}|C_l)\ p(C_l)} \tag{3.5.1}$$

where the denominator of the entity on the right hand side, i.e., the sum over k of the product of the likelihood and the prior, is a normalization constant. It is straightforward to see from (3.5.1) that the ability to classify a data point or the posterior probability essentially depends on knowing the likelihood, $p(\mathbf{x}|C_k)$. If we assume that the data points under consideration takes the form of continuous random variables, the probability density characterizing each class can be modeled as multivariate Gaussian of the form

$$p(\mathbf{x}|C_k) = \frac{1}{(2\pi)^{d/2}|\Sigma_k|^{1/2}} \exp(-\frac{1}{2}(\mathbf{x} - \mu_k)^T {\Sigma_k}^{-1}(\mathbf{x} - \mu_k)) \ . \tag{3.5.2}$$

In LDA, it is usually assumed that all classes, C_k and C_l, have the same covariance matrix such that $\Sigma_k = \Sigma, \forall k, l \in K$ and the hyperplane separating both classes is a straight line. Therefore, to compare the two classes it is sufficient to take the logarithm of the ratio since the logarithm is a monotonic

function. By doing this we obtain

$$\begin{aligned}\log \frac{p(C_k|\mathbf{x})}{p(C_l|\mathbf{x})} &= \log \frac{p(\mathbf{x}|C_k)}{p(\mathbf{x}|C_l)} + \log \frac{\pi_k}{\pi_l} \\ &= \log \frac{\pi_k}{\pi_l} - \frac{1}{2}(\mu_k + \mu_l)^T \Sigma^{-1}(\mu_k - \mu_l) + \mathbf{x}^T \Sigma^{-1}(\mu_k - \mu_l) \ .\end{aligned} \tag{3.5.3}$$

It is easy to see that (3.5.3) is a linear function of $\mathbf{x}$, where the normalization factors as well as the quadratic part in the exponents have been eliminated due to the equality constraints on the covariance matrix, Σ. It should be noted that at the decision boundary, (3.5.3) equals zero. Furthermore, if we apply the optimal Bayes classification method based on the MAP, the linear discriminant function can be defined as

$$\delta_k(\mathbf{x}) = \log \pi_k - \frac{1}{2}\mu_k^T \Sigma^{-1} \mu_k + \mathbf{x}^T \Sigma^{-1} \mu_k \tag{3.5.4}$$

and the decision rule is described by

$$\hat{C}_k(\mathbf{x}) = \underset{k}{\operatorname{argmax}}\ \delta_k(\mathbf{x}) \tag{3.5.5}$$

where the prior π_k, mean μ_k, and covariance Σ, $\forall k \in K$ can be estimated from the training data as

$$\hat{\pi}_k = N_k / L \tag{3.5.6}$$

where N_k is the number of training data vector belonging to class k,

$$\hat{\mu}_k = \frac{1}{N_k} \sum_{i=1}^{N_k} \mathbf{x}_i \tag{3.5.7}$$

and

$$\hat{\Sigma} = \frac{1}{L - K} \sum_{k=1}^{K} \sum_{i=1}^{N_k} (\mathbf{x}_i - \hat{\mu}_k)(\mathbf{x}_i - \hat{\mu}_k)^T. \tag{3.5.8}$$

Conversely, if the covariances are not assumed to be equal i.e. $\Sigma_k \neq \Sigma_l$, the eliminations in (3.5.3) do not occur and the quadratic elements in $\mathbf{x}$ are retained, thus leaving us with the quadratic discriminant analysis (QDA) classifier. The quadratic discrimination function in this case is therefore given by

$$\delta_k(\mathbf{x}) = \log \pi_k - \frac{1}{2} \log |\Sigma_k| - \frac{1}{2}(\mathbf{x} - \mu_k)^T \Sigma_k^{-1} (\mathbf{x} - \mu_k) \tag{3.5.9}$$

and the classification of a data vector can be done by adopting the decision rule given in (3.5.5).

3.6 Support Vector Machines Classification Techniques

The SVM is a non-parametric, learning technique that has been successfully applied to many real world problems involving data classification [2], [52]. It is a statistical pattern recognition technique that is based on the principle of structural risk minimization and is known to generalize well. Rooted in the concepts of geometry and convex optimization [53], it has the ability to find global and non-linear classification solutions and as a result it is widely used in the fields of data mining and machine learning [52].

In this section, the SVM algorithms is described. Furthermore, how it can be applied to solve both temporal and spatio-temporal spectrum sensing problems is demonstrated in multi-antenna CR networks under single and multiple PUs considerations. To show the efficacy of the SVM classifier, an algorithm for realizing a novel blind feature that is based on the eigenvalues of the sample covariance matrix of the received primary signals which has the capability to enhance the performance of the SVM for signal classification is first presented. Next, the spectrum sensing problem under multiple PUs scenario is formulated as a multiple class signal detection problem where intuitively, each class is comprised of one or more sub-classes and generalized

expressions for the possible classes are provided. Then, the eigenvalues features and error correcting output codes (ECOC) based multi-class * SVM (MSVM) algorithms is investigate for solving the multiple class spectrum sensing problem using two different coding strategies. Finally, the performance of the proposed SVM based detectors is shown in terms of probability of detection, probability of false alarm, receiver operating characteristics curves and overall classification accuracy.

3.6.1 Algorithm for the Realization of Eigenvalues Based Feature Vectors for SUs Training

In this sub-section, the procedure for extracting the eigenvalue based feature for training the SUs is described. During the training interval, given that the PU(s) operate at a carrier frequency f_c and the transmitted signal of the p-th PU is sampled at the rate of f_s by the SU, the $M \times 1$ observation vector at the receiver can be defined as [32]

$$\mathbf{x}(n) = [x_1(n), x_2(n), ..., x_M(n)]^T. \tag{3.6.1}$$

If we assume that there are P transmitting PUs, the received signal vector can be expressed as

$$\mathbf{x}(n) = \sum_{p=1}^{P} \boldsymbol{\phi}_p s_p(n) + \boldsymbol{\eta}(n), \tag{3.6.2}$$

where

$$\boldsymbol{\phi}_p = [\phi_{1,p}, \phi_{2,p}, ..., \phi_{M,p}]^T \tag{3.6.3}$$

$$\boldsymbol{\eta}(n) = [\eta_1(n), \eta_2(n), ..., \eta_M(n)]^T \tag{3.6.4}$$

*In this context, the term multi-class denotes more that two classes.

where the vector $\boldsymbol{\phi}_p$ represents the channel gain between the p-th PU and the antennas of the SU. If we take N consecutive samples of the transmitted PU signal for the eigenvalue computation, the corresponding signal and noise vectors can be defined as

$$\begin{aligned} \mathbf{X} &= [\mathbf{x}^T(n), \mathbf{x}^T(n-1), ..., \mathbf{x}^T(n-N+1)]^T \\ \mathbf{S} &= [\mathbf{s}_1^T(n), \mathbf{s}_2^T(n), ..., \mathbf{s}_P^T(n)]^T \\ \boldsymbol{\eta} &= [\boldsymbol{\eta}^T(n), \boldsymbol{\eta}^T(n-1), ..., \boldsymbol{\eta}^T(n-N+1)]^T \end{aligned} \tag{3.6.5}$$

where $\mathbf{s}_p(n) = [s_p(n), s_p(n-1), ..., s_p(n-N+1)]$. If we let the matrix of the channel coefficients for the N consecutive samples of the p-th PU's signal be represented by Φ_{MN}^p, then we can write

$$\Phi_{MN}^p = \begin{pmatrix} \boldsymbol{\phi}_p^1 \\ \boldsymbol{\phi}_p^2 \\ \vdots \\ \boldsymbol{\phi}_p^N \end{pmatrix}$$

and the channel coefficient matrix when all the P PUs are simultaneously transmitting, $\boldsymbol{\Phi} = [\Phi_{MN}^1, \Phi_{MN}^2, ..., \Phi_{MN}^P]$, of order $MN \times P$ can be represented as

$$\boldsymbol{\Phi} = \begin{pmatrix} \boldsymbol{\phi}_1^1 & \boldsymbol{\phi}_2^1 & \cdots & \boldsymbol{\phi}_P^1 \\ \boldsymbol{\phi}_1^2 & \boldsymbol{\phi}_2^2 & \cdots & \boldsymbol{\phi}_P^2 \\ \vdots & \vdots & \ddots & \vdots \\ \boldsymbol{\phi}_1^N & \boldsymbol{\phi}_2^N & \cdots & \boldsymbol{\phi}_P^N \end{pmatrix}.$$

The PUs' signals jointly received by all the antennas of the SU during the sampling interval can therefore be expressed in a matrix form as

$$\mathbf{X} = \boldsymbol{\Phi}\ \mathbf{S} + \boldsymbol{\eta}. \tag{3.6.6}$$

Furthermore, the statistical covariance matrix of the received signals can be

written in terms of the PU (source) signals and the noise at the receiver as

$$\mathbf{R}_x = \mathbf{\Phi}\mathbf{R}_s\mathbf{\Phi}^H + \sigma_n^2\mathbf{I}_{MN}, \tag{3.6.7}$$

where $\mathbf{R}_s = \mathbb{E}[\mathbf{S}\mathbf{S}^H]$ is the statistical covariance matrix of the transmitted primary signal, $\mathbf{I}_{MN}$ is the identity matrix of order MN and $(.)^H$ denotes Hermitian transpose. However, in blind spectrum sensing being considered, the primary signal and the PU-SU channel is not known at the SUs, as such it is difficult to determine $\mathbf{R}_s$ in isolation as required by (3.6.7). For most practical realization therefore, it is easier to derive the eigenvalues features by using the received signals' covariance matrix that is computed over finite samples yielding an approximated form of (3.6.7) expressed as

$$\tilde{\mathbf{R}}_x = \mathbf{X}\mathbf{X}^H \ . \tag{3.6.8}$$

In general, $\tilde{\mathbf{R}}_x$ is a symmetric and Toeplitz matrix which under H_0, follows an uncorrelated complex Wishart distribution such that $\tilde{\mathbf{R}}_x \sim \mathcal{W}_M(N, \Sigma)$ with M dimensions over finite samples N known as the degrees of freedom and Σ is the population covariance matrix described by [54], [55]

$$\Sigma = \frac{1}{N}\mathbb{E}[\mathbf{X}\mathbf{X}^H] = \sigma_n^2\mathbf{I}_M \ \cdot \tag{3.6.9}$$

Similarly, under H_1 $\tilde{\mathbf{R}}_x$ follows a correlated complex Wishart distribution with population covariance matrix, Σ described by

$$\Sigma = \mathbf{\Phi}\mathbf{R}_s\mathbf{\Phi}^H + \sigma_n^2\mathbf{I}_M \tag{3.6.10}$$

where the correlation in this case is due to the presence of the PU signal, $\mathbf{R}_s$. To derive the required training features for the learning machine, the eigenvalues of the matrix in (3.6.8) is computed [56]. It is pertinent to state

here that if $M > P$, the eigenvalues thus derived not only has the capability to increase the feature space for support vector machines both also provides the SUs additional information about the number of active PUs under the hypothesis H_1, albeit not their locations.

3.6.2 Binary SVM Classifier and Eigenvalue Based Features for Spectrum Sensing Under Single PU Scenarios

Under single PU scenario, similar to (2.2.1), the spectrum sensing problem is simply a binary classification problem of the form

$$x_m(n) = \begin{cases} \eta_m(n) & H_0 : PU \quad absent \\ \phi(su^m)s(n) + \eta_m(n) & H_1 : PU \quad present. \\ \forall m \in M \end{cases} \tag{3.6.11}$$

where $x_m(n)$ is the instantaneous signal received at the m-th antenna of the SU. Suppose that D independent but identically distributed samples of vector of eigenvalues are collected for training purposes so that $\mathcal{S} = \{(\mathbf{x}_1, y_1), (\mathbf{x}_2, y_2), \cdots, (\mathbf{x}_D, y_D)\}$ is the set of training examples where $\mathbf{x}_i \in \mathcal{R}^M$ is an M-dimensional feature vector and $y_i \in \{-1, 1\}$ is the corresponding class label. If the training samples are linearly separable, the desire is to use the data set $\mathcal{S}$ to find the hyperplane that optimally separates the positive and the negative classes as depicted by Figure 3.2. However, if the training data are obtained under low SNR condition, overlapping would occur between the classes and consequently the training samples would not be linearly separable in their original feature space. To counteract the effect of overlapping, an appropriate non-linear mapping function (kernel function), $\beta(\mathbf{x})$, is introduced with careful choice of kernel parameters in order to transform the non-linearly separable data to a higher dimensional feature space where it could become linearly separable.

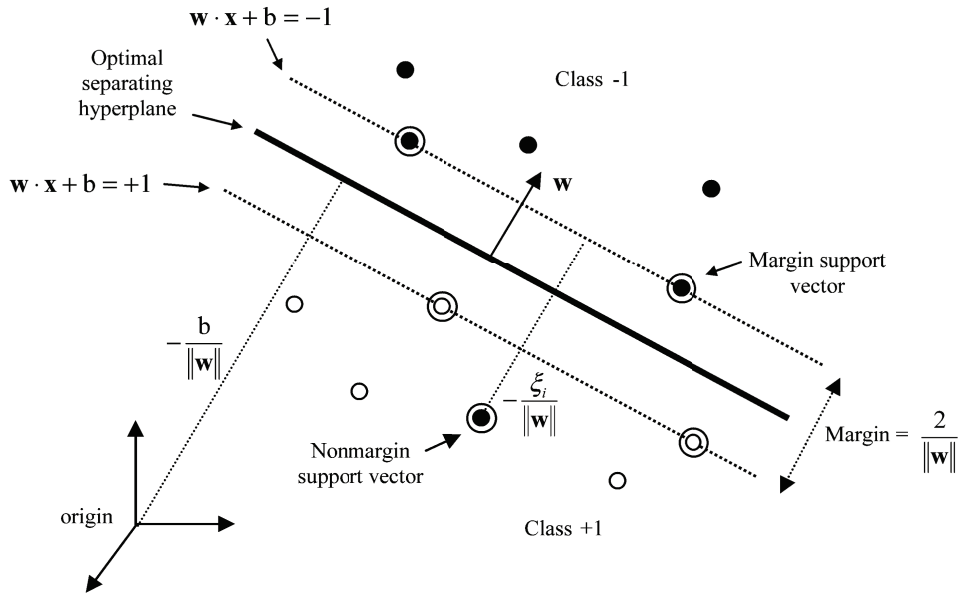

Figure 3.2. Support vector machines geometry showing non-linearly separable hyperplane [2]

The implicit objective is to minimize the actual error on the training data set $\{\mathbf{x}_i\}_{i=1}^{D}$, denoted by $\frac{1}{D}\sum_{i=1}^{D} y_i f(\mathbf{x}_i) < 0$, where $f(\mathbf{x})$ is the prediction on $\mathbf{x}$ and an error is considered to have occurred if $f(\mathbf{x}_i) \neq y_i$. In order to achieve the goal, the margin between the supporting hyperplanes of the two classes given by $\frac{2}{\|\mathbf{w}\|}$ is maximized where $\mathbf{w}$ is the weight vector which is normal to the separating hyperplane. Furthermore, to avoid over-fitting the data, minimum misclassification is allowed through the introduction of a slack variable ξ_i, to produce a soft margin classifier [46] so that data points for which $\xi_i = 0$ are correctly classified and are either on the margin or on the correct side of the margin while those for which $0 < \xi_i \leq 1$ lie inside the margin but are on the correct side of the decision boundary. Therefore, for an error to occur it follows that the corresponding ξ_i must exceed unity so that $\sum_i \xi_i$ is an upper bound on the number of training errors. A natural way to assign an extra cost for errors is to incorporate it into the objective

function for the optimization problem as [46], [57]

$$\begin{aligned} \underset{\mathbf{w},b,\xi}{\text{minimize}} \quad & \langle \mathbf{w}.\mathbf{w} \rangle + \Gamma \sum_{i=1}^{D} \xi_i \\ \text{subject } to \quad & y_i(\langle \mathbf{w}.\beta(\mathbf{x}_i) \rangle + b) \geq 1 - \xi_i, \\ & \xi_i \geq 0, \quad i = 1, 2, ..., D. \end{aligned} \tag{3.6.12}$$

where $\langle \mathbf{w}.\mathbf{w} \rangle$ denotes inner product otherwise written as $\mathbf{w}^T\mathbf{w}$, b is the bias describing the perpendicular distance between the origin and the separating hyperplane and Γ is a soft margin parameter sometimes referred to as the box constraint [46], [58].

To solve the resulting convex optimization problem, the Langrangian function, $\mathcal{L}$ is introduced so that (3.6.12) can be written in the primal form as

$$\begin{aligned} \mathcal{L}_p = \mathcal{L}(\mathbf{w}, b, \xi, \alpha, \psi) = \Bigg\{ & \frac{1}{2}\langle \mathbf{w}.\mathbf{w} \rangle + \Gamma \sum_{i=1}^{D} \xi_i - \sum_{i=1}^{D} \psi_i \xi_i \\ & - \sum_{i=1}^{D} \alpha_i [y_i(\langle \mathbf{w}.\beta(\mathbf{x}_i) \rangle + b) - 1 + \xi_i] \Bigg\} \end{aligned} \tag{3.6.13}$$

where α_i and ψ_i are positive Langrangian multipliers and the training data for which $\alpha_i > 0$, are the support vectors. By applying the Karush-Kuhn-Tucker (KKT) conditions [53] which essentially requires that the derivatives of (3.6.13) with respect to $\mathbf{w}$, b and ξ vanish, we obtain

$$\frac{\partial \mathcal{L}_p}{\partial \mathbf{w}} = 0 \Longrightarrow \mathbf{w} = \sum_{i=1}^{D} y_i \alpha_i \beta(\mathbf{x}_i) \tag{3.6.14}$$

$$\frac{\partial \mathcal{L}_p}{\partial b} = 0 \Longrightarrow \sum_{i=1}^{D} y_i \alpha_i = 0 \tag{3.6.15}$$

$$\frac{\partial \mathcal{L}_p}{\partial \xi} = 0 \Longrightarrow \alpha_i + \psi_i = \Gamma \tag{3.6.16}$$

Since $\psi_i \geq 0$, it implies that $0 \leq \alpha_i \leq \Gamma$ where the value of Γ sets an upper limit on the Langrangian optimization variable α_i. It should be noted that the value of Γ offers a trade-off between accuracy of data fit and regularization and as such, it must be chosen carefully. For most practical realization, it is easier to solve the dual form of the problem defined in (3.6.13) which can be obtained by plugging (3.6.14), (3.6.15) and (3.6.16) into (3.6.13) as

$$\begin{aligned}
\mathcal{L}(\mathbf{w}, b, \xi, \alpha, \psi) &= \frac{1}{2}\langle \mathbf{w}.\mathbf{w} \rangle + \Gamma \sum_{i=1}^{D} \xi_i - \sum_{i=1}^{D} \psi_i \xi_i - \sum_{i=1}^{D} \alpha_i [y_i(\langle \mathbf{w}.\beta(\mathbf{x}_i) \rangle + b) - 1 + \xi_i] \\
&= \Bigg\{ \frac{1}{2} \sum_{i=1}^{D} \sum_{j=1}^{D} y_i y_j \alpha_i \alpha_j \langle \beta(\mathbf{x}_i).\beta(\mathbf{x}_j) \rangle + (\alpha_i + \psi_i) \sum_{i=1}^{D} \xi_i - \sum_{i=1}^{D} \psi_i \xi_i \\
&\quad - \sum_{i=1}^{D} \sum_{j=1}^{D} y_i y_j \alpha_i \alpha_j \langle \beta(\mathbf{x}_i).\beta(\mathbf{x}_j) \rangle - b \sum_{i=1}^{D} y_i \alpha_i + \sum_{i=1}^{D} \alpha_i - \sum_{i=1}^{D} \alpha_i \xi_i \Bigg\} \\
&= \sum_{i=1}^{D} \alpha_i - \frac{1}{2} \sum_{i=1}^{D} \sum_{j=1}^{D} y_i y_j \alpha_i \alpha_j \langle \beta(\mathbf{x}_i).\beta(\mathbf{x}_j) \rangle. \qquad (3.6.17)
\end{aligned}$$

Thus, equivalently, the solution to the original minimization problem expressed in the primal form in (3.6.13) is found by maximizing the dual form (3.6.17) over α as [59]

$$\begin{aligned}
\underset{\alpha}{\text{maximize}} \quad & \sum_{i=1}^{D} \alpha_i - \frac{1}{2} \sum_{i=1}^{D} \sum_{j=1}^{D} y_i y_j \alpha_i \alpha_j \langle \beta(\mathbf{x}_i).\beta(\mathbf{x}_j) \rangle \\
\text{subject to} \quad & \sum_{i=1}^{D} y_i \alpha_i = 0 \ , \quad 0 \leq \alpha_i \leq \Gamma, \ \forall i
\end{aligned} \qquad (3.6.18)$$

Finally, using the quadratic programming algorithm [53], the convex optimization problem in (3.6.18) can be solved for optimal value of α, denoted as α^* which in turn can be used to obtain optimal weight vector, $\mathbf{w}^*$ from (3.6.14) as

$$\mathbf{w}^* = \sum_{i=1}^{D} y_i \alpha_i^* \beta(\mathbf{x}_i). \qquad (3.6.19)$$

What remains now is to calculate the bias, b. It is known that any training example satisfying (3.5.15) is a support vector, denoted as $\mathbf{x}_s$ and also

satisfies the KKT complementarity condition given by

$$y_s(\mathbf{w}^*.\beta(\mathbf{x}_s) + b) = 1. \tag{3.6.20}$$

If we substitute (3.6.19) into (3.6.20) and let α^* be the set of Langrangian multiplier, α corresponding to the set of support vectors for which $\alpha > 1$, we obtain

$$y_s(\sum_{j\in S} y_j\alpha_j\langle\beta(\mathbf{x}_j).\beta(\mathbf{x}_s)\rangle + b) = 1 \tag{3.6.21}$$

where S denotes the set of indices of the support vectors. Multiplying (3.6.21) through by y_s, we will have

$$y_s^2(\sum_{j\in S} y_j\alpha_j\langle\beta(\mathbf{x}_j).\beta(\mathbf{x}_s)\rangle + b) = y_s \tag{3.6.22}$$

and since $y_s \in \{-1, 1\}$, it follows that, $y_s^2 = 1$ so that the bias, b is computed as

$$b = y_s - \sum_{j\in S} y_j\alpha_j\langle\beta(\mathbf{x}_j).\beta(\mathbf{x}_s)\rangle. \tag{3.6.23}$$

It is noteworthy that instead of using an arbitrary support vector, $\mathbf{x}_s$, a better approach is to take an average over all support vectors in S and by so doing we derive our optimal b, i.e. b^* as

$$b^* = \frac{1}{N_{\tilde{s}}}\sum_{s\in S}\left(y_s - \sum_{j\in S} y_j\alpha_j\langle\beta(\mathbf{x}_j).\beta(\mathbf{x}_s)\rangle\right) \tag{3.6.24}$$

where $N_{\tilde{s}}$ is the number of support vectors. The relevant kernel based SVM classifier can then be derived and used to predict the status of the PU via the class of the new observed data vector, $\mathbf{x}^{new}$, as

$$y(\mathbf{x}^{new}) = sgn\left(\sum_{j=1}^{N_s} y_j\alpha_j K(\mathbf{x}_j, \mathbf{x}^{new}) + b^*\right). \tag{3.6.25}$$

where the inner product in the feature space, $\langle\beta(\mathbf{x}_j).\beta(\mathbf{x}_k)\rangle$, is replaced by

an appropriate kernel function, $K(\mathbf{x}_j, \mathbf{x}_k)$ which is used for mapping the data to high dimensional space. Potential candidates for kernel are linear, polynomial and the Gaussian radial basis functions. Suffice to say at this point that the exact form of the mapping function need not be known or explicitly calculated because the inner product itself is sufficient to provide the required mapping and thus significantly reduces the computational burden [46]. The SVM based spectrum sensing algorithm for single PU scenario is presented in Algorithm 3.6.

Algorithm 3.6: SVM classifier based sensing algorithm for single PU

---

i. Given the training set, $\mathcal{S} = \{\mathbf{x}_i, y_i\}_{i=1}^{D} \in \{H_0, H_1\}$, where $\mathbf{x}_i \in R^N$, select appropriate mapping function, $\beta(\mathbf{x})$ and associated kernel parameters.

ii. Generate matrix $\mathbf{H}$, where $\mathbf{H}_{ij} = y_i y_j \langle \beta(\mathbf{x}_i), \beta(\mathbf{x}_j) \rangle$.

iii. Select suitable value for the box constraint parameter, Γ.

iv. Solve the optimization problem in (3.6.18) for the optimal values, α^* such that $\sum_{i=1}^{D} \alpha_i - 0.5\boldsymbol{\alpha}^T \mathbf{H} \boldsymbol{\alpha}$ is maximized, subject to $0 \leq \alpha_i \leq \Gamma$, and $\sum_{i=1}^{D} \alpha_i y_i = 0$, $\forall i$.

v. Evaluate $\mathbf{w}^*$ using (3.6.19).

vi. Determine the set of support vectors, S for which $\alpha^* > 0$.

vii. Calculate b^* using (3.6.24).

viii. Classify each new data vector, $\mathbf{x}^{new}$ using (3.6.25) to infer PU's status, H_0 or H_1 .

3.6.3 Multi-class SVM Algorithms for Spatio-Temporal Spectrum Sensing Under Multiple PUs Scenarios

One significant limitation of the conventional SVM (CSVM) algorithm described in subsection (3.6.2) is that it is designed to solve binary classification

(two class) problems and as a result, it is directly applicable for performing *temporal* spectrum sensing such as in scenarios with only one operating PU. In this sub-section, the focus is on spectrum sensing under multiple PUs scenarios.

3.6.4 System Model and Assumptions

A PU-SU network where the SUs are operating in the coverage areas of P PU transmitters is considered. The PUs are assumed to be geographically separated but operating within the same frequency band such as in a cellular network where the possibility of frequency re-use in nearby cells is offered as depicted in Figure 3.3. Here, the SUs are assumed to be cooperating in order to jointly detect the availability of spectrum holes both in *time* and *space* in conjunction with the secondary base station (SBS). It is further assumed that the PUs activities are such that when all PUs are inactive, spectrum holes are available both temporally and spatially at the PUs' locations. However, when there are $p < P$ active PUs, spatial spectrum holes will be available in time at some $p' = P - p$ PUs' geographical locations (the coverage areas of the p' inactive PUs) which if detected can be utilized by the SUs during the p' PUs' idle period. It is thought that such spatially available bands could be used for base-to-mobile communications as well as mobile-to-mobile communications that is being proposed as an integral part of the next-generation cellular networks [60].

In general, if we let $S(P, p)$ denote a particular class in which p out of P PUs are active during any sensing interval, the spectrum sensing task under this scenario can be formulated as a multiple hypothesis testing problem

$$H_0 : x_m(n) = \eta_m(n) \tag{3.6.26}$$

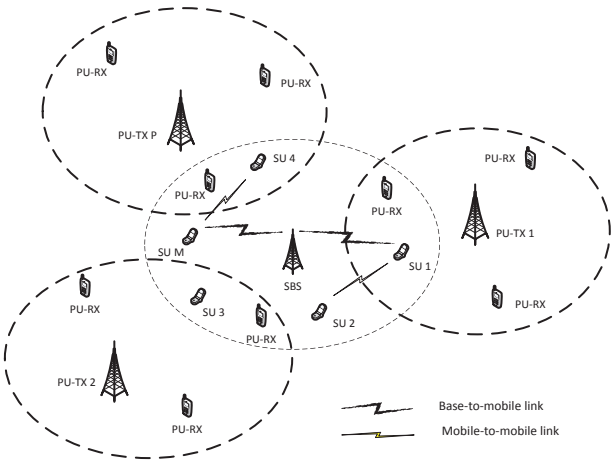

Figure 3.3. Cognitive radio network of primary and secondary users.

$$H_1^{S(P,p)} : x_m(n) = \sum_{\tilde{p}=1}^{p} \phi_{\tilde{p}}(su^m) s_{\tilde{p}}(n) + \eta_m(n),\ p = \{1, \cdots, P\} \qquad (3.6.27)$$

where H_0 implies that *all* PUs are absent and $H_1^{S(P,p)}$ means that *at least one* PU is present. Furthermore, $x_m(n)$ is the instantaneous signal received at the m-th antenna of the SU over bandwidth ω of interest within which the PUs operate, $\tilde{p}$ is the index of the active PU(s) for a specific state in the p-th class and $\phi_{\tilde{p}}(su^m)$ is the gain coefficient of the channel between the $\tilde{p}$-th PU and the m-th antenna of the SU. The remaining parameters in (3.6.27) are $s_{\tilde{p}}(n)$ which is the instantaneous PU signal assumed to be BPSK modulated with variance, $\mathbb{E}|s_{\tilde{p}}(n)|^2 = \sigma^2_{s_{\tilde{p}}}$, and $\eta_m(n)$ which is assumed to be circularly symmetric complex Gaussian noise with mean, zero and variance, $\mathbb{E}|\eta_m(n)|^2 = \sigma^2_\eta$. Under H_0, all PUs are inactive, so no primary signal is detected and it corresponds to the null hypothesis. On the other hand, $H_1^{S(P,p)}$ corresponds to *composite* alternative hypothesis where in this consideration it is assumed that at any given time there is/are $p \in \{1, ..., P\}$ active PUs during the sensing interval indicated by p in the superscript, $S(P, p)$. It is apparent that under multiple PUs scenarios, intuitively there are P classes of alternative hypothesis each of which may comprise of one or

more sub-classes that may be viewed as different system state. The goal is to develop a system that is able to learn the peculiar attributes that uniquely characterize each of the states under the composite alternative hypothesis in order to be able to distinguish them from one another using this knowledge. From the foregoing, it can be seen that $H_1^{S(P,p)}$ represents each of the P classes of alternative hypothesis resulting from the multiple PU spectrum sensing problem formulation and may thus be re-written as

$$H_1^{S(P,p)} = \begin{cases} H_1^{S(P,1)} \\ H_1^{S(P,2)} \\ \vdots \\ H_1^{S(P,P)} \end{cases} \tag{3.6.28}$$

where for an arbitrarily large P ($P \gg 1$), $H_1^{S(P,1)}$ describes the possible independent occurrences of the PUs where only one PU is active during the sensing duration. This can be written as

$$H_1^{S(P,1)} = H_1^p : \phi_p(su^m)s_p(n) + \eta_m(n), \quad \forall p \in \{1, \cdots, P\}. \tag{3.6.29}$$

If we let $\binom{P}{p} = \frac{P!}{(P-p)!\,p!}$ denote the total number of possible combinations in the p-th class, then it is easy to see that $H_1^{S(P,1)}$ class comprises of $\binom{P}{1}$ states as shown in (3.6.29). Similarly, the second class, $H_1^{S(P,2)}$ which corresponds to the case where any two PUs are active simultaneously can be described as comprising of $\binom{P}{2}$ states which can be expressed as

$$H_1^{S(P,2)} = \begin{cases} H_1^{1,p} : \phi_1(su^m)s_1(n) + \phi_p(su^m)s_p(n) + \eta_m(n), \quad \forall p = 2, \cdots, P \\ H_1^{2,p} : \phi_2(su^m)s_2(n) + \phi_p(su^m)s_p(n) + \eta_m(n), \quad \forall p = 3, \cdots, P \\ \vdots \\ H_1^{P-1,P} : \sum_{P-1}^{P} \phi_p(su^m)s_p(n) + \eta_m(n) \end{cases} \tag{3.6.30}$$

Furthermore if we consider every possible states in the $H_1^{S(P,3)}$ class where there are three simultaneously active PUs, we will have $\binom{P}{3}$ states which can be described as

$$H_1^{S(P,3)} = \begin{cases} H_1^{1,2,p} : \sum_{i=1}^{2} \phi_i(su^m)s_i(n) + \phi_p(su^m)s_p(n) + \eta_m(n), \\ \qquad\qquad \forall p = 3, ..., P \\ H_1^{1,3,p} : \sum_{i=1,3} \phi_i(su^m)s_i(n) + \phi_p(su^m)s_p(n) + \eta_m(n), \\ \qquad\qquad \forall p = 4, ..., P \\ H_1^{1,4,p} : \sum_{i=1,4} \phi_i(su^m)s_i(n) + \phi_p(su^m)s_p(n) + \eta_m(n), \\ \qquad\qquad \forall p = 5, ..., P \\ \qquad\qquad \vdots \\ H_1^{1,P-1,P} : \sum_{p=1,P-1}^{P} \phi_p(su^m)s_p(n) + \eta_m(n) \\ H_1^{2,3,p} : \sum_{i=2}^{3} \phi_i(su^m)s_i(n) + \phi_p(su^m)s_p(n) + \eta_m(n), \\ \qquad\qquad \forall p = 4, ..., P \\ H_1^{2,4,p} : \sum_{i=2,4} \phi_i(su^m)s_i(n) + \phi_p(su^m)s_p(n) + \eta_m(n), \\ \qquad\qquad \forall p = 5, ..., P \\ \qquad\qquad \vdots \\ H_1^{2,P-1,P} : \phi_2(su^m)s_2(n) + \sum_{p=P-1}^{P} \phi_p(su^m)s_p(n) + \eta_m(n) \\ H_1^{3,4,p} : \sum_{i=3}^{4} \phi_i(su^m)s_i(n) + \phi_p(su^m)s_p(n) + \eta_m(n), \\ \qquad\qquad \forall p = 5, ..., P \\ H_1^{3,5,p} : \sum_{i=3,5} \phi_i(su^m)s_i(n) + \phi_p(su^m)s_p(n) + \eta_m(n), \\ \qquad\qquad \forall p = 6, ..., P \\ \qquad\qquad \vdots \\ H_1^{3,P-1,P} : \phi_3(su^m)s_3(n) + \sum_{p=P-1}^{P} \phi_p(su^m)s_p(n) + \eta_m(n) \\ \qquad\qquad \vdots \\ H_1^{P-2,P-1,P} : \sum_{p=P-2}^{P} \phi_p(su^m)s_p(n) + \eta_m(n). \end{cases} \tag{3.6.31}$$

By following similar line of reasoning, the expressions for all classes of alternative hypothesis that describe every possible PU states in the network can be generated. The $\binom{P}{P}$ combination where all PUs are simultaneously active

during the sensing interval is only one state and it corresponds to the P-th class of alternative hypothesis which can be expressed as

$$H_1^{S(P,P)} = H_1^{1,\cdots,P-1,P} : \sum_{p=1}^{P} \phi_p(su^m) s_p(n) + \eta_m(n). \tag{3.6.32}$$

For any given network comprising P PUs, from (3.6.28) to (3.6.32) it is apparent that there are $1 + \sum_{p=1}^{P} \binom{P}{p}$ distinguishable hypotheses whose attribute has to be learnt by the SUs in order to be able to efficiently detect available spectrum opportunities and fully optimize the usage of the spectrum resources. It should be noted though, that each one of the $j \in \sum_{p=1}^{P} \binom{P}{p}$ alternative hypotheses states not only indicates the presence of the PU activity in the network but also provides additional information about the specific location(s) of the active PUs. It is opined that if the SUs are properly trained, they will be able to determine the geographical location(s) where spatial spectrum hole is/are available at any given point in time which can be utilized by employing appropriate interference mitigating transmit technique such as beamforming.

Furthermore, in the multiple hypotheses sensing problem, the SUs' detection performance metrics, probability of detection (Pd) defined as $p(H_1|H_1)$, also describes the ability of the detector to classify the frequency band being monitored as busy (occupied) when one or more PU is active. Similarly, the probability of false alarm (Pfa) defined as $p(H_1|H_0)$, describes classifying the band of interest as being used when in reality all PU(s) are inactive. In addition, since the interest is to determine the actual status of every PU during any sensing duration, it is important that a more pertinent metric referred to as classification accuracy (CA) be introduced which can be defined as, $CA \triangleq p(H^y|H^y)$ where H^y represents the true network's state including the idle state. In the context of the multi-class problems, it is possible for one or more states in a given class to be classified more accurately than oth-

ers within the same class, or in another class. Therefore, if i and q denote the class and state index respectively, the overall classification accuracy over all hypotheses is defined as

$$CA_{ovr} = \frac{1}{(Y_P + 1)} \left\{ \sum_{i=1}^{P} \sum_{q=1}^{Q_i} p(H_i|H_i)\ p(H_q|H_q) + p(H_0|H_0) \right\} \tag{3.6.33}$$

where P is the total number of classes, Q_i is the number of states in the i^{th} class, $Y_P = \mathbf{card}(\bigcup_{i=1}^{P} Q_i)$ is the total number of states present in all classes being considered under H_1, and $\mathbf{card}(G)$ implies cardinality. For the sake of emphasis, it should be noted here that if $Q_i = \mathbf{card}(Q_i),\ \forall\ i, j \in P, \exists j : Q_i \neq Q_j$. It is also worth reiterating that CA_{ovr} is a performance metric that describes the capability of the spectrum sensing scheme to correctly indicate the number of active PUs and their respective geographical locations during the sensing interval. A good spectrum sensing scheme should be designed to maximize CA_{ovr} so as to avoid causing intolerable interference to the PUs' transmissions and to minimize P_{fa} in order to optimize use of radio resources.

3.6.5 Multi-class SVM Algorithms

In reality, due to mutual interference the number of active transmitters that can simultaneously transmit in the same spectral band within a given geographical area is limited [61]. It follows therefore that for large P, the actual number of PUs to be considered is far smaller than P. To describe the application of the proposed MSVM algorithm based technique, let us consider a simple multiple user scenario where there are two PUs in the network (i.e. P = 2) so that in addition to the null hypothesis, there are $2^P - 1$ alternative hypotheses for consideration in our spectrum sensing problem. In this case, the vector of possible states that describe the activities of the PUs is represented as $[x, y] \in \{[0, 0], [0, 1], [1, 0], [1, 1]\}$ where $x, y = 0$

and $x, y = 1$ implies PU is absent and present respectively. The multiple hypothesis testing problem (3.6.26) and (3.6.27) in this scenario, translates to a four-hypothesis testing problem comprising of one null hypothesis and three alternative hypotheses defined as

$$x_m(n) = \begin{cases} \eta_m(n) & H_0 : both \;\; PUs \;\; absent \\ \phi_1(su^m)s_1(n) + \eta_m(n) & H_1^1 : only \;\; PU_1 \;\; present \\ \phi_2(su^m)s_2(n) + \eta_m(n) & H_1^2 : only \;\; PU_2 \;\; present \\ \sum_{k=1}^{K} \phi_k(su^m)s_k(n) + \eta_m(n) & H_1^{1,2} : both \;\; PUs \;\; present \end{cases} \quad \forall m \in M. \tag{3.6.34}$$

Under this operating condition, it is assumed that only one of the four states defined in (3.6.34) can exist during any sensing duration while the PUs are also assumed to be geographically located such that a spatial spectrum hole can be declared within the operating environment of any inactive PU and in the coverage areas of both PUs in the event that both PUs are inactive. To address this multi-class signal detection problem, the approach is to learn the attributes of the received PU(s) signals using the MSVM algorithms.

In general, the implementation of the MSVM classification technique can be approached in two ways. One way is the direct approach where multi-class problem is formulated as a single, large, all-in-one optimization problem that considers all support vectors at once [62]. However, the number of parameters to be estimated through this method tends to increase as the number of classes to be discriminated increases. Besides, the method is less stable which affects the classifier's performance in terms of classification accuracy [2]. The alternative approach which was adopted in this study is to treat the multi-class problem as multiple binary classification tasks and requires the construction of multiple binary SVM models from the training data by using one-versus-all (OVA) or one-versus-one (OVO) methods [62], [63], [64]. In this application, the data set that were collected under each of

the four hypotheses represents each system state respectively and can also be viewed as the unique classes that we seek to be able to distinguish.

In the one-versus-all (OVA) otherwise known as the one-versus-rest approach, $J = 2^P$ binary SVM models are constructed for J classes where the j^{th} SVM, $\forall j \in J$ is trained on two classes of labeled data set. This pair of classes are realized by assigning positive labels to all the data points in the j^{th} class while negative labels are assigned to all remaining training data points. So, given D training data points in the data set, $\mathcal{S} = \{(\mathbf{x}_1, y_1), (\mathbf{x}_2, y_2), \cdots, (\mathbf{x}_D, y_D)\}$, where $\mathbf{x}_i \in R^n$, $i = 1, \cdots, D$ and $y_i \in \{1, \cdots, J\}$ is the class to which $\mathbf{x}_i$ belongs, the j^{th} SVM solves the optimization problem defined in the primal form as

$$\begin{aligned} \underset{\mathbf{w}^j, b^j, \xi^j}{\text{minimize}} \quad & \langle \mathbf{w}^j . \mathbf{w}^j \rangle + \Gamma^+ \sum_{i|y_i=j}^{D} \xi_i^j + \Gamma^- \sum_{i|y_i \neq j}^{D} \xi_i^j \\ \text{subject to} \quad & (\langle \mathbf{w}^j . \beta(\mathbf{x}_i) \rangle + b^j) \geq 1 - \xi_i^j, \quad if \ y_i = j \\ & (\langle \mathbf{w}^j . \beta(\mathbf{x}_i) \rangle + b^j) \leq -1 + \xi_i^j, \quad if \ y_i \neq j \\ & \xi_i^j \geq 0, \quad i = 1, \cdots, D. \end{aligned} \tag{3.6.36}$$

where as in (3.6.12) the labeled training examples are mapped into high dimensional feature plane via appropriately selected non-linear kernel function $\beta(\mathbf{x})$, Γ^+ and Γ^- remain as penalty parameters and $\sum_i \xi_i^j$ is an upper bound on the number of training errors. It should be noted that in the problem formulation of the original binary SVM, the soft margin objective function in (3.6.23) assigns equal cost, Γ to both positive and negative misclassifications in the penalty component. Here, this has been modified in order to accommodate the imbalance in the number of training examples in the two classes arising under the OVA scheme, as a cost sensitive learning approach which addresses the sensitiveness of the SVM algorithm to class imbalance

training data [52]. In addition, by assigning different cost in a way that takes the imbalance into consideration, the overall misclassification errors is reduced owing to the fact that the tendency for the decision hyperplane to skew towards the class that has smaller number of training examples is considerably mitigated. Appropriate values for the penalty parameters can be obtained by setting the ratio $\frac{\Gamma^+}{\Gamma^-}$ to the ratio $\frac{\mathbf{card}(C_{maj})}{\mathbf{card}(C_{min})}$ where C_{maj} and C_{min} refers to the majority and minority class respectively.

As in the case of the CSVM, during the training, a classifier model that maximizes the margin, $\frac{2}{\|\mathbf{w}^j\|}$ between any given pair of classes is desired by minimizing $\frac{1}{2}\langle \mathbf{w}^j.\mathbf{w}^j \rangle$ where the constant term $\frac{1}{2}$ is introduced for mathematical convenience. However, this is easier to achieve if the procedure outlined in (3.6.13) to (3.6.18) is followed and (3.6.36) is transformed to the dual form expressed as

$$\begin{aligned} &\underset{\alpha^j}{\text{maximize}} \quad \sum_{i=1}^{D} \alpha_i^j - \frac{1}{2}\sum_{i=1}^{D}\sum_{l=1}^{D} y_i^j y_l^j \alpha_i^j \alpha_l^j \langle \beta(\mathbf{x}_i).\beta(\mathbf{x}_l) \rangle \\ &\text{subject to} \quad \sum_{i=1}^{D} y_i^j \alpha_i^j = 0 \ , \quad 0 \leq \alpha_i^{+,j} \leq \Gamma^+, \ 0 \leq \alpha_i^{-,j} \leq \Gamma^-, \ \forall i \end{aligned} \tag{3.6.37}$$

where $\alpha_i^{+,j}$ and $\alpha_i^{-,j}$ are the Langrangian multipliers of the positive and negative training examples for the j^{th} model, respectively. By solving (3.6.37) $\forall j$, J decision functions described by

$$\sum_{i=1}^{N_s^j} y_i^j \alpha_i^j K(\mathbf{x}_i^j, \mathbf{x}^{new}) + b^j, \quad \forall j \in J \tag{3.6.38}$$

are obtained for classifying new data point, $\mathbf{x}^{new}$ and determining the actual state of the PU network.

Another coding strategy that can be used to address the multi-class spectrum sensing problem via the MSVM algorithm is the one-versus-one (OVO) scheme where each binary learner trains only on a pair of classes, $j_j, j_q \in J$ at a time. In this technique, all training examples in class j_j are

considered to be the positive class whereas those in the j_q class are treated as the negative class. All remaining examples, $J\backslash\bar{j}$ where $\bar{j} = \{j_j \cup j_q\}$ are simply ignored. Therefore, similar to (3.6.36), the formulation of the optimization problem in the primal form using the OVO method can be described by [62]

$$\begin{aligned} \underset{\mathbf{w}^{jq},b^{jq},\xi^{jq}}{\text{minimize}} \quad & \langle \mathbf{w}^{jq}.\mathbf{w}^{jq}\rangle + \Gamma \sum_{i=1}^{\bar{D}} \xi_i^{jq} \\ \text{subject to} \quad & (\langle \mathbf{w}^{jq}.\beta(\mathbf{x}_i)\rangle + b^{jq}) \geq 1 - \xi_i^{jq}, \quad if\ y_i = j \\ & (\langle \mathbf{w}^{jq}.\beta(\mathbf{x}_i)\rangle + b^{jq}) \leq -1 + \xi_i^{jq}, \quad if\ y_i = q \\ & \xi_i^{jq} \geq 0, \quad i = 1, ..., \bar{D}. \end{aligned} \tag{3.6.39}$$

where $\bar{D} = \mathbf{card}(\bar{j})$. The dual form of (3.6.39) expressed as

$$\begin{aligned} \underset{\alpha^{jq}}{\text{maximize}} \quad & \sum_{i=1}^{\bar{D}} \alpha_i^{jq} - \frac{1}{2} \sum_{i=1}^{\bar{D}} \sum_{j=1}^{\bar{D}} y_i^{jq} y_l^{jq} \alpha_i^{jq} \alpha_l^{jq} \langle \beta(\mathbf{x}_i).\beta(\mathbf{x}_l)\rangle \\ & \text{subject to} \ \sum_{i=1}^{\bar{D}} y_i \alpha_i^{jq} = 0\ , \quad 0 \leq \alpha_i^{jq} \leq \Gamma,\ \forall i \end{aligned} \tag{3.6.40}$$

is solved for every possible jq pair and $\binom{J}{2}$ SVM decision functions

$$\sum_{i=1}^{N_s^{jq}} y_i^{jq} \alpha_i^{jq} K(\mathbf{x}_i^{jq}, \mathbf{x}^{new}) + b^{jq}, \quad \forall jq\ pair \tag{3.6.41}$$

are obtained for classifying new data point, $\mathbf{x}^{new}$.

3.6.6 Predicting PUs' Status via ECOC Based Classifier's Decoding

The ECOC scheme is a framework that enables us to design how the pairs of classes that we train on using the OVO or OVA methods are selected. It

also allows us to take advantage of the dependencies among different labels and the predictions made by the individual SVM classifier model towards minimizing the overall classification error [64], [65]. From the perspective of the ECOC, spectrum sensing task may be viewed as a typical telecommunication problem where the source is the PU-SU channel being sensed, the transmitted information is the true state of the PU activities encoded in the actual class of the new observations that we wish to predict, the communication channel is comparable to both the training feature as well as the MSVM learning algorithms and with the aid of ECOC scheme the errors that may be introduced through the choice of the training features and the learning machines can be corrected at the SU receiver.

For the OVA model in (3.6.36), to implement the ECOC scheme a coding matrix, $\mathcal{M} \in \{+1, -1\}^{J \times L}$ is simply constructed where J is the number of classes in the entire training data set and L is the number of binary learners that are required to solve the multi-class problem. It should be noted that for the OVA method, $J = L$, and a straightforward approach for constructing the coding matrix $\mathcal{M}$ is to choose a square, symmetric matrix with $+1s$ on the leading diagonal *only* so that $Tr(\mathcal{M}) = J$. The coding matrix for implementing the OVA scheme where $J = L = 4$ is designed as shown in Table 3.1.

Table 3.1. One-versus-all coding matrix

	l_1	l_2	l_3	l_4
j_1	+1	-1	-1	-1
j_2	-1	+1	-1	-1
j_3	-1	-1	+1	-1
j_4	-1	-1	-1	+1 .

To apply the OVA matrix above to solve the four-class problem in (3.6.34), during the learning phase for deriving the decision model, the first binary learner l_1 in the first column is trained by assigning the positive label to all the training examples in the j_1 class (row 1) while all the training examples in the remaining j_2 through j_4 classes (rows 2 to 4) are assigned the negative label as shown. For the second learner, l_2 in column 2, positive label is assigned to all the training examples in the j_2 row and negative label is assigned to all the training examples in the remaining rows. So in general, for the n-th learner, we assign positive label to all the examples in the n-th row and negative label to training examples in the rest rows to obtain all required $J = 4$ decision models.

Similarly, in the implementation of the OVO scheme sometimes referred to as the *all pairs* method, the coding matrix, $\mathcal{M} \in \{+1, -1, 0\}^{J \times L}$ is chosen in such a way that the l-th learner trains on two classes only. Assuming that this learner is used to train on the j-th and q-th classes, the rows of $\mathcal{M}$ that corresponds to the j-th and q-th classes of interest are labeled +1 and -1 respectively while all remaining rows are ignored by assigning 0s to them. This procedure is repeated until all required $\binom{J}{2}$ decision functions are realized. Table 3.2 shows the OVO scheme coding matrix $\mathcal{M}$ for solving the four-class problem in (3.6.34)

Table 3.2. One-versus-one coding matrix

	l_1	l_2	l_3	l_4	l_5	l_6
j_1	+1	+1	+1	0	0	0
j_2	-1	0	0	+1	+1	0
j_3	0	-1	0	-1	0	+1
j_4	0	0	-1	0	-1	-1 .

It is pertinent to mention at this juncture that while the OVO and OVA coding strategies appear to have gained popularity, the multiple SVM models approach to multi-class problem can also be implemented by using a coding matrix that is chosen in a way that the positive and negative labels are randomly assigned to the classes during the training phase [63]. One advantage of this approach is the flexibility of employing variable number of binary learners, doing so with very minimal performance loss.

It could be observed that in the two popular ECOC strategies described above, each class of the training data in the multiple hypothesis problem is associated with a row of $\mathcal{M}$ thereby resulting in a unique codeword for each class. One way of decoding the class for a new (test) data point is by comparing the codeword that is formed by merging the predictions of all the learners with the ECOC unique codeword for each class and the test data is classified as belonging to the class with the smallest Hamming distance. This is very similar to the class prediction in CSVM, where to classify new data point, $\mathbf{x}^{new}$, the sign of (3.6.25) is used. However, this approach entirely ignores the confidence level that the actual score produced by each binary classifier attaches to its prediction. To overcome this disadvantage, the loss-weighted decoding strategy can be employed which takes into account every predictor's score for the test point as calculated from the decision function in (3.6.25).

In the loss-weighted decoding, if the set of predicted scores for a new observation $\mathbf{x}^{new}$, jointly returned by the MSVM learners' decision models is denoted by

$$\Theta(\mathbf{x}^{new}) = \{\theta_{l_1}(\mathbf{x}^{new}), \cdots, \theta_{l_L}(\mathbf{x}^{new})\} \tag{3.6.42}$$

for L learners, where θ_{l_l} is the actual predicted score produced by the margin-based decision model of the l-th learner, then a test data point is classified as belonging to the class $\hat{j} \in \{1, ...J\}$ that offers the minimum sum of binary

losses over all learners. This is obtained by using the expression [65]

$$\hat{j} = \underset{j}{\operatorname{argmin}} \frac{\sum_{l=1}^{L} |m_{jl}| g(m_{jl,\theta_{l_l}})}{\sum_{l=1}^{L} |m_{jl}|} \tag{3.6.43}$$

where $\hat{j}$ is the predicted class for the test data point, m_{jl} refers to the element jl of $\mathcal{M}$, (i.e. the label for class j of learner l) and $g(.,.)$ is an appropriate binary loss function specifically chosen for the classifier. In general, for the SVM classifier, a good choice for the binary loss is the hinged function whose score domain lies in $(-\infty, \infty)$, and is defined by

$$g(y_l, \theta_l) = \frac{max(0, 1 - y_l \theta_{l_l})}{2} \tag{3.6.44}$$

where y_l is the class label for the l-th binary learner of the class being considered. In this study, (3.6.43) is used to obtain the class of the new test data point which corresponds to the true state of the PU activities that we wish to predict during the spectrum sensing interval.

3.7 Numerical Results and Discussion

In this section, the performance of the proposed schemes is evaluated for both the single and multiple PU scenarios. The CSVM algorithm was applied to the single PU case while for the multiple PU scenario the MSVM algorithm was implemented. The results are quantified in terms probability of detection, probability of false alarm, receiver operating characteristics curves (ROC), area under ROC (AuC) and overall classification accuracy.

3.7.1 Single PU Scenario

Under this scenario, the aim is simply to detect the presence or absence of the PU. So for the purpose of simulation, under H_1, it is assumed that the PU signal is $BPSK$ modulated, with transmit power equals one Watt. It is

further assumed that the PU-SU channel is complex additive white Gaussian noise with $\phi(su^m)$ modeled as a Rayleigh distributed random variable and the noise power is denoted by η_m^2. The noise and the PU's signal are assumed to be uncorrelated. By cross-validation, the CSVM kernel width parameter, σ is 64 and the box constraint, Γ is 0.8. A total of 2000 set of eigenvalues was generated through 2000 random realizations of the channels, out of which 400 were used for training and the rest for testing purpose. To demonstrate the robustness of the eigenvalue derived features, comparisons are made with energy † based features. The performance of the scheme is evaluated under different values of the number of received signal samples, SU antenna number and operating SNR.

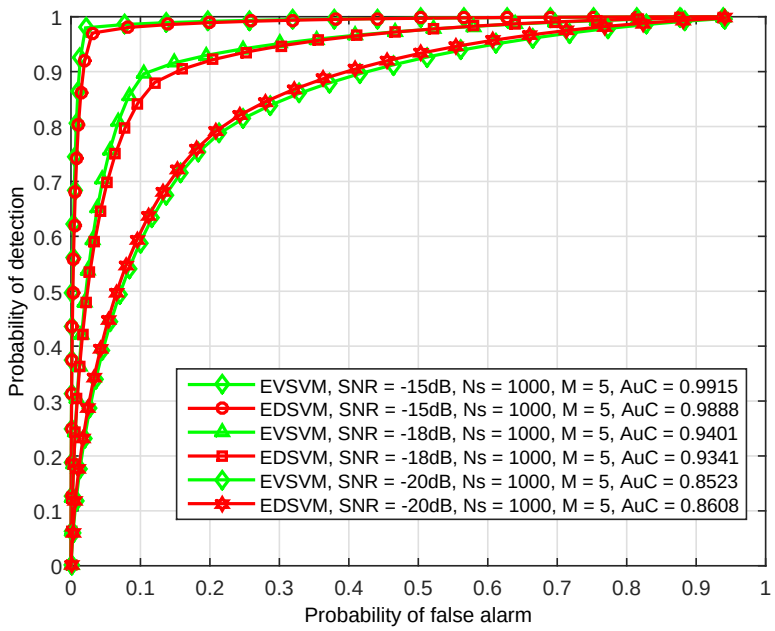

Figure 3.4. ROC performance comparison showing EV based SVM and ED based SVM schemes under different SNR range, number of antenna, $M = 5$, and number of samples, $N_s = 1000$.

Figure 3.4 shows the performance of the proposed eigenvalue feature based SVM binary classifier (EVSVM) in terms of the ROC curves for fixed

†The procedure for the realization of the energy based features and associated statistical properties is described in Chapter four of this thesis.

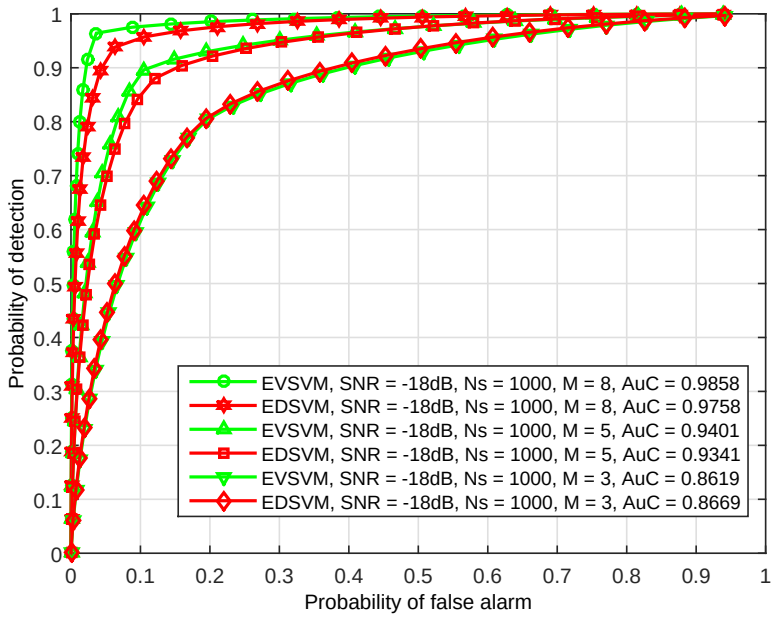

Figure 3.5. ROC performance comparison showing EV based SVM and ED based SVM schemes with different number of antenna, M, SNR = -18 dB, and number of samples, $N_s = 1000$.

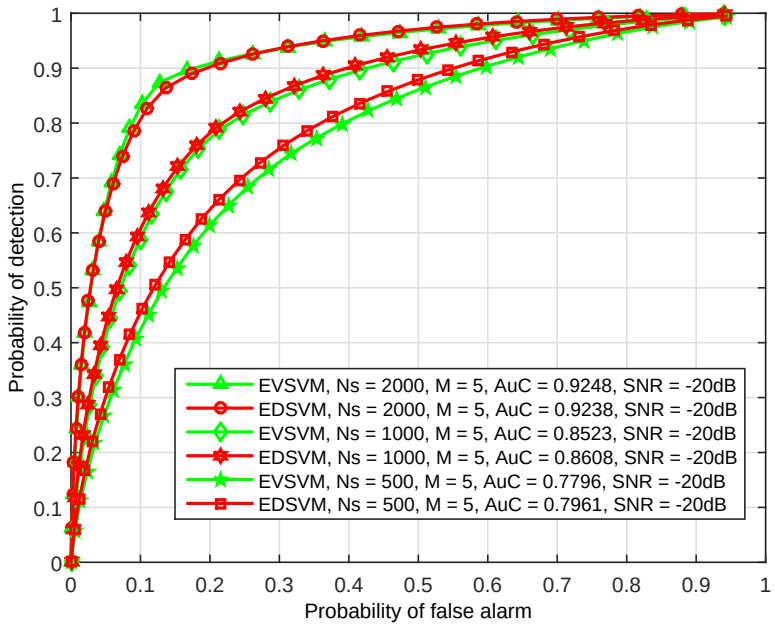

Figure 3.6. ROC performance comparison showing EV based SVM and ED based SVM schemes with different number of samples, N_s, number of antenna, $M = 5$, and SNR = -20 dB .

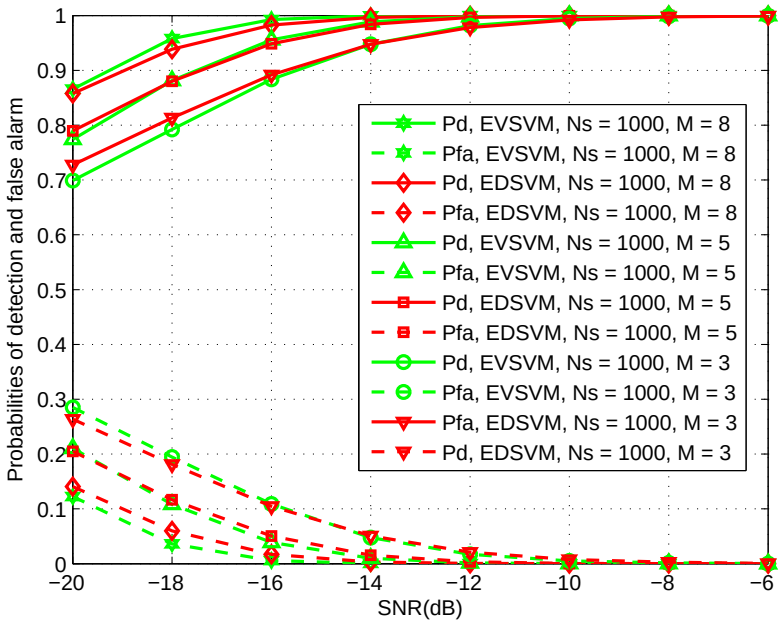

Figure 3.7. Performance comparison between EV based SVM and ED based SVM schemes showing probability of detection and probability of false alarm versus SNR, with samples number, $N_s = 1000$, number of antenna, $M = 3$, 5 and 8.

number of received signal samples, $N_s = 1000$ and number of SU antennas, $M = 5$ when the SNR = -15 dB, -18 dB and -20 dB. As seen, EV based SVM outperforms the ED based SVM. For example, at the $Pfa = 0.1$, the Pd of 0.9 is achieved by the EVSVM scheme whereas the EDSVM achieves 0.85 at SNR of -18 dB. Additionally, for the EVSVM scheme, as the SNR is increased from -20 dB to -18 dB, the Pd is raised correspondingly from 0.6 to 0.9 providing a 30% gain in performance. The various cases of SNR conditions considered indicates that the new EVSVM scheme outperforms the EDSVM method which demonstrates the strength of the feature derived from eigenvalues to enhance the capability of the SVM binary classifier. In particular, within the SNR range of interest, it can noted that the EVSVM scheme offers significant improvement in the detection of spectrum holes. This is in addition to the fact that it provides the SU useful information about the number of active PUs through the presence of non-

repeating eigenvalues in the derived features. Furthermore, the performance improvement of the EVSVM scheme is discernible at SNR of -15 dB by computing the AuC where it is seen that the EVSVM scheme yields an AuC of 0.9915 against 0.9888 yielded by the EDSVM.

In Figure 3.5, the effect of varying number of SU antenna, M is shown on the performance of the proposed scheme with fixed number of received signal samples, $N_s = 1000$ while SNR is kept at -18 dB. As seen, when M is increased from 3 to 5, 30% improvement in performance is observed when Pfa is 0.1, that is, Pd is increased from 0.6 to 0.9. On the other hand, the EDSVM methods yields only 25% improvement, where Pd is increased from 0.6 to 0.85. Figure 3.6 shows the impact of varying the number of attributes of the feature vector has on the performance for a fixed number of SU antennas, $M = 5$ and operating SNR = -20 dB. As we increase N_s from 500 to 2000, the EVSVM scheme is seen to yield a rise in Pd from 0..42 to 0.82. The EDSVM however, achieve an increase in Pd from 0.43 to 0.8 when the Pfa is kept at 0.1. This indicates that a more accurate detection result is obtained when a considerably high number of received signal samples are processed.

Figure 3.7 depicts the Pd and Pfa performance for the EVSVM and EDSVM schemes over an SNR range of -20 dB to -6 dB. For the investigation, the number of samples, N_s is 1000 and the antenna number, M considered are 3, 5 and 8. Here, for the proposed EVSVM method, it can be seen that when M is 8, Pd increased from 0.86 to 0.96 as the SNR is increased from -20 dB to -18 dB while the Pfa dropped correspondingly from 0.12 to 0.03 over the same SNR range. It can further be observed that at SNR of -18 dB, with the same antenna number, $M = 8$, the EVSVM scheme attains Pd of 0.96 while the Pfa is kept well below 0.1. In the case of the EDSVM method, we observe a trend similar to that exhibited by the EVSVM in terms of Pd and Pfa versus SNR. However, the EVSVM tech-

nique outperforms the EDSVM which is evident if we consider for instance the performance of both methods where they both meet the CR IEEE 802.22 requirement at SNR = -18 dB and SU antenna number, $M = 8$. Here, we observe a margin of about 2 % in Pd (0.93 to 0.95) and Pfa (0.05 to 0.03). Furthermore, with increase in M from 3 to 8 and when SNR = -20 dB the EVSVM offers a rise in Pd from 0.7 to 0.88 (about 18% gain) and a drop in Pfa from 0.29 to 0.11 which corresponds to a 18% fall whereas for the EDSVM the rise in Pd is from 0.72 to 0.88 (about 16% gain) and drop in Pfa is from 0.28 to 0.12 (about 16% drop). From the foregoing, it is evident that the SVM technique exhibits a robust performance even when prior knowledge of the feature's underlying distribution is lacking or not taken into consideration. In addition, the eigenvalue based scheme exhibits a very good performance in comparison with the EDSVM scheme and its strength is seen to especially lie in relatively high number of antennas and sample number. However, the performance improvement accrue credibly makes up for its relatively high implementation complexity. The increased performance of the EVSVM method indicates a significant potential for improving the usage of the radio spectrum resources.

3.7.2 Multiple PUs Scenario

To validate the multi-class algorithms described in this chapter, in our simulation we consider a PU-SU network comprising of two operating fixed PUs whose activity is to be monitored. The geographical location of the PUs are assumed to be known by the SBS and the PUs are assumed to be operating at SNR of 0 dB and -3 dB respectively. Under H_1, it is assumed that the PUs' signal is $BPSK$ modulated and the channel gain between the PUs and the individual SU, $\phi(su^m)$ is modeled as a Rayleigh distributed, zero mean complex random variable. The PU-SU channel is assumed to be quasi-static during the training and testing period and characterized by complex

additive white Gaussian noise with power, η_m^2. Furthermore, the PUs' signals and the noise are assumed to be uncorrelated. By cross-validation, the MSVM kernel scale parameter, σ is 10 and the box constraint, Γ is 1. For the implementation of the OVA scheme though, the corresponding values for box constraint parameters, Γ^+ and Γ^- are obtained from the ratio of the pair of classes being considered as discussed in sub-section (3.6.4). For easy comparison with other supervised schemes discussed in this chapter we used the energy based feature and generated 2000 set of feature vectors out of which 400 were used for training and the rest for testing purpose. The performance of the scheme is evaluated through 1000 random realizations of the PU-SU channels under different values of the number of received signal samples, cooperating SUs, and operating SNR.

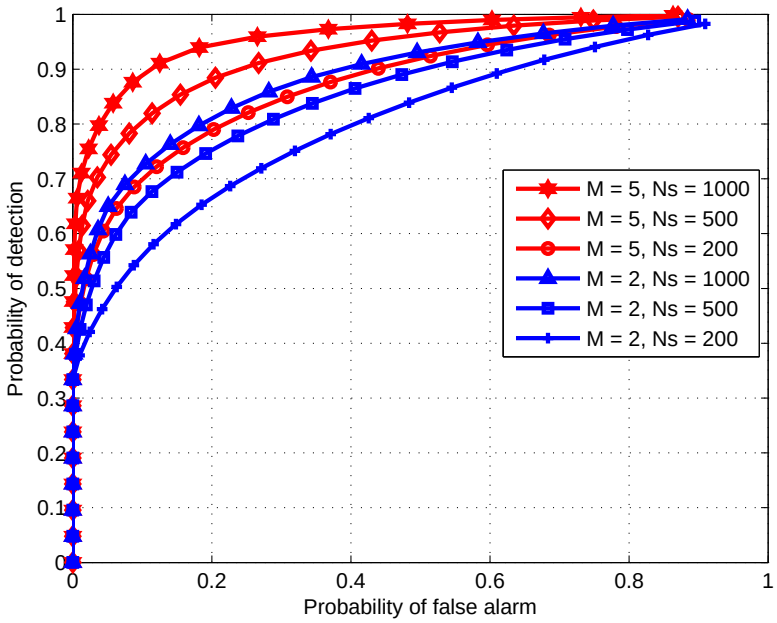

Figure 3.8. ROC curves for CSVM with number of PU = 2, number of antennas, M = 2 and 5, number of samples, N_s = 500,1000 at SNR = -15dB.

In Figure 3.8, the performance of linear kernel based CSVM classifier is shown when used for temporal spectrum sensing under multiple PUs scenarios using the *roc*. Due to the class imbalance we applied cost sensitive

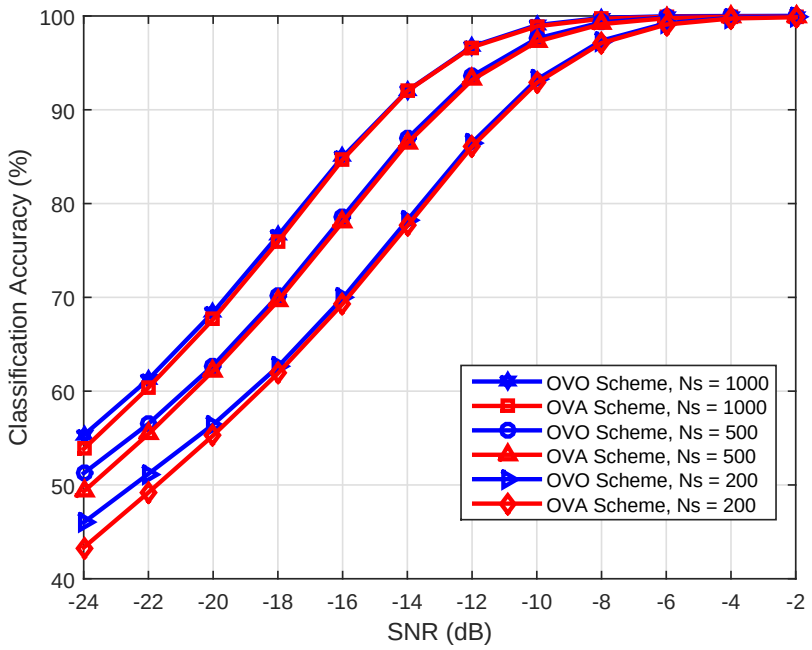

Figure 3.9. Comparison between OVO and OVA coding Schemes with number of PU = 2, number of sensors, M = 5, number of samples, N_s = 200, 500 and 1000.

learning technique and investigated the effect of the number of cooperating sensors, by increasing M from 2 to 5 while we vary the number of sensing samples, N_s, of the PUs' signal from 200 to 1000 at a fixed SNR of -15 dB. It can be seen that the system's performance improves when the number of sensors, M is increased. For example, given that N_s is 1000, at a considerably low false alarm probability of 0.1, the detection probability achieved by the scheme is about 0.73 when $M = 2$ while at $M = 5$, the Pd is attained is about 0.9 indicating a detection probability gain of approximately 17%. Similarly, given the same operational Pfa of 0.1, as N_s is increased from 200 to 1000, a rise in Pd from 0.56 to 0.73 is observed when $M = 2$ and from 0.7 to 0.9 when $M = 5$ yielding a detection probability gain of about 17% and 20% respectively. It is worth reiterating here, however, that the ROC only provides us information about the detector's performance when the target is to determine temporal available of spectrum hole. To evaluate the capabil-

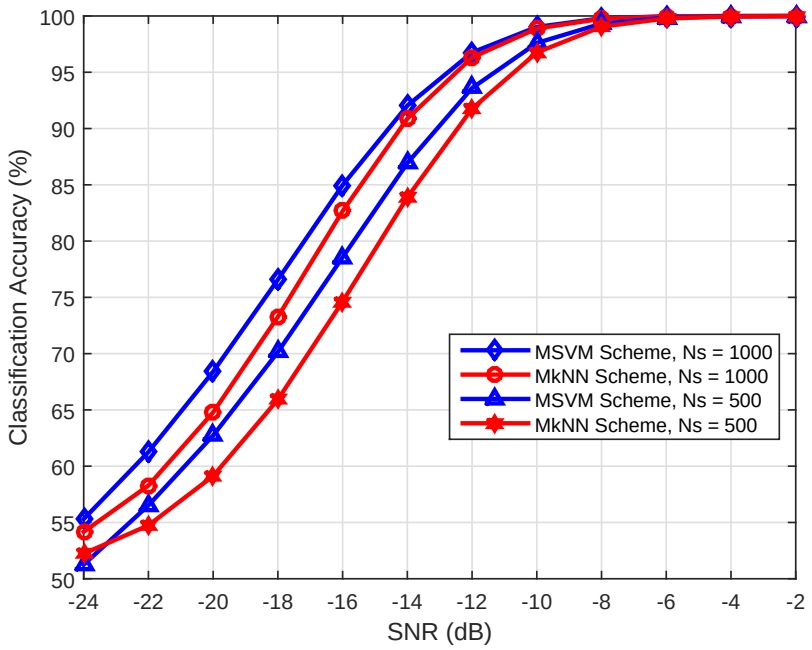

Figure 3.10. Comparison between OVO-MkNN and OVO-MSVM, with number of PU = 2, number of sensors, M = 5, number of samples, $N_s = 500$ and 1000.

ity of the proposed SVM detector considering spatial-temporal detection of unused bands, we resort to using CA as a more appropriate metric of choice.

In Figure 3.9, the comparison between the OVO and OVA coding schemes is shown under different N_s given $M = 5$ cooperating sensors. Here, an agreement between the performance of the two schemes in terms of CA is observed over the entire SNR range considered. This leaves us with the understanding that any of the two schemes may be used without any significant performance loss. However, the implementation complexity of the each of the schemes as highlighted in sub-section (3.6.4) is worth considering. Figure 3.10 shows the comparison between the performance of the proposed MSVM classifier and the multi-class kNN (MkNN) classifier with 5 neighbors, evaluated at $M = 5$ and $N_s = 500$ and 1000. It can be seen here that the MSVM scheme has an advantage over the MkNN scheme especially in the low SNR regime. For instance, at the SNR of -20 dB, the MkNN

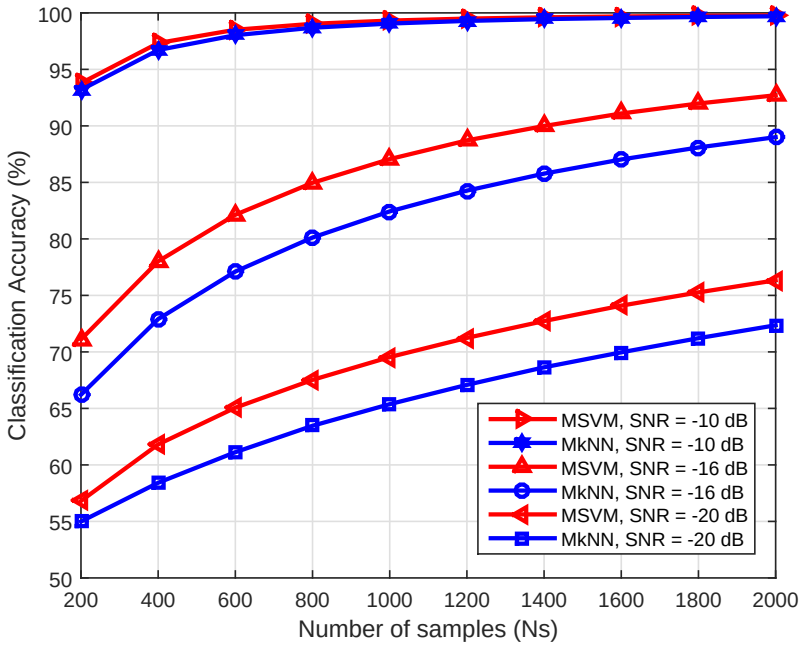

Figure 3.11. Comparison between OVO-MkNN and OVO-MSVM, with number of PU = 2, number of sensors, M = 5 at SNR = -10 dB, -16 dB and -20 dB.

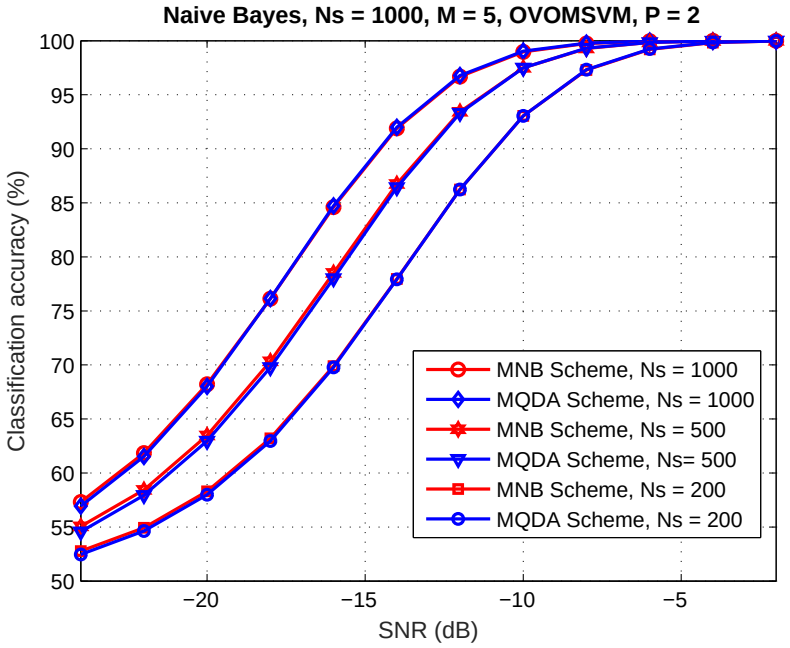

Figure 3.12. Comparison between OVO-MNB and OVO-MQDA, with number of PU = 2, number of sensors, M = 5, number of samples, N_s = 200, 500 and 1000.

scheme attains the CA of about 59% while the MSVM yields 64% at $N_s = 500$ and when $N_s = 1000$, MkNN scheme provides CA of 65% against 69% obtained from MSVM scheme. Both schemes are however observed to yield an increase in CA as the SNR is increased.

The effect of increasing N_s is seen in Figure 3.11 where the CA of the proposed MSVM method is evaluated over different choices of N_s at the SNR of -10 dB, -16 dB and -20 dB respectively. As expected, it can be seen that CA increases as N_s is increased from 200 to 2000. Figure 3.12, the performance comparison between two parametric classifiers considered at the outset this chapter is shown, namely, the naive Bayes and quadratic discriminant analysis classifiers under multi-class consideration using the OVO scheme. Here, M is fixed at 5 while N_s is varied between 200 and 1000. It can be seen that the performance of the two schemes are essentially identical over the entire SNR range considered. For instance, at $SNR =$ -24 dB, CA rises from about 52% to approximately 57% when N_s is increased from 200 to 1000. Similarly, as SNR is increased from -24 dB to -10 dB, CA is seen to to rise from 57% to about 93% at N_s equals 200 and from 57% to 99% when N_s is raised to 1000. Furthermore, by comparing Figure 3.9 and Figure 3.12, it can be observed that the performance of these two parametric techniques approaches that of the two non-parametric classifiers considered. However, the parametric methods require that we have the knowledge of the dataset's underlying statistical distribution. These results bring to the fore the viability of the proposed methods for spatial spectrum hole detection while also demonstrating the robustness of the SVM classifier in comparison with other supervised non-parametric classifier widely applied in data mining applications.

3.8 Summary

In this chapter, the performance of supervised classifier based methods for spectrum sensing in cognitive radio networks was investigated. Using both energy features as well as features derived from the eigenvalues of sample covariance matrix of the primary signals which are computed in finite time and the error correcting output code techniques, the key performance metrics of the classifiers are evaluated. Simulations shows that the proposed detectors are robust to temporal and joint spatio-temporal detection of spectrum holes in scenarios with single and multiple primary users. In particular, it is demonstrated that the SVM, which is a non-parametric technique can be successfully applied even in scenarios where the prior knowledge of the underlying statistical distribution of the data samples may not be available. In the next chapter, semi-supervised learning algorithms will be presented. These will be considered with a view to deploying them in mobile SUs to perform spectrum sensing. A novel channel tracking techniques for improving their classification performance under this condition will also be examined.

Chapter 4

ENHANCED SEMI SUPERVISED PARAMETRIC CLASSIFIERS FOR SPECTRUM SENSING UNDER FLAT FADING CHANNELS

4.1 Introduction

Semi-supervised learning techniques in general do not require labeling information. This is in contrast to the supervised learning methods discussed in Chapter 3 where completely labeled data set are required to derive decision functions that are needed for classifying unseen data points. However, in some cases, it may be necessary that these algorithms be provided supervisory signal for few training examples. In most of the semi-supervised learning algorithms, typically, the only supervisory information required is the knowledge of the number of clusters represented in the training data

and a valid assumption of the underlying probability distribution that models the training data. In some instances, the algorithms are able to make use of the partially labeled or unlabeled data to capture the shape of the underlying distribution and generalize to new samples [43]. In the spectrum sensing problem, a very important motivation for adopting semi supervised algorithms is the significant saving in memory requirements for storing additional supervisory signal information for all training examples.

In this chapter, two prominent semi-supervised learning algorithms are studied, namely; the K-means and Expectation-Maximization (EM) parametric classifiers and their capability for solving our spectrum sensing problem is evaluated. Furthermore, SUs that are depending on these classifiers for spectrum sensing under slow fading Rayleigh channel conditions are considered and a novel technique for enhancing their performance under this scenario is proposed. In particular, mobile SUs that are operating in the presence of scatterers are considered and the performance degradation of their sensing capability is examined. To improve the performance under this condition, the use of Kalman filter based channel estimation technique is investigated for tracking the temporally correlated slow fading channel and aiding the classifiers to update the decision boundary in real time. In the following two sections, the procedure for implementing the K-means and Expectation-Maximization (EM) semi supervised classification algorithms for addressing our spectrum hole detection problem is first described.

4.2 K-means Clustering Technique and Application in Spectrum Sensing

The K-means clustering technique otherwise referred to as the Lloyds algorithm is known as one of the workhorses of machine learning [66]. It is a prototype-based, partitional clustering method designed to find a user-

specified number of clusters, K represented by their centroids in a dataset [44]. A cluster is a set of objects in which all objects are very similar to the cluster's representative, usually the centroid or mean (average of all the points in the cluster). To describe how the K-means algorithm works and demonstrate the applicability in solving spectrum sensing problem, let us again consider a simple sensing network comprising a PU and M SUs as depicted in Figure 4.1. The SU system is such that the secondary base station (SBS) is located at the cell center and it is assumed that the SUs are cooperating to detect the presence or absence of the PUs. For spatial diversity, during the training interval, the SUs performs sensing at their respective locations and report their measurements to the SBS where clustering can easily be performed due to the enormity of the data involved. Following from (2.2.1), the spectrum sensing under this scenario can be expressed as a binary hypothesis testing problem of the form

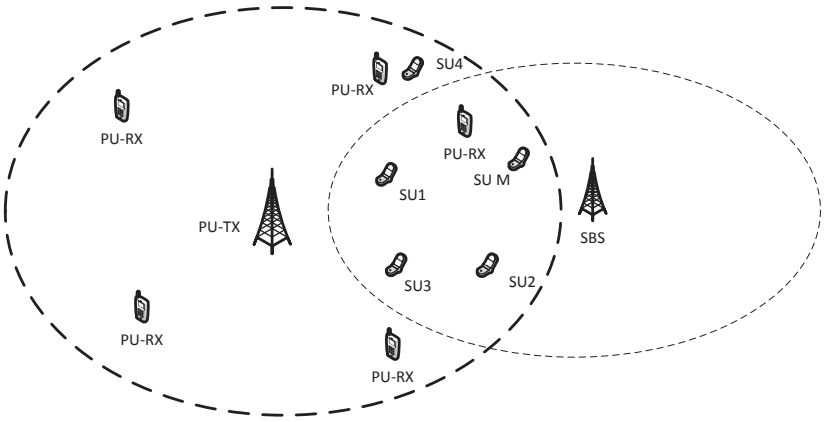

Figure 4.1. Cooperative spectrum sensing network of single PU and multiple SUs.

$$H_0 : x_m(n) = \eta_m(n) \tag{4.2.1}$$

$$H_1 : x_m(n) = \phi(su^m)s(n) + \eta_m(n) \tag{4.2.2}$$

where all parameters are as previously defined. In this study, it is assumed that the PU-SU channel modeled by $\phi(su^m)$ is quasi-static throughout the training and testing interval and the sensing energy measurements obtained by the SUs under each state of the PU's activity, H_0 and H_1 are considered to belong to the respective cluster. The SUs are further considered to be single antenna devices and the sensing results transmitted by each SU is treated as an attribute of the M dimensional feature vector.

4.2.1 Energy Features Realization

During the training interval, given that the PU operates at a carrier frequency f_c and bandwidth ω, if the received PU signal is sampled at the rate of f_s by each SU, the energy samples sent to the SBS for training purpose can be estimated as

$$\boldsymbol{x}_i = \frac{1}{N_s} \sum_{n=1}^{N_s} |x_m(n)|^2 \tag{4.2.3}$$

where $n = 1, 2, \cdots, N_s$ and $N_s = \tau f_s$ is the number of samples of the received PU signal used for computing the energy sample at the SU while τ is the duration of sensing time for each energy sample realization. When the PU is idle, the probability density function (PDF) of $\boldsymbol{x}_i$ follows Chi-square distribution with $2N_s$ degrees of freedom and when N_s is large enough (say, $N_s \simeq 250$) [30], this PDF can be approximated as Gaussian through the central limit theorem (CLT) with mean, $\mu_0 = \sigma_\eta^2$ and variance, σ_0^2 expressed

as [67]

$$\begin{aligned}\sigma_0^2 &= \mathbb{E}[(\boldsymbol{x}_i - \mu_0)^2] \\ &= \mathbb{E}[(\frac{1}{N_s}\sum_{n=1}^{N_s}|x_m(n)|^2 - \sigma_\eta^2)^2] \\ &= \frac{1}{N_s}\mathbb{E}[(|\eta_m(n)|^2 - \sigma_\eta^2)^2] \\ &= \frac{1}{N_s}\mathbb{E}[(|\eta_m(n)|^4 - 2\sigma_\eta^2|\eta_m(n)|^2 + \sigma_\eta^4] \\ &= \frac{1}{N_s}\mathbb{E}[(|\eta_m(n)|^4 - 2\sigma_\eta^4 + \sigma_\eta^4] \\ &= \frac{1}{N_s}\mathbb{E}[(|\eta_m(n)|^4 - \sigma_\eta^4]. \end{aligned} \tag{4.2.4}$$

However, for an additive white Gaussian noise, $\mathbb{E}|\eta(n)|^4 = 2\sigma_n^4$ so that we have

$$\sigma_0^2 = \frac{1}{N_s}\sigma_{\eta,m}^4, \forall m \in M. \tag{4.2.5}$$

Similarly, when the PU is active, the distribution of $\boldsymbol{x}_i$ can be approximated as Gaussian with mean, $\mu_1 = |\phi(x_{su}^m)|^2\sigma_s^2 + \sigma_\eta^2$ and variance, σ_1^2 derived as

$$\sigma_1^2 = \mathbb{E}[(\boldsymbol{x}_i - \mu_1)^2] \tag{4.2.6}$$

For simplicity, if we momentarily drop the channel effect, $\phi(x_{su}^m)$, (4.2.6) can be written as

$$\begin{aligned}\sigma_1^2 &= \mathbb{E}[(\frac{1}{N_s}\sum_{n=1}^{N_s}|x_m(n)|^2 - (\sigma_s^2 + \sigma_\eta^2))^2] \\ &= \frac{1}{N_s}\mathbb{E}[(|s(n) + \eta_m(n)|^2 - (\sigma_s^2 + \sigma_\eta^2))^2]. \end{aligned} \tag{4.2.7}$$

If it is assumed that the primary signal, $s(n)$ is complex modulated independent and identically distributed ($i.i.d$) random process, $s_r(n) + s_i(n)$, where the additional subscript, r and i denotes the *real* and *imaginary*

components, with mean zero and variance, $\mathbb{E}[|s(n)|^2] = \sigma_s^2$, and the noise, $\eta_m(n) \sim \mathcal{CN}(0, \sigma_\eta^2)$, is circularly symmetric complex Gaussian $i.i.d$ random process, $\eta_{m,r}(n) + \eta_{m,i}(n)$, with mean zero and variance, $\mathbb{E}[|\eta_m(n)|^2] = \sigma_\eta^2$. Further, if we assume that the primary signal, $s(n)$ is independent of noise, $\eta_m(n)$ such that $\mathbb{E}[s(n)\eta_m(n)] = 0$, $\mathbb{E}[s_r^2(n)] = \mathbb{E}[s_i^2(n)] = \frac{\sigma_s^2}{2}$, $\mathbb{E}[s_r(n)s_i(n)] = 0$, $\mathbb{E}[s^2(n)] = 0$, $\mathbb{E}[s(n)] = 0$, $\mathbb{E}[\eta_{m,r}^2(n)] = \mathbb{E}[\eta_{m,i}^2(n)] = \frac{\sigma_\eta^2}{2}$, $\mathbb{E}[\eta_{m,r}(n)\eta_{m,i}(n)] = 0$, $\mathbb{E}[\eta_m(n)] = 0$, then (4.2.7) can be re-expressed as

$$
\begin{aligned}
\sigma_1^2 &= \frac{1}{N_s}\mathbb{E}\left[\left(\left([s_r(n)+\eta_{m,r}(n)]^2 + [s_i(n)+\eta_{m,i}(n)]^2\right) - \left(\sigma_s^2+\sigma_\eta^2\right)\right)^2\right] \\
&= \frac{1}{N_s}\mathbb{E}\left[\left(|s(n)|^2 + |\eta_m(n)|^2 + 2s_r(n)\eta_{m,r}(n) + 2s_i(n)\eta_{m,i}(n) - \sigma_s^2 - \sigma_\eta^2\right)^2\right] \\
&= \frac{1}{N_s}\mathbb{E}\Big[|s(n)|^4 + |s(n)|^2|\eta_m(n)|^2 + 2|s(n)|^2 s_r(n)\eta_{m,r}(n) + 2|s(n)|^2 s_{p,i}(n) \\
&\quad \eta_{m,i}(n) - |s(n)|^2\sigma_s^2 - |s(n)|^2\sigma_\eta^2 + |s(n)|^2|\eta_m(n)|^2 + |\eta_m(n)|^4 + 2s_r(n)\eta_{m,r}(n) \\
&\quad |\eta_m(n)|^2 + 2s_i(n)\eta_{m,i}(n)|\eta_m(n)|^2 - |\eta_m(n)|^2\sigma_s^2 - |\eta_m(n)|^2\sigma_\eta^2 + 2s_r(n)\eta_{m,r}(n) \\
&\quad |s(n)|^2 + 2s_r(n)\eta_{m,r}(n)|\eta_m(n)|^2 + 4s_r^2(n)\eta_{m,r}^2(n) + 4s_r(n)s_i(n)\eta_{m,r}(n)\eta_{m,i}(n) \\
&\quad - 2s_r(n)\eta_{m,r}(n)\sigma_s^2 - 2s_r(n)\eta_{m,r}(n)\sigma_\eta^2 + 2s_i(n)\eta_{m,i}(n)|s(n)|^2 + 2s_i(n)\eta_{m,i}(n) \\
&\quad |\eta_m(n)|^2 + 4s_r(n)s_i(n)\eta_{m,r}(n)\eta_{m,i}(n) + 4s_i^2(n)\eta_{m,i}^2(n) - 2s_i(n)\eta_{m,i}(n)\sigma_s^2 - \\
&\quad 2s_i(n)\eta_{m,i}(n)\sigma_\eta^2 - \sigma_s^2|s(n)|^2 - \sigma_s^2|\eta_m(n)|^2 - 2s_r(n)\eta_{m,r}(n)\sigma_s^2 - 2s_i(n)\eta_{m,i}(n) \\
&\quad \sigma_s^2 + \sigma_s^4 + \sigma_\eta^2\sigma_s^2 - \sigma_\eta^2|s(n)|^2 - \sigma_\eta^2|\eta_m(n)|^2 - 2s_r(n)\eta_{m,r}(n)\sigma_\eta^2 - 2s_i(n)\eta_{m,i}(n) \\
&\quad \sigma_\eta^2 + \sigma_\eta^2\sigma_s^2 + \sigma_\eta^4\Big] \\
&= \frac{1}{N_s}\Big[\mathbb{E}[|s(n)|^4] + \sigma_s^2\sigma_\eta^2 - \sigma_s^4 - \sigma_s^2\sigma_\eta^2 + \sigma_\eta^2\sigma_s^2 + \mathbb{E}[|\eta_m(n)|^4] - \sigma_\eta^2\sigma_s^2 - \sigma_\eta^4 + \\
&\quad \frac{4\sigma_s^2\sigma_\eta^2}{4} + \frac{4\sigma_s^2\sigma_\eta^2}{4} - \sigma_s^4 - \sigma_s^2\sigma_\eta^2 + \sigma_s^4 + \sigma_\eta^2\sigma_s^2 - \sigma_\eta^2\sigma_s^2 - \sigma_\eta^4 + \sigma_\eta^2\sigma_s^2 + \sigma_\eta^4\Big] \\
&= \frac{1}{N_s}\Big[\mathbb{E}[|s(n)|^4] + \mathbb{E}[|\eta_m(n)|^4] + 2\sigma_s^2\sigma_\eta^2 - \sigma_s^4 - \sigma_\eta^4\Big] \\
&= \frac{1}{N_s}\Big[\mathbb{E}[|s(n)|^4] + \mathbb{E}[|\eta_m(n)|^4] - (\sigma_s^2 - \sigma_\eta^2)^2\Big]. \qquad (4.2.8)
\end{aligned}
$$

At this point if we restore the channel effect on the received primary signal,

$s(n)$, we obtain

$$\sigma_1^2 = \frac{1}{N_s}[|\phi(x_{su}^m)|^4\mathbb{E}|s(n)|^4 + \mathbb{E}|\eta(n_m)|^4 - (|\phi(x_{su}^m)|^2\sigma_s^2 - \sigma_\eta^2)^2], \forall m \in M. \tag{4.2.9}$$

4.2.2 The K-means Clustering Algorithm

Let us suppose that by using (4.2.3) we collect energy feature vector set, $\mathcal{S} = \{\mathbf{x}_i\}_{i=1}^D \in \{H_0, H_1\}$, $\mathbf{x}_i \in R^M$, where M in this instance is the dimension of our feature vector which also corresponds to the number of cooperating SUs, the K-means problem is to minimize the within cluster sum of squares error, for a pre-determined and fixed number of clusters in $\mathcal{S}$. Let K be the fixed number of clusters and $S_k \subset \mathcal{S}$, where $k = 1, \cdots, K$ is the subset index such that $\mathcal{S} = \{S_k\}_{k=1}^K$. If a feature vector, $\mathbf{x}_j$ belongs to cluster $k \in \mathcal{S}$, the K-means problem formulation can be written as [68]

$$\begin{aligned} \underset{S}{\text{minimize}} \quad & \sum_{k=1}^{k}\sum_{j\in S_k} \|\mathbf{x}_j - \mathbf{C}_k\|^2 \\ \text{subject } to \quad & \mathbf{C}_k = \frac{1}{\mathbf{card}(S_k)}\sum_{j\in S_k}\mathbf{x}_j, \ \bigcup_{k=1}^{K} S_k = \mathcal{S}. \end{aligned} \tag{4.2.10}$$

where **card** implies the cardinality function. The K-means clustering algorithm which finds a partition in which objects within each cluster are as close to each other as possible, and as far as possible from objects in other clusters and that can be used for computing the cluster centroids at the SBS is presented in Algorithm 4.1. Although the algorithm will converge to a point, it is important to note that this may not necessarily be the minimum of the sum of squares. This is owing to the fact that the optimization problem in (4.2.10) is non-convex and thus the algorithm is a heuristic, which converges to a local minimum. The algorithm moves objects between clusters and stops when there is no change in assignments from one iteration to the

next such that the sum cannot be decreased further. The result, however, is a set of clusters that are as compact and well-separated as possible for every sensor.

After the training process, let $\mathbf{C}_k^*$ denote the M dimensional vector of centroids obtained for the k-th cluster by K-means clustering algorithm, if the classifier thereafter receives a test feature vector, $\mathbf{x}^{new}$, the classifier uses the decision rule described by

$$\hat{\mathbf{C}}_k(\mathbf{x}^{new}) = \underset{k}{\operatorname{argmin}}\ \delta_k(\mathbf{x}^{new}) \tag{4.2.11}$$

where $\delta_k(\mathbf{x}^{new}) = \|\mathbf{x}^{new} - \mathbf{C}_k^*\|_2^2$, $\forall k \in \{1, \cdots, K\}$, to determine the cluster, $\hat{\mathbf{C}}_k$ to which $\mathbf{x}^{new}$ belongs and hence, the status of the PUs' activities.

Algorithm 4.1: K-means Clustering Algorithm for Cooperative Spectrum Sensing in CR Networks

---

1. $\forall\ m = 1, ..., M$, initialize cluster centroids
   $\mathbf{C}_1, ..., \mathbf{C}_K$, $\forall\ k = 1, ..., K$ given $\mathcal{S}$, K.
2. **do repeat**
3. **for** $k \leftarrow 1$ to K
4. **do** $S_k \leftarrow \{\ \}$
5. **for** $i \leftarrow 1$ to D
6. **do** $k \leftarrow argmin_k \|\mathbf{C}_k - \mathbf{x}_i\|^2$
7. $S_k \leftarrow S_k \cup \{\mathbf{x}_i\}$
8. **do** $\mathbf{C}_k \leftarrow |S_k|^{-1} \sum_{\mathbf{x}_i \in S_k} \mathbf{x}_i, \forall\ k$
9. **until convergence**
10. $\mathbf{C}_{H0}^* \leftarrow min\{|\mathbf{C}_1^*|, ..., |\mathbf{C}_K^*|\}$

4.3 Multivariate Gaussian Mixture Model Technique for Cooperative Spectrum Sensing

A mixture model is a probabilistic model for representing the presence of subset of data within a set of observations, without requiring that a set of label be used to identify the subset to which an individual observation belongs [69]. Conventionally, a mixture model is considered as the mixture distribution which represents the probability distribution of observations in an entire set. The goal in mixture model problems is essentially to make statistical inferences about the properties of the subset and to derive the properties of the overall set from those of the subset given only observations contained in the superset, while the identity information about the subset may be hidden (unknown).

Mixture models can take different forms depending on the underlying probability distribution that models the observation data in the set under consideration. A Gaussian mixture model (GMM) for example, is a weighted sum of multivariate Gaussian probability densities of the form [70]

$$f(\mathbf{x}|\theta) = \sum_{k=1}^{K} \pi_k \ \psi(\mathbf{x}|\boldsymbol{\mu}_k, \Sigma_k), \tag{4.3.1}$$

where θ is the collection of all governing GMM parameters comprising π_k, $\boldsymbol{\mu}_k$, and Σ_k, $\forall k \in K$, $\pi_k : 0 \leq \pi_k \leq 1$, is the mixing coefficient or weighting factor normalized over all k so that $\sum_{k=1}^{K} \pi_k = 1$, and $\psi(\mathbf{x}|\boldsymbol{\mu}_k, \Sigma_k)$ is the Gaussian density function defined as

$$\psi(\mathbf{x}|\boldsymbol{\mu}_k, \Sigma_k) = \frac{1}{(2\pi)^{M/2}|\Sigma_k|^{1/2}} \exp\left\{ -\frac{1}{2}(\mathbf{x} - \boldsymbol{\mu_k})^T \Sigma_k^{-1} (\mathbf{x} - \boldsymbol{\mu_k}) \right\}. \tag{4.3.2}$$

Out the outset, it was established that the energy features can be modeled as Gaussian variable via the CLT, thus the M dimensional energy samples vector realized using (4.2.3) under both network states in (4.2.1) and (4.2.2)

for all sensors in the network may be treated as a mixture of Gaussian.

For the set of training energy vector $\mathcal{S}$, the Gaussian PDF may be expressed as

$$p(\mathcal{S}|\theta) = p(\mathbf{x}_1, \cdots, \mathbf{x}_D|\theta) \tag{4.3.3}$$

which following from the $i.i.d$ nature of $\mathbf{x}_i \in \mathcal{S}$, $\forall i$ may be re-expressed as

$$\begin{aligned} p(\mathcal{S}|\theta) &= p(\mathbf{x}_1|\theta) \cdots p(\mathbf{x}_D|\theta) \\ &= \prod_{i=1}^{D} p(\mathbf{x}_i|\theta) \end{aligned} \tag{4.3.4}$$

whose log-likelihood may be written as

$$\begin{aligned} \ln\Big[p(\mathcal{S}|\theta)\Big] &= \ln\Big[\prod_{i=1}^{D} p(\mathbf{x}_i|\theta)\Big] \\ &= \sum_{i=1}^{D} \ln\Big\{\sum_{k=1}^{K} \pi_k \psi(\mathbf{x}_i|\boldsymbol{\mu}_k, \Sigma_k)\Big\}. \end{aligned} \tag{4.3.5}$$

At this point, it could be noted that due to the presence of the summation over k term, appearing inside the logarithm in (4.3.5), it is impossible to obtain close form analytical solutions to our distribution parameters of interest via the maximum likelihood estimator. Nevertheless, there exist a number of iterative methods for maximizing the likelihood function and one such method that is widely adopted is the EM which will now considered [17], [46].

4.3.1 Expectation Maximization Clustering Algorithm for GMM

The EM algorithm introduced by Dempster et al in [71] is an elegant and powerful method that allows us to obtain maximum likelihood solutions to the parameter estimation problem in (4.3.5). Here, it is considered that maximizing the likelihood function requires that the derivatives with respect to the mixture distribution parameters of interest, π_k, $\boldsymbol{\mu}_k$ and Σ_k vanish. By

adopting this informal approach, to derive $\boldsymbol{\mu}_k$, we simply differentiate (4.3.5) with respect to the means as

$$\begin{aligned}\frac{\partial}{\partial \boldsymbol{\mu}_k} \ln \Big[p(\mathcal{S}|\theta)\Big] &= \frac{\partial}{\partial \boldsymbol{\mu}_k}\Bigg[\sum_{i=1}^{D} \ln\Bigg\{\sum_{k=1}^{K} \pi_k \psi(\mathbf{x}_i|\boldsymbol{\mu}_k, \Sigma_k)\Bigg\}\Bigg] \\ &= \sum_{i=1}^{D} \frac{\pi_k \ \psi(\mathbf{x}_i|\boldsymbol{\mu}_k, \Sigma_k)}{\sum_{j=1}^{K} \pi_j \ \psi(\mathbf{x}_i|\boldsymbol{\mu}_j, \Sigma_j)} \Sigma_k^{-1}(\mathbf{x}_i - \boldsymbol{\mu}_k) \qquad (4.3.6)\end{aligned}$$

If we define a parameter, r_{ik} as the posterior probability or responsibility which the k-th cluster takes for explaining data point $\mathbf{x}_i$, and let this be represented as

$$r_{ik} = \frac{\pi_k \ \psi(\mathbf{x}_i|\boldsymbol{\mu}_k, \Sigma_k)}{\sum_{j=1}^{K} \pi_j \ \psi(\mathbf{x}_i|\boldsymbol{\mu}_j, \Sigma_j)}. \qquad (4.3.7)$$

By setting the derivative in (4.3.6) to zero, we obtain

$$\sum_{i=1}^{D} r_{ik} \ \Sigma_k^{-1}(\mathbf{x}_i - \boldsymbol{\mu}_k) = 0 \qquad (4.3.8)$$

and if we multiply through by Σ_k, the mean, $\boldsymbol{\mu}_k$ is derived as

$$\begin{aligned}\boldsymbol{\mu}_k &= \frac{1}{\sum_{i=1}^{D} r_{ik}} \sum_{i=1}^{D} r_{ik} \ \mathbf{x}_i \\ &= \frac{1}{D_k} \sum_{i=1}^{D} r_{ik} \ \mathbf{x}_i \qquad (4.3.9)\end{aligned}$$

where it is taken that $D_k = \sum_{i=1}^{D} r_{ik}$. From the general understanding of mean, D_k may be viewed as the actual number of data points assigned to cluster k whose weighted mean is $\boldsymbol{\mu}_k$. Similarly, the responsibility term, r_{ik} may be seen as the respective weights associated with each data point, $\mathbf{x}_i$.

Next we consider the derivation of the expression for the covariance ma-

trix, Σ_k. We proceed by differentiating (4.3.5) with respect to Σ_k as

$$\frac{\partial}{\partial \Sigma_k} \ln \Big[p(\mathcal{S}|\theta) \Big] = \frac{\partial}{\partial \Sigma_k} \Big[\sum_{i=1}^{D} \ln \Big\{ \sum_{k=1}^{K} \pi_k \psi(\mathbf{x}_i|\boldsymbol{\mu}_k, \Sigma_k) \Big\} \Big]. \tag{4.3.10}$$

By assuming that Σ_k is non-singular and symmetric, and invoking the matrix derivative, $\frac{\partial |\Sigma|^k}{\partial \Sigma} = k|\Sigma|^k \Sigma^{-T}$, and also setting the right hand side (R.H.S) of (4.3.10) to zero we will have

$$\begin{aligned}
0 &= \sum_{i=1}^{D} \Bigg\{ \frac{\pi_k \ \big[\big\{ \psi(\mathbf{x}_i|\boldsymbol{\mu}_k, \Sigma_k)(\mathbf{x}_i - \boldsymbol{\mu}_k)(\mathbf{x}_i - \boldsymbol{\mu}_k)^T \Sigma_k^{-1} \big\} - \big\{ \psi(\mathbf{x}_i|\boldsymbol{\mu}_k, \Sigma_k) \big\} \big]}{\sum_{j=1}^{K} \pi_j \ \psi(\mathbf{x}_i|\boldsymbol{\mu}_j, \Sigma_j)} \Bigg\} \\
&= \sum_{i=1}^{D} \Bigg\{ \frac{\pi_k \ \psi(\mathbf{x}_i|\boldsymbol{\mu}_k, \Sigma_k)(\mathbf{x}_i - \boldsymbol{\mu}_k)(\mathbf{x}_i - \boldsymbol{\mu}_k)^T \Sigma_k^{-1}}{\sum_{j=1}^{K} \pi_j \ \psi(\mathbf{x}_i|\boldsymbol{\mu}_j, \Sigma_j)} \Bigg\} \ - \\
&\qquad \sum_{i=1}^{D} \Bigg\{ \frac{\psi(\mathbf{x}_i|\boldsymbol{\mu}_k, \Sigma_k)}{\sum_{j=1}^{K} \pi_j \ \psi(\mathbf{x}_i|\boldsymbol{\mu}_j, \Sigma_j)} \Bigg\} \\
&= \sum_{i=1}^{D} \Big\{ r_{ik} \ (\mathbf{x}_i - \boldsymbol{\mu}_k)(\mathbf{x}_i - \boldsymbol{\mu}_k)^T \Big\} \Sigma_k^{-1} - \sum_{i=1}^{D} \Big\{ r_{ik} \Big\}
\end{aligned} \tag{4.3.11}$$

where the responsibility, r_{ik} has used as defined in (4.3.7). Further, by multiplying both sides of (4.3.11) by Σ_k, and re-arranging, we obtain

$$\Sigma_k \ \sum_{i=1}^{D} r_{ik} = \sum_{i=1}^{D} r_{ik} \ (\mathbf{x}_i - \boldsymbol{\mu}_k)(\mathbf{x}_i - \boldsymbol{\mu}_k)^T \tag{4.3.12}$$

so that the covariance matrix, Σ_k can be derived as

$$\Sigma_k = \frac{1}{D_k} \sum_{i=1}^{D} r_{ik} \ (\mathbf{x}_i - \boldsymbol{\mu}_k)(\mathbf{x}_i - \boldsymbol{\mu}_k)^T. \tag{4.3.13}$$

Finally, we will consider extracting the expression for the mixing coefficient, π_k. This is achieved by maximizing with respect to π_k subject to the constraint, $\sum_{k=1}^{K} \pi_k = 1$. By applying Langrangian method of multiplier, the optimization problem is solved by differentiating the expression

$$\ln \big[p(\mathcal{S}|\theta) \big] + \alpha \big[\sum_{k=1}^{K} \pi_k - 1 \big] \tag{4.3.14}$$

with respect to, π_k and setting the result to zero, yielding

$$\begin{aligned} 0 &= \frac{\partial}{\partial \pi_k}\Big\{ \ln\big\{p(\mathcal{S}|\theta)\big\} + \alpha\big\{\sum_{k=1}^{K}\pi_k - 1\big\}\Big\} \\ &= \frac{\partial}{\partial \pi_k}\Big[\sum_{i=1}^{D}\ln\Big\{\sum_{k=1}^{K}\pi_k\psi(\mathbf{x}_i|\boldsymbol{\mu}_k,\Sigma_k)\Big\} + \alpha\big\{\sum_{k=1}^{K}\pi_k - 1\big\}\Big\}\Big] \\ &= \sum_{i=1}^{D}\frac{\psi(\mathbf{x}_i|\boldsymbol{\mu}_k,\Sigma_k)}{\sum_{j=1}^{K}\pi_j\ \psi(\mathbf{x}_i|\boldsymbol{\mu}_j,\Sigma_j)} + \alpha \end{aligned} \tag{4.3.15}$$

If we apply (4.3.7), (4.3.15) becomes

$$-\alpha = \frac{\sum_{i=1}^{D}\ r_{ik}}{\pi_k} \tag{4.3.16}$$

so that if we multiply through by π_k, and sum both sides over k, we obtain

$$-\alpha\sum_{k=1}^{K}\pi_k = \sum_{k=1}^{K}\sum_{i=1}^{D}\ r_{ik}. \tag{4.3.17}$$

Further, by substituting $\sum_{k=1}^{K}\pi_k = 1$ and $D_k = \sum_{i=1}^{D} r_{ik}$, in (4.3.17), we will arrive at

$$\alpha = -\sum_{k=1}^{K} D_k = -D, \tag{4.3.18}$$

the total number of data points in all K clusters. Finally, if we substitute (4.3.18) into (4.3.16), we have

$$D = \frac{\sum_{i=1}^{D}\ r_{ik}}{\pi_k} \Rightarrow \pi_k = \frac{D_k}{D}. \tag{4.3.19}$$

From (4.3.19), it is obvious that the mixing coefficient for the k-th component is given by the average responsibility it takes o explain all data points associated with it. Furthermore, it should be noted that all our parameters of interest for the k-th component, π_k, $\boldsymbol{\mu}_k$ and Σ_k, depend in some way on the responsibility, r_{ik}, which in turn depends on all other components, as indicated in (4.3.7). In view of this interlocked nature, the optimal solutions

derived in (4.3.9), (4.3.13) and (4.3.19) are not in closed form so that we will have to resort to an iterative technique to solve our spectrum sensing problem via the EM algorithm. An iterative EM algorithm used in this study is presented in Algorithm 4.2.

As could be seen in Algorithm 4.2, the first step in the implementation of the EM technique for solving the mixture model problem is to set initial values for the cluster parameters of all components and use them to compute the log-likelihood. These initial values are also used to compute the responsibility (posterior probability) for all clusters in the expectation step. In the maximization step, the responsibility values derived from the expectation step are in turn used to obtain the values for mixing coefficient, mean and covariance matrix for all components. Then, the log-likelihood is re-compute again and convergence is checked for. The process of computing the responsibility, mixing proportion, mean and covariances is then repeated until convergence is achieved and optimal cluster parameters are obtained for all components in the mixture. It should be noted, though, that the EM algorithm is known to converge to a local optimal solution [71].

Algorithm 4.2: EMGMM Clustering Algorithm for CR Spectrum Sensing

1. **Initialization:** Choose the initial estimates $\pi_k^{(1)}$, $\boldsymbol{\mu}_k^{(1)}$, $\Sigma_k^{(1)}$, $\forall k \in K$ and using (4.3.5), compute the initial log-likelihood,

$$\ln\big[p(\mathcal{S}|\theta^{(1)}\big] = \tfrac{1}{D}\big[\sum_{i=1}^{D} \ln\big\{\sum_{k=1}^{K} \pi_k^{(1)} \psi(\mathbf{x}_i|\boldsymbol{\mu}_k^{(1)}, \Sigma_k^{(1)}\big\}\big].$$

2. $l \leftarrow 1$
3. **do repeat**
4. **Expectation step:** Using (4.3.7) compute responsibility, $r_{ik}^{(l)}$,

$$r_{ik}^{(l)} = \frac{\pi_k^{(l)}\ \psi(\mathbf{x}_i|\boldsymbol{\mu}_k^{(l)}, \Sigma_k^{(l)})}{\sum_{j=1}^{K} \pi_j^{(l)}\ \psi(\mathbf{x}_i|\boldsymbol{\mu}_j^{(l)}, \Sigma_j^{(l)})},\ i = 1, \cdots, D,\ \forall k \in K,$$

and

$$D_k^{(l)} = \sum_{i=1}^{D} r_{ik}^{(l)}, \forall k \in K.$$

5. **Maximization step:** Using (4.3.19), (4.3.9) and (4.3.13), compute the mixing coefficients, $\pi_k^{(l+1)}$, means, $\boldsymbol{\mu}_k^{(l+1)}$ and covariances, $\Sigma_k^{(l+1)}$,

$$\pi_k^{(l+1)} = \frac{D_k^{(l)}}{D}, \forall k \in K,$$
$$\boldsymbol{\mu}_k^{(l+1)} = \frac{1}{D_k^{(l)}} \sum_{i=1}^{D} r_{ik}^{(l)}\ \mathbf{x}_i, \forall k \in K,$$
$$\Sigma_k^{(l+1)} = \frac{1}{D_k^{(l)}} \sum_{i=1}^{D} r_{ik}^{(l)}\ (\mathbf{x}_i - \boldsymbol{\mu}_k^{(l+1)})(\mathbf{x}_i - \boldsymbol{\mu}_k^{(l+1)})^T, \forall k \in K.$$

6. **Convergence check:** Re-compute the log-likelihood,

$$\ln\big[p(\mathcal{S}|\theta^{(l+1)}\big] = \tfrac{1}{D}\big[\sum_{i=1}^{D} \ln\big\{\sum_{k=1}^{K} \pi_k^{(l+1)} \psi(\mathbf{x}_i|\boldsymbol{\mu}_k^{(l+1)}, \Sigma_k^{(l+1)}\big\}\big].$$

7. $l \leftarrow l + 1$
8. **until convergence**
9. $\boldsymbol{\mu}_{H0}^* \leftarrow min\{|\boldsymbol{\mu}_1^*|, ..., |\boldsymbol{\mu}_K^*|\}$

If the set of optimal parameters derived from the algorithm is denoted by $\{\pi_k^*\}_{k=1}^K$, $\{\boldsymbol{\mu}_K^*\}_{k=1}^K$ and $\{\Sigma_k^*\}_{k=1}^K$, given a test energy vector $\mathbf{x}^{new}$, the cluster $\hat{\mathbf{C}}_k$ to which the test point belongs is determined by first computing the log-likelihood for all clusters using $\ln\{\pi_k^* \cdot \psi(\mathbf{x}^{new}|\boldsymbol{\mu}_k^*, \Sigma_k^*)\}$, and then making a decision according to

$$\hat{\mathbf{C}}_k(\mathbf{x}^{new}) = \underset{k}{\text{argmax}} \left\{ \ln\{\pi_k^* \cdot \psi(\mathbf{x}^{new}|\boldsymbol{\mu}_k^*, \Sigma_k^*)\},\ \forall k = \{1, \cdots, K\} \right\}. \quad (4.3.20)$$

From the foregoing, in comparison with K-means, which models the data set as a collection of K spherical regions and does deterministic assignment of data points to clusters in which case every data point belongs exactly to a one cluster, thus viewed as a *hard* assignment technique, the EMGMM employs a probabilistic approach which models the data as a collection of K Gaussians with each data point having a degree of membership in each cluster, and thus may be viewed as a form of $soft$ assignment technique. The demerits of EMGMM however, lies in that like K-means, the number of clusters has to be known beforehand, the solution depends strongly on the initialization and the fact that it can only model convex clusters [72].

4.3.2 Simulation Results and Discussion

In this sub-section, the performance of the K-means and EMGMM algorithms for spectrum sensing is investigated. In particular, for simplicity a scenario whereby the SUs experience near LOS propagation from the PU is assumed such that the magnitude of the PU-SU channel coefficient, $|\phi(x_{su}^m)|$, is considered to be fairly the same for the sensors. It is also assumed that the PU-SU channel is quasi-static throughout the learning and testing duration. Furthermore, a two-SU, single-PU network is considered and the data set, $\mathcal{S} = \{\mathbf{x}_i\}_{i=1}^{D} \in \{H_0, H_1\}$, $\mathbf{x}_i \in R^2$ is assumed to be collected across the active and idle states of the PU. The PU is also assumed to switch states in a predetermined manner known to the SUs so that there is no overlapping in the data collection process. Under this setting, the underlying distribution of $\mathcal{S}$ may be characterized by GMM, essentially as a linear combination of two Gaussian components with different means and covariances. The PU transmit power is assumed to be one Watt and the noise is complex AWGN with power, σ_η^2.

In Figure 4.2, the constellation plot of the K-means classifier's input and output at SNR of -13 dB, the sample number, $N_s = 2000$ and sensor num-

ber, $M = 2$ is shown. Under the operating condition shown, the clusters can be seen to be overlapping and by examining the output of the algorithm, we notice how all data points are *strictly* assigned to one of the two classes as described. It is clear to see here that K-means algorithm made some clustering error on both clusters which invariably affects the overall classification performance in terms of the spectrum hole detection.

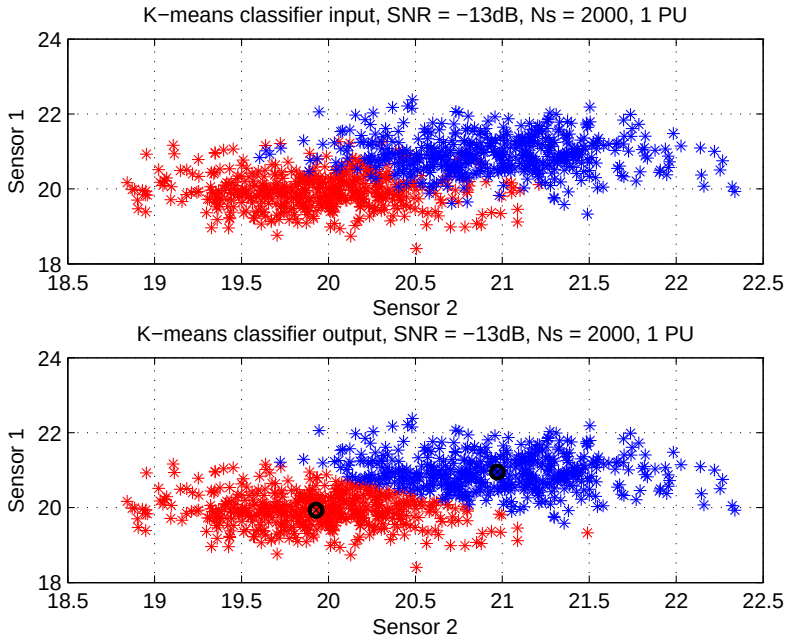

Figure 4.2. Constellation plot showing clustering performance of K-means algorithm, SNR = -13dB, number of PU, $P = 1$, number of sensors, $M = 2$, number of samples, $Ns = 2000$.

In Figure 4.3, the performance of the K-means algorithm in terms of ROC curve is shown. Antenna number, M is set to 2 while SNR and N_s are both varied. Given Pfa of 0.1, it can be seen that as N_s is increased from 1000 to 2000, Pd rises from 0.82 to 0.95 at SNR of -13 dB and from about 0.52 to 0.78 when SNR equals -15 dB, thus suggesting an improvement of about 13% and 26% respectively. Similarly, at the same Pfa, when N_s is fixed at 1000, Pd rises from 0.52 to 0.81 (about 29 % gain) and 0.78 to 0.95 (about 17% gain) at N_s equals 2000 when SNR is raised from -15 dB

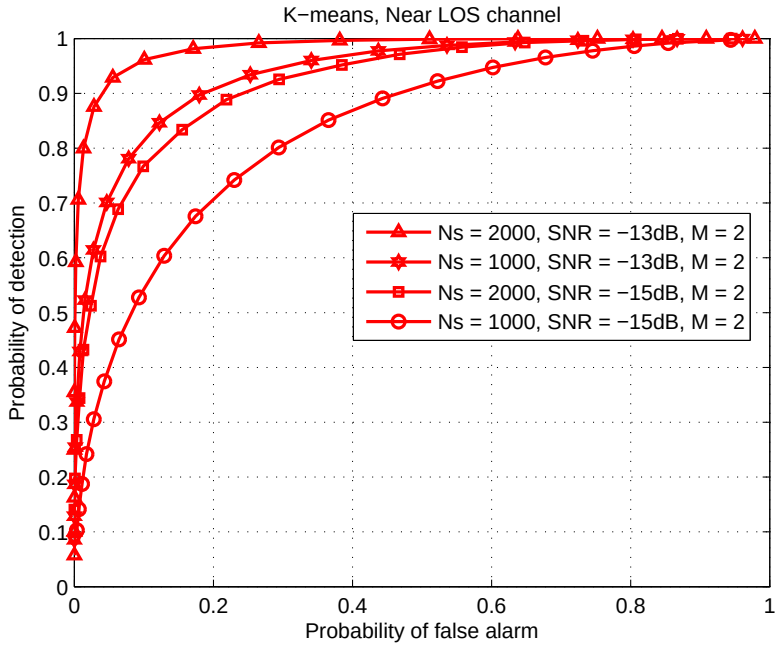

Figure 4.3. ROC curves showing the sensing performance of the K-means algorithm, number of PU, $P = 1$, number of sensors, $M = 2$, number of samples, $Ns = 1000$ and 2000, SNR = -13 dB and -15 dB.

to -13 dB. As expected, this also suggests that the scheme offers significant performance gain with increase in SNR. Using the same PU-SU operating scenario, the performance of the GMM scheme is investigated in Figure 4.4 at SNR of -13 dB and sample number, $N_s = 2000$ where the constellation plot of Gaussian mixture with two components is shown as well as the contours of its corresponding probability density as obtained using the EM algorithm. Here, the capability of the EM algorithm to recognize and capture the user specified Gaussian components that are present in the mixture is also clearly seen. Although, the two bivariate normal components overlap, it is seen here that their peaks are reasonably distinguishable, thereby making clustering feasible. In Figure 4.5, the constellation plot of the training data is shown along with the estimated posterior probability for every data points which is used for deriving other underlying statistical properties of the clusters that are represented in the training data. In performing clustering, the data

points are assigned to one of the two components in the mixture distribution corresponding to the highest posterior probability as shown in Figure 4.6.

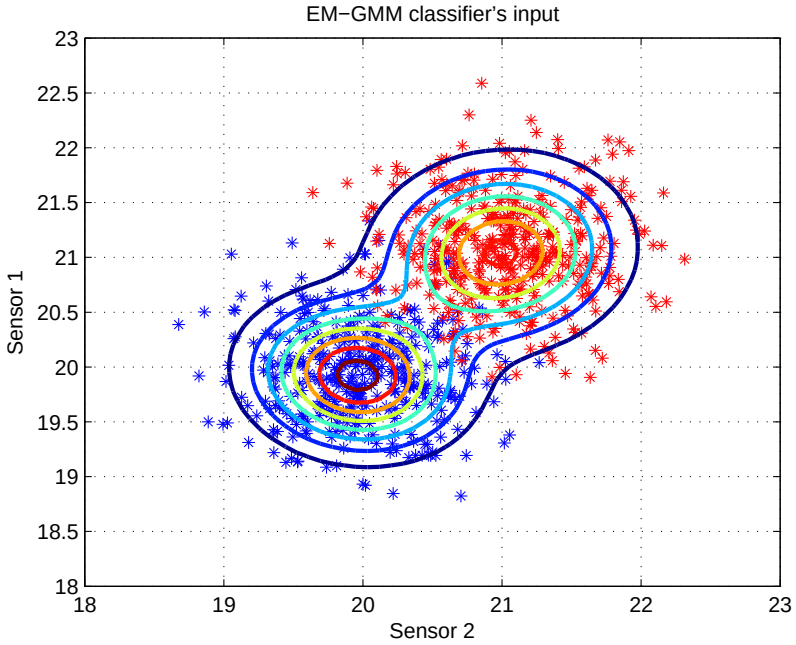

Figure 4.4. Constellation plot showing probability distribution of mixture components, SNR = -13dB, number of PU, $P = 1$, number of sensors, $M = 2$, number of samples, $Ns = 2000$.

Figure 4.7 shows the *roc* of the EM based GMM spectrum sensing scheme where we investigated the performance of the scheme using N_s of 1000 and 2000 while the SNR is set to -13 dB and -15 dB. It can be seen here that at the Pfa of 0.1, detection probability increases from 0.4 to 0.7 (about 30% gain in Pd) when M = 2, SNR = -15 dB and N_s is increased from 1000 to 2000. Similar trend in performance improvement can be observed when the SNR is adjusted from -15 dB to -13 dB, given M = 2 and N_s equals 1000 where Pd rises rapidly from about 0.4 to 0.8, corresponding to a gain of about 40%.

These observable improvements indicate that in the low SNR regime, as the sample number is increased (more time is spent in sensing) or the receive SNR improves, the clusters become more distinct and identifiable and at the

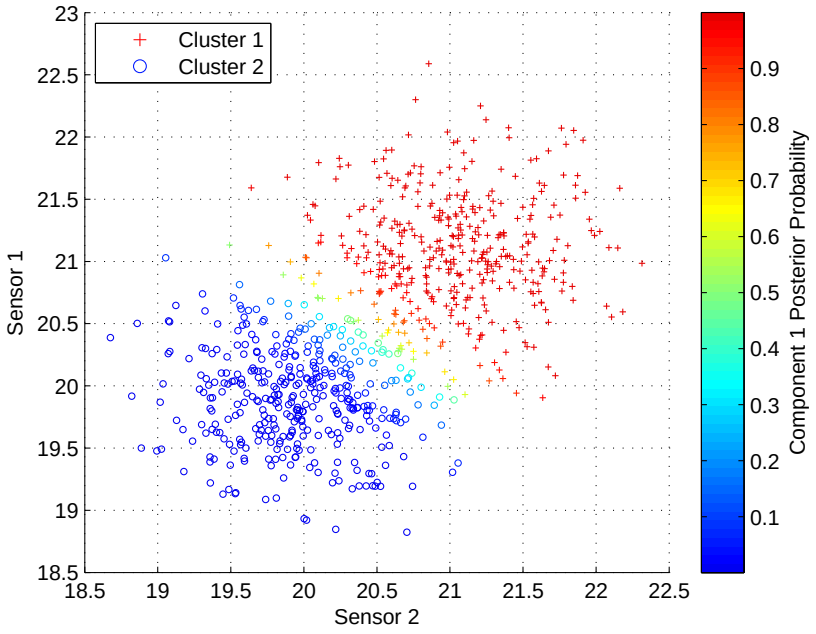

Figure 4.5. Constellation plot showing the mixture components' posterior probability derived from the E-M algorithm, number of PU, $P = 1$, number of sensors, $M = 2$, number of samples, $Ns = 2000$, SNR = -13 dB .

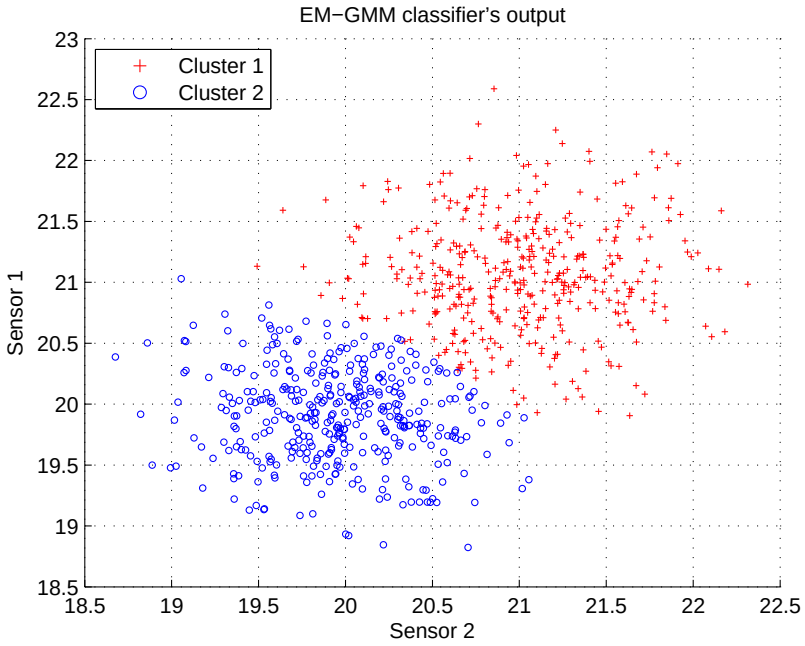

Figure 4.6. Constellation plot showing the clustering capability of the E-M algorithm, number of PU, $P = 1$, number of sensors, $M = 2$, number of samples, $Ns = 2000$, SNR = -13 dB.

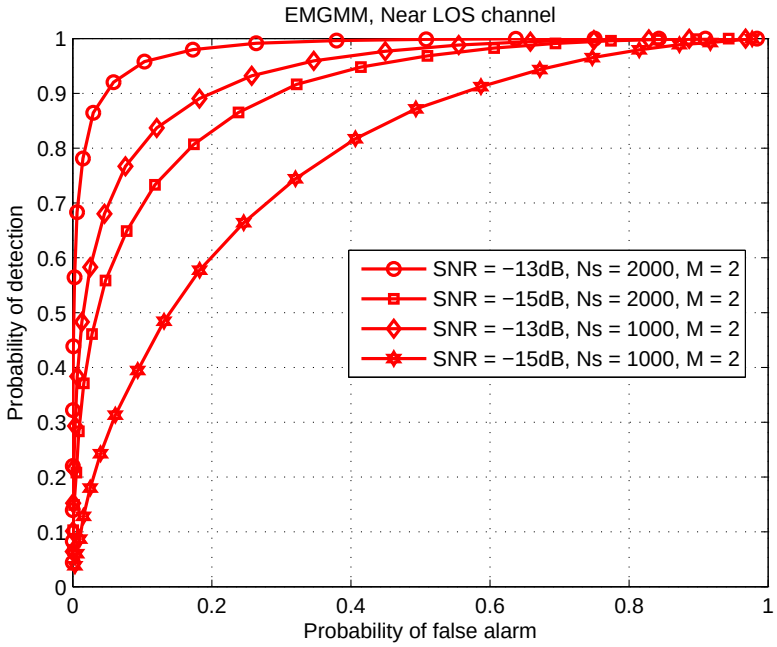

Figure 4.7. ROC curves showing the sensing performance of the E-M algorithm, number of PU, $P = 1$, number of sensors, $M = 2$, number of samples, $Ns = 1000$ and 2000, SNR = -13 dB and -15 dB.

same time the representative components are more clearly separable, thus benefiting the GMM based sensing algorithm.

4.4 Enhancing the Performance of Parametric Classifiers Using Kalman Filter

As evident from the above consideration, well trained parametric classifiers such as the one based on K-means and EMGMM are capable of generating excellent decision boundary for data classification. However, their performance could degrade severely when deployed under time varying channel conditions such as when SUs are mobile in the presence of scatterers. In this section, the aim is to address this problem by employing the Kalman filter based channel estimation technique for tracking the temporally correlated slow fading channel and aiding the classifiers to update the decision boundary in real time. In the succeeding sub-sections, the sensing problem

under flat fading channel conditions and the proposed solution is investigated. The performance of the enhanced classifiers is quantified in terms of average probabilities of detection and false alarm.

4.4.1 Problem Statement

A spectrum sensing network consisting of a fixed PU transmitter (PU-TX), a collaborating sensor node (CSN) co-locating with the PU, a secondary base station (SBS) which plays the role of a data clustering center as well as the SUs' coordinator and M SUs as illustrated in Figure 4.8 is considered. It is assumed that the PU's activity is such that it switches alternately between active and inactive states allowing the SUs to be able to opportunistically use its dedicated frequency band and operate within the PU's coverage area. During the training phase, all SUs sense the energy of the PU-SU channel at their respective locations during both states and report it to the SBS where clustering is performed and appropriate decision boundary is generated. It is assumed that the training data from individual SU is independent but identically distributed.

Let us suppose that based on the decision boundary that is generated from the training data, the PU has been declared to be inactive while all the SUs are stationary. Consider also that SU-c3 that is initially at point 'A' is using the PU's band while having to transit to another location designated point 'B' as shown. The channel condition characterizing the SU's trajectory is assumed to be flat fading (e.g. traveling through a heavily built-up urban environment). This description equally applies where multiple mobile SUs share the PU's band and are able to cooperate. Since the training process of a learning technique normally takes a long time, under this scenario it is impractical for the mobile SU(s) to undergo re-training while in motion owing to the dynamic nature of the channel gain and if sensing information is exchanged among SUs, it could be received incorrectly due to the channel

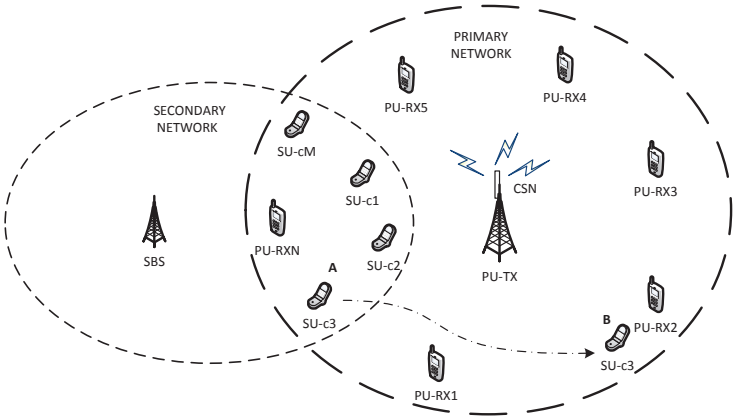

Figure 4.8. A spectrum sensing system of a primary user and mobile secondary users networks.

fading and noise resulting in performance loss [73], [74]. In addition, significant amount of energy and other resources are required to communicate sensing results periodically to other users and in a bid to conserve resources, SUs may prefer not to share their results [75]. To be able to detect the status of the PU activities correctly and efficiently, the onus is therefore on the individual mobile SU as it travels to cater to making well informed decision by dynamically adjusting its decision boundary at the SBS in a manner that the changes in channel conditions are taken into consideration, doing so with minimal cooperation overhead.

To address this challenge, in this study a framework is proposed whereby each SU incorporates a channel tracking sub-system that is based on the Kalman filtering algorithm which enables the SU to obtain an online, unbiased estimate of the true channel gain as it travels. The estimated channel gain can then be used to generate energy features for updating its decision boundary in real time. To investigate the capability of the proposed scheme, without loss of generality, let us adopt the energy vectors based K-means clustering platform earlier described in subsection 4.2.2 due to its simplicity.

4.4.2 System Model, Assumptions and Algorithms

Consider that the PU transmitter is located at a coordinate $\mathbf{x}_{pu}$ as shown in Figure 4.8 and the mobile SU of interest SU-c3, is located initially at $\mathbf{x}_{su}^{m}$. During the training period, all SUs carry out sensing of the PU's channel at their respective locations and collectively report the estimated energy to the SBS where K-means clustering is performed and the cluster centroids are computed. The jointly reported sensing data can be used to obtain a 'high-dimensional' decision plane at the SBS and can enable immobile SUs to be able to take advantage of space diversity which helps contain hidden node problem. Prior to SU-c3 being in motion, let $\phi(\mathbf{x}_{su}^{m}, n)$ represent the channel gain between the PU-TX and SU-c3 at a time instant n. Given that the PU signals are statistically independent, an estimate of the discrete-time signal received at the SU-c3 terminal can be written as

$$x_m(n) = \begin{cases} s(n)\phi(\mathbf{x}_{su}^{m}, n) + \eta_m(n), & H_1 : PU\ present \\ \eta_m(n), & H_0 : PU\ absent \end{cases} \tag{4.4.1}$$

where the channel coefficient $\phi(\mathbf{x}_{su}^{m}, n)$ is assumed to be zero-mean, unit-variance complex Gaussian random variable whose magnitude squared is the power attenuation $P^{att}_{\mathbf{x}_{pu}\rightarrow\mathbf{x}_{su}^{m}}$, between PU-TX and SU-c3 which can be described by

$$\begin{aligned} P^{att}_{\mathbf{x}_{pu}\rightarrow\mathbf{x}_{su}^{m}} &= |\phi(\mathbf{x}_{su}^{m}, n)|^2 \\ &= L_p(\|\mathbf{x}_{pu} - \mathbf{x}_{su}^{m}\|_2) \cdot \delta_{\mathbf{x}_{pu}\rightarrow\mathbf{x}_{su}^{m}} \cdot \gamma_{\mathbf{x}_{pu}\rightarrow\mathbf{x}_{su}^{m}}, \end{aligned} \tag{4.4.2}$$

where $\|\cdot\|_2$ implies Euclidean norm, $L_p(\rho) = \rho^{-d}$ is the path loss component over distance ρ, d is the path loss exponent, $\delta_{\mathbf{x}_{pu}\rightarrow\mathbf{x}_{su}^{m}}$ is the shadow fading component and $\gamma_{\mathbf{x}_{pu}\rightarrow\mathbf{x}_{su}^{m}}$ represents the small scale fading factors. The remaining parameters in (4.5.1) are $s(n)$ which is the instantaneous

PU signal assumed to be complex Gaussian with mean zero and variance $\mathbb{E}|s(n)|^2 = \sigma_s^2$ and $\eta_m(n)$, which is assumed to be an independent and identically distributed circularly symmetric complex zero-mean Gaussian noise with variance $\mathbb{E}|\eta_m(n)|^2 = \sigma_\eta^2$. Throughout this consideration, the shadow fading effect is assumed to be quasi-static and the channel gain, $\phi(\mathbf{x}_{su}^m, n)$ is assumed to be time-invariant while SU-c3 is stationary at point 'A' during training and becomes a fading process as it transits from point 'A' at coordinate $\mathbf{x}_{su}^m$ to point 'B' at coordinate $\mathbf{x}_{su}^j$. It is further assumed that in order to reduce cooperation overhead, although the traveling SU is to be aided by the SBS and other collaborating device within the network, it is primarily responsible for the continuous monitoring of the PU's activities while using the PU's band and would vacate the band immediately when the PU becomes active.

4.4.3 Energy Vectors Realization for SUs Training

During the training interval, given that the PU operates at a carrier frequency f_c and bandwidth ω, if the transmitted PU signal is sampled at the rate of f_s by each SU, the energy samples sent to the SBS for training purpose can be estimated as [67]

$$\mathbf{x}_i = \frac{1}{N_s} \sum_{n=1}^{N_s} |x_m(n)|^2 \tag{4.4.3}$$

where $n = 1, 2, \cdots, N_s$ and $N_s = \tau f_s$ is the number of samples of the received PU signal used for computing the training energy sample at the SU while τ is the duration of sensing time for each energy sample realization. Let $\mathcal{S} = \{\mathbf{x}_1, ..., \mathbf{x}_\mathcal{L}\}$ be the set of training energy vectors obtained at the SBS during the training period where $\mathbf{x}_i \in R^q$, and q is the dimension of each training energy vector which corresponds to the number of collaborating SUs and antenna per SU. If $\mathbf{x}_i \in \{H_0, H_1\}$ is fed into the parametric

classifier, the output of the classifier is the cluster centroids (means) that can be used to generate the decision boundary which optimally separates the two clusters, H_0, H_1. This decision boundary can then be used for the classification of new data points when the classifier is deployed in an environment similar to where it has been trained given any desired false alarm probability. However, in the realistic deployment scenario under consideration involving a mobile SU which travels through a fading channel environment where frequent re-training is impractical, relying on the hitherto, optimal decision threshold obtained at the initial point of training would result in detection error. Therefore, in order to achieve high probability of detection and low false alarm, the cluster centroids computed at the SBS have to be continuously updated and the decision boundary adjusted correspondingly.

4.4.4 Tracking Decision Boundary Using Kalman Filter Based Channel Estimation

In order to be able to track the changes in the cluster centroids under slow fading channel condition occasioned by the mobility of the SU, the Kalman filtering technique is introduced to enable the mobile SU to obtain an online, unbiased estimate of the temporally correlated fading channel gain. Since the PU is assumed to be alternating between the active and inactive states, a collaborating sensor node (CSN) that is co-locating with the PU is activated during the SU's travel period. The sensor node's duty is to broadcast a signal known to the SUs (e.g. pilot signal) periodically during the PU's idle interval for the benefit of the mobile SUs to enable centroid update and avoid causing harmful interference to the PU's service. The role of the CSN in the proximity of the PU is similar to that of the *helper node* used for authenticating the PU's signal in [76] and the rationale behind incorporating a sensor node co-locating with the PU is to ensure that the

channel between the PU and the mobile SU is captured by the CSN-to-mobile SU channel. It should be noted that our model is equally applicable in the case where there are multiple and/or mobile PUs and can accommodate any other collaborating sensor node selection method. The mobile SU on the other hand makes a prediction of the dynamic channel gain based on its speed of travel and combines this prediction with the noisy observation from the collaborating node via the Kalman filtering algorithm to obtain an unbiased estimate of the true channel gain.

Let the discrete-time observation at the mobile SU terminal due to the transmitted signal by the CSN be described by

$$z(t) = s(t)\phi(t) + \varrho(t) \tag{4.4.4}$$

where $s(t)$ is a known pilot signal, $\varrho(t)$ is a zero mean complex additive white Gaussian noise at the receiver with variance, σ_{ϱ}^2 and $\phi(t)$ is a zero mean circularly complex Gaussian channel gain with variance σ_{ϕ}^2, t is the symbol time index. If we let T_s be the symbol period of the pilot signal, the normalized Doppler frequency of the fading channel is $f_d T_s$ where f_d is the maximum Doppler frequency in Hertz defined by $f_d = \frac{v}{\lambda}$, v is the speed of the mobile and λ is the wavelength of the received signal. The magnitude of the instantaneous channel gain, $|\phi|$ is a random variable whose PDF is described by

$$p_{\phi}(\phi) = \frac{2\phi}{\nu} \exp(\frac{-\phi^2}{\nu}), \phi \geq 0 \tag{4.4.5}$$

where ϕ is the fading amplitude and $\nu = \overline{\phi^2}$ is its mean square value. Furthermore, the phase of $\phi(t)$ is assumed to be uniformly distributed between 0 and 2π. It should be noted, though, that by virtue of the location of CSN in the network, it is assumed that $\phi(t)$ also captures the channel gain between the PU-TX and SU-c3 during every observation interval. For the flat fading

Rayleigh channel, the following Jake's Doppler spectrum is often assumed

$$S_{\phi}(f) = \begin{cases} \frac{1}{\pi f_d \sqrt{1-(f/f_d)^2}}, & |f| \leq f_d \\ 0, & |f| > f_d \end{cases} \tag{4.4.6}$$

where f is the frequency shift relative to the carrier frequency. The corresponding autocorrelation coefficient of the observation signal, $z(t)$ under this channel condition is given by [77]

$$\begin{aligned} R_{\phi}(\epsilon) &= \mathbb{E}[\phi(\kappa) \cdot \phi^*(\kappa - \epsilon)] \\ &= \sigma_{\phi}^2 J_0(2\pi f_d \epsilon) \end{aligned} \tag{4.4.7}$$

for lag ϵ where $J_0(\cdot)$ is the zeroth order Bessel function of the first kind. It should be noted that in the actual deployment for cognitive radio, the idle time of the PU is long enough so that it is possible to periodically obtain the noisy observation (measurement) of the channel gain, $z(t)$ during the PU's idle time [61]. The mobile SU can apply the Kalman filter algorithm described in subsection (4.5.3) to obtain an unbiased estimate $\tilde{\phi}$, of the true fading channel gain ϕ which can then be used to update the cluster centroids at the SBS and also for tracking the temporally dynamic optimal decision boundary.

Since the target is to use the Kalman filtering to realize the best estimate $\tilde{\phi}$ of ϕ, a prediction of the dynamic evolution of the channel gain is required in addition to the noisy observation $z(t)$. For simplicity, it is proposed that the first order autoregressive model ($AR-1$) be used since it has been shown to be sufficient to capture most of the channel tap dynamics in Kalman filter based channel tracking related problems [77]. It should be noted too, that the $AR-1$ model is widely acceptable as an approximation to the Rayleigh fading channel with Jake's Doppler spectrum [78], [79]. The $AR-1$ model for approximating the magnitude of time varying complex channel gain can

be expressed as

$$\phi_t^{AR-1} = \alpha \cdot \phi_{t-1}^{AR-1} + \zeta(t) \tag{4.4.8}$$

where t is the symbol index, $0 < \alpha < 1$ and $\zeta(t)$ is complex additive white Gaussian noise with variance $\sigma_\zeta^2 = (1-\alpha^2)\sigma_\phi^2$. When $\alpha = 1$, the $AR-1$ model for the dynamic evolution of ϕ in (4.5.8) becomes a random walk model [77]. One way of obtaining the coefficient of the $AR-1$ model, α expressed as

$$\alpha = \frac{R_\phi^{AR-1}[1]}{R_\phi^{AR-1}[0]} \tag{4.4.9}$$

is by using correlation matching criterion whereby the autocorrelation function of the temporally correlated fading channel is matched with the autocorrelation function of the approximating AR model for lags 0 and 1 such that $R_\phi^{AR-1}[0] = R_\phi[0]$ and $R_\phi^{AR-1}[1] = R_\phi[1]$. However, if the evolution of the dynamic channel gain is modeled by a higher order AR process, the required coefficients can be obtained by solving the Yule-Walker set of equations [79].

Remarks: The optimal estimate of the channel gain that is obtained via the Kalman filter is sufficient to enable the mobile SU avoid frequent and total dependence on the CSN or other SUs for information regarding the status of PU-TX and the associated overhead.

4.4.5 Kalman Filtering Channel Estimation Process

At this point having obtained α, the observation equation (4.5.4) is combined with the state evolution equation (4.5.8) to form a Kalman filter set of equations as [22]

$$\hat{\phi}_{t|t-1} = \alpha\hat{\phi}_{t-1|t-1} \tag{4.4.10}$$

$$M_{t|t-1} = \alpha^2 M_{t-1|t-1} + \sigma_\zeta^2 \tag{4.4.11}$$

$$K_t = \frac{M_{t|t-1}}{M_{t|t-1} + \sigma_\varrho^2} \tag{4.4.12}$$

$$\hat{\phi}_{t|t} = \hat{\phi}_{t|t-1} + K_t(z(t) - \alpha\hat{\phi}_{t|t-1}) \tag{4.4.13}$$

$$M_{t|t} = (1 - K_t)M_{t|t-1} \tag{4.4.14}$$

where K_t is the Kalman gain , $M_{t|t}$ is the variance of the prediction error and $\hat{\phi}_{t|t}$ is the desired optimal estimate of ϕ_t. It is pertinent to mention here that in the rare event that the PU is active for an unexpectedly prolonged period of time so that it becomes impossible to obtain an observation, the situation can be treated as missing observation. Suppose this occurs at a time t, the Kalman filtering prediction step described by (4.5.10) and (4.5.11) remains the same while the correction step in (4.5.13) and (4.5.14) will become

$$\hat{\phi}_{t|t} = \hat{\phi}_{t|t-1} \tag{4.4.15}$$

$$M_{t|t} = M_{t|t-1} \tag{4.4.16}$$

and if the period of missing observation is extremely prolonged, the significance on the detection of PU status is that the mobile SU loses its ability to track the fading channel for that period so that the only effect taken into consideration is the path loss. Consequently, it could be seen that even under this situation the proposed scheme does not perform worse than the alternative where the channel tracking is not considered (path loss only model). A simple algorithm for implementing the proposed enhanced classifier is presented in Algorithm 4.3.

Algorithm 4.3: Kalman Filter Enhanced Parametric Classifier Based Spectrum Sensing Algorithm

1. Generate cluster centroids, $C_k \ \forall \ k = 1, ..., K$ at the SBS using **Algorithm 4.1**.
2. Initialize parameters α, $M_{t-1|t-1}$ and σ_ζ^2 at the SUs.
3. **if** SU begins motion, $t \leftarrow 1$
4. **repeat**
5. SU obtains $z(t)$ in (4.5.4) during PU's idle interval and computes $\hat{\phi}_{t|t}$ and $M_{t|t}$ using (4.5.10) to (4.5.14).
6. Compute new energy samples at SU using $\hat{\phi}_{t|t}$ in step 5 and update cluster centroids at the SBS.
7. Use updated centroids from step 6 to decide the PU status, H_0 or H_1.
8. $t \leftarrow t + 1$
9. **until** SU ends motion
10. **end if**

4.5 Simulation Results and Discussion

For simulation purpose, the average power of the fading process is normalized to unity and the mobile SU under consideration (SU-c3) is assumed to be equipped with an omnidirectional antenna while traveling at a constant velocity of 6 km/hr. A single PU is considered which operates alternately in the active and inactive modes, so that the number of clusters, K is 2. The symbol frequency of the PU is 10 ksymbol/s transmitted at the central carrier frequency of 1.8 GHz. As the SU travels, to model the effects of the scatterers, it is assumed that a total of 128 equal strength rays at uniformly distributed angles of arrival impinge on the receiving antenna, so that we have a normalized Doppler frequency of 1e-3. During training the path

loss exponent, d is assumed equals to 3 while the shadow fading component $\delta_{\mathbf{x}_{pu}\rightarrow\mathbf{x}_{su}^{m}}$ and the small scale fading factor, $\gamma_{\mathbf{x}_{pu}\rightarrow\mathbf{x}_{su}^{m}}$ are both assumed equal to 1, the PU signal is BPSK and transmit power is 1 Watt. The training energy samples at the SUs are computed using $N_s = 1000$. When SU is in motion, the waveform of the temporally correlated Rayleigh fading process to be tracked is generated using the modified Jake's model described in [80]. To test the enhanced classifier, it is assumed that the mobile SU-c3's trajectory is at an approximately constant average distance to PU-TX throughout the duration of travel and energy samples for updating the centroids are computed using $N_s = 1000$.

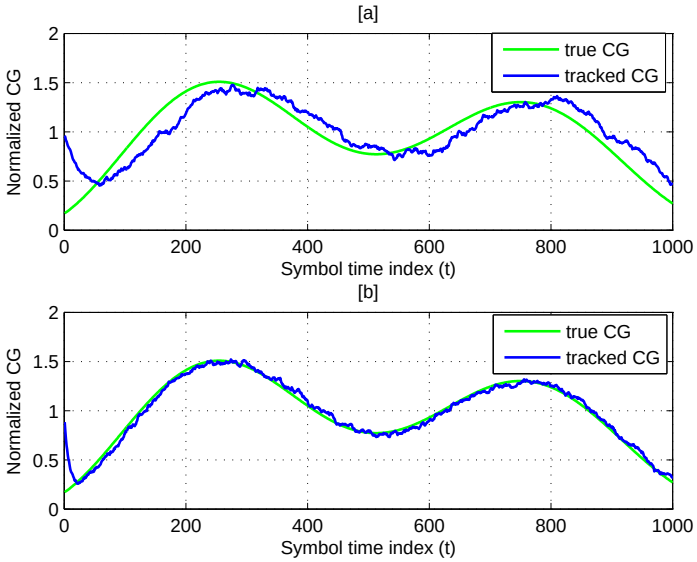

Figure 4.9. Time varying channel gain (CG) tracked at [a] $SNR = 5\ dB$ and [b] $SNR = 20\ dB$.

In Figure 4.9, the ability of the Kalman filter is shown in tracking the true channel gain when the pilot signals are received from the CSN at SNR of 5 dB and 20 dB respectively over an observation window of 1000 symbol duration. It could be seen that as the pilot's SNR is increased, the performance of the tracker also improves. The mean square error performance of the AR-1 based Kalman filter is shown in Figure 4.10 at normalized Doppler

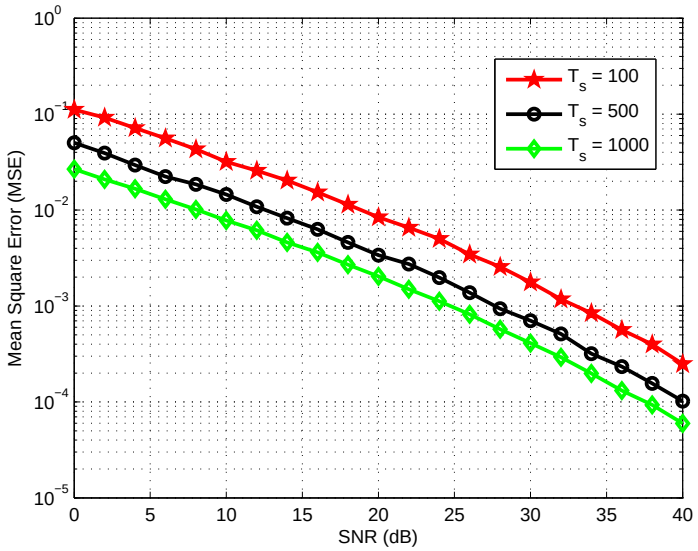

Figure 4.10. Mean square error performance of the AR-1 based Kalman filter at normalized Doppler frequency = 1e-3, tracking duration, T_s = 100, 500 and 1000 symbols.

frequency of 1e-3 where at the same SNR the tracking error reduces for different duration of tracked pilot symbols (tracking duration). This shows that the longer the tracking duration the better the overall performance of the tracker. It is also seen that the average error reduces from 5e-2 to 16e-5 with increase in tracking SNR from 0 dB to 40 dB when the tracking duration, T_s = 1000. The effect of the number of PU's signal samples, N_s used for computing the energy features for training, tracking and testing on the average probabilities of detection (Pd_{Av}) and false alarm (Pfa_{Av}) is shown in Figure 4.11. Here, a considerable improvement in Pd_{Av} is observed as N_s is increased from 1000 to 2000. In Figure 4.12, the performance of the enhanced classifier is shown in terms of Pd_{Av} and Pfa_{Av} and compared with the path loss only model. Here, the pilot symbols from the CSN are assumed to be received at the SNR of 5 dB each time the decision boundary is updated. When the PU's signal is received at SNR of 20 dB, it could be seen that the enhanced classifier attains Pd_{Av} of unity at zero Pfa_{Av} while at PU's operating SNR of 0 dB, Pd_{Av} of about 0.91 is achieved at Pfa_{Av}

equals 0.07 in spite of the degradation in sensing path. This is in contrast to what obtains from the path loss only model where at the SNR of 20 dB, Pd_{Av} is only about 0.83 at a non-zero Pfa_{Av}. In summary, a performance improvement of about 20 percent is observable in the enhanced scheme.

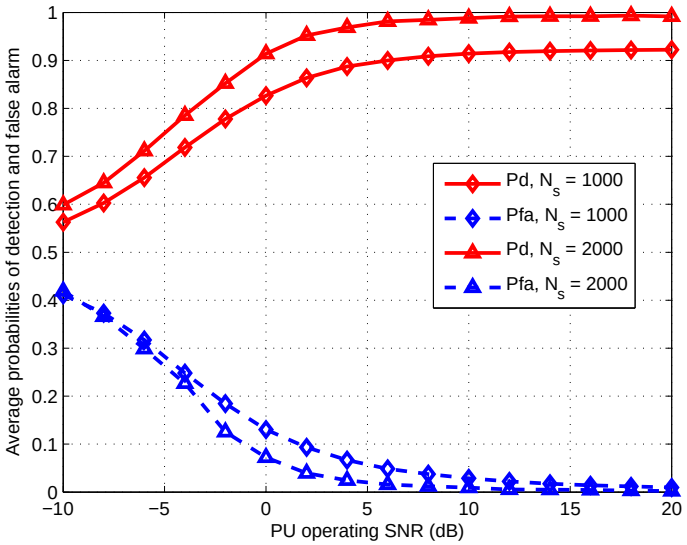

Figure 4.11. Average probabilities of detection and false alarm vs SNR, tracking $SNR = 5$ dB, number of samples, $N_s = 1000$ and 2000, tracking duration = 1000 symbols.

4.6 Summary

In this chapter, the use of semi-supervised learning algorithms for spectrum sensing in CR networks is considered. In particular, the K-means and GMM based EM algorithms were investigated. Simulation reveals that the classifiers possess excellent classification capabilities which make them appealing for detecting unused spectrum holes especially in scenarios with fixed-located PUs and SUs. Furthermore, the use of these parametric classifiers for spectrum sensing was investigated under slow varying flat fading conditions involving mobile SUs and a novel, Kalman filter based channel estimation technique was proposed to enhance their performance. Again,

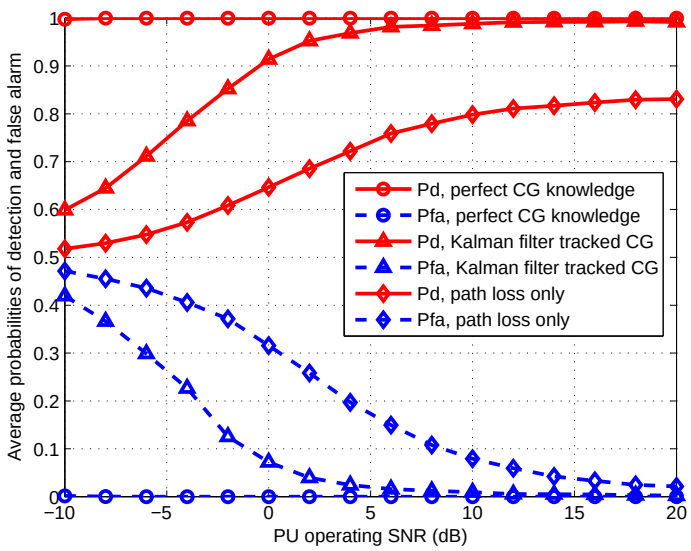

Figure 4.12. Average probabilities of detection and false alarm vs SNR, tracking $SNR = 5\ dB$, number of samples, $N_s = 2000$, tracking duration = 1000 symbols.

simulation results show that under this spectrum sensing condition and by utilizing few collaborating secondary devices, the proposed scheme offers significant performance improvement with minimal cooperation overhead. In the following chapter, an unsupervised learning algorithm that overcomes some of the limitations of the semi-supervised algorithms will be presented.

Chapter 5

UNSUPERVISED VARIATIONAL BAYESIAN LEARNING TECHNIQUE FOR SPECTRUM SENSING IN COGNITIVE RADIO NETWORKS

5.1 Introduction

One of the limitations of the K-means and EM algorithms presented in Chapter 4 is that they are both known to converge to locally optimal solution. The K-means algorithm in particular, is sensitive to initialization and as a result it is possible for two different initializations to yield considerably different clustering results [68]. In a similar vein, the EM algorithm is susceptible to singularity problem which may occur if a Gaussian component collapses onto a particular data point [46]. They also require a priori knowledge of the number of signal classes or clusters represented in the training data, thereby

making them unsuitable in spectrum sensing applications where such a priori information is not available or where the number of PU is not fixed.

In this chapter, the variational Bayesian learning for GMM (VBGMM) is proposed and investigated. This technique provides a framework that overcomes some of the weaknesses of the semi-supervised methods previously considered. In addition, the VBGMM offers a robust clustering technique which can enable the CR device to autonomously learn the characteristics of its operating environment and adapts its actions accordingly [81]. First, the principle of factorized approximation to true posterior distribution on which the VBGMM learning is based is described via the consideration of variational inference technique for univariate Gaussian. Next, building on this premise an extension to the mixture model will be considered. Finally, how the VBGMM method can be adopted to solve our spectrum sensing problem will be demonstrated.

5.2 The Variational Inference Framework

Let us consider a fully Bayesian model comprising of a set of observed (measured) and latent (hidden) continuous variables as well as parameters where it is assumed that all variables and parameters are assigned prior distributions. If we let the set of all observed variables be represented by $\boldsymbol{\mathcal{X}}$ and the set of all latent variables and parameters be denoted by $\boldsymbol{\Theta}$, where $\boldsymbol{\mathcal{X}} = \{\boldsymbol{X}_1, \boldsymbol{X}_2, \cdots, \boldsymbol{X}_N\}$ and $\boldsymbol{\Theta} = \{\boldsymbol{\theta}_1, \boldsymbol{\theta}_2, \cdots, \boldsymbol{\theta}_N\}$, are sets of N, $i.i.d$ random variables, the joint distribution over all observed and latent variables and parameters, $p(\boldsymbol{\mathcal{X}}, \boldsymbol{\Theta})$ constitutes the probability model to be considered. Since it is intractable to estimate the posterior directly, the desire is to obtain an approximation for the posterior distribution, $p(\boldsymbol{\Theta}|\boldsymbol{\mathcal{X}})$ and the model evidence, $p(\boldsymbol{\mathcal{X}})$ such that

$$p(\boldsymbol{\Theta}|\boldsymbol{\mathcal{X}}) \approx q(\boldsymbol{\Theta}) \tag{5.2.1}$$

where over all the latent variables, a variational distribution, $q(\boldsymbol{\Theta})$ is defined so that for any choice of $q(\boldsymbol{\Theta})$, the decomposition of the log marginal probability can be expressed as [46], [82], [83]

$$\ln p(\boldsymbol{\mathcal{X}}) = \mathcal{L}(q) + KL(q\|p). \tag{5.2.2}$$

The first term on the R.H.S of (5.2.2) is known as the variational free energy and it can be defined as

$$\mathcal{L}(q) = \int q(\boldsymbol{\Theta}) \ln \left\{ \frac{p(\boldsymbol{\mathcal{X}}, \boldsymbol{\Theta})}{q(\boldsymbol{\Theta})} \right\} d\boldsymbol{\Theta} \tag{5.2.3}$$

and the second term is given by

$$KL(q\|p) = -\int q(\boldsymbol{\Theta}) \ln \left\{ \frac{p(\boldsymbol{\Theta}|\boldsymbol{\mathcal{X}})}{q(\boldsymbol{\Theta})} \right\} d\boldsymbol{\Theta}. \tag{5.2.4}$$

The second term, $KL(q\|p)$ is known as the Kullback-Leibler divergence between $q(\boldsymbol{\Theta})$ and the true posterior distribution, $p(\boldsymbol{\Theta}|\boldsymbol{\mathcal{X}})$ which satisfies the condition, $KL(q\|p) \geq 0$ (i.e. must be non-negative) and equals to zero when $q(\boldsymbol{\Theta}) = p(\boldsymbol{\Theta}|\boldsymbol{\mathcal{X}})$. Since the log of evidence, $\ln p(\boldsymbol{\mathcal{X}})$ is fixed with respect to q, it follows from (5.2.2) that $\mathcal{L}(q)$ is a lower bound on $\ln p(\boldsymbol{\mathcal{X}})$ and that $\mathcal{L}(q) \leq \ln p(\boldsymbol{\mathcal{X}})$. In performing inference, the goal then becomes making $q(\boldsymbol{\Theta})$ as close as possible to the true posterior by selecting the distribution $q(\boldsymbol{\Theta})$ that minimizes $KL(q\|p)$.

However, it is difficult to deal with the posterior $p(\boldsymbol{\Theta}|\boldsymbol{\mathcal{X}})$, hence instead of minimizing $KL(q\|p)$, an option is to maximize $\mathcal{L}(q)$ by restricting $q(\boldsymbol{\Theta})$ to a family of distribution that offer tractable solutions [82], [84]. It should be noted, though, that it is unrealistic to make $KL(q\|p) = 0$, so this technique will not provide exact result but an approximation. In practice, to generate the required family of approximating distribution, factorized distributions approach is often used where it is assumed that the elements of the latent

variables, $\boldsymbol{\Theta}$ can be partitioned into different groups $\boldsymbol{\Theta}_i$ where $i = 1, ..., M$ such that [46]

$$q(\boldsymbol{\Theta}) = \prod_{i=1}^{M} q_i(\boldsymbol{\Theta}_i). \tag{5.2.5}$$

If we substitute (5.2.5) into (5.2.3), and for the sake of simplicity, also let $q_j = q_j(\boldsymbol{\Theta}_j)$, we will obtain

$$\begin{aligned} \mathcal{L}(q) = \int q_j \ln \tilde{p}(\boldsymbol{\mathcal{X}}, \boldsymbol{\Theta}_j) d\boldsymbol{\Theta}_j - \int q_j \ln q_j \; d\boldsymbol{\Theta}_j \\ + \; constant \end{aligned} \tag{5.2.6}$$

where the joint distribution, $\tilde{p}(\boldsymbol{\mathcal{X}}, \boldsymbol{\Theta}_j)$ is defined by the relation

$$\ln \tilde{p}(\boldsymbol{\mathcal{X}}, \boldsymbol{\Theta}_j) = \mathbb{E}_{i \neq j}[\ln p(\boldsymbol{\mathcal{X}}, \boldsymbol{\Theta})] \; + \; constant. \tag{5.2.7}$$

In (5.2.7), $\mathbb{E}_{i \neq j}[\cdots]$ implies taking the expectation with respect to factorized distribution q, over all variables $\boldsymbol{\Theta}_i$ for $i \neq j$. If we rearrange (5.2.6), it can be seen that the lower bound function, $\mathcal{L}(q)$ becomes a negative KL divergence between $\tilde{p}(\boldsymbol{\mathcal{X}}, \boldsymbol{\Theta}_j)$ and $q_j(\boldsymbol{\Theta}_j)$, i.e.

$$\begin{aligned} \mathcal{L}(q) = \int q_j \ln \frac{\tilde{p}(\boldsymbol{\mathcal{X}}, \boldsymbol{\Theta}_j)}{q_j} \; d\boldsymbol{\Theta}_j \; + \; constant \\ = - \; KL(q_j \| \tilde{p}_j). \end{aligned} \tag{5.2.8}$$

It is worth noting here, that minimizing KL divergence is equivalent to maximizing the lower bound given by (5.2.8) and thus, we have the minimum when

$$q_j(\boldsymbol{\Theta}_j) = \tilde{p}(\boldsymbol{\mathcal{X}}, \boldsymbol{\Theta}_j). \tag{5.2.9}$$

Hence, by combining (5.2.7) and (5.2.9), the optimal solution $q_j^*(\boldsymbol{\Theta}_j)$ is obtained as

$$\ln q_j^*(\boldsymbol{\Theta}_j) = \mathbb{E}_{i \neq j}[\ln p(\boldsymbol{\mathcal{X}}, \boldsymbol{\Theta})] \; + \; constant \tag{5.2.10}$$

where the constant term can be taken care of by taking the exponential of

both sides and normalizing the distribution $q_j^*(\boldsymbol{\Theta}_j)$ as

$$q_j^*(\boldsymbol{\Theta}_j) = \frac{\exp(\mathbb{E}_{i\neq j}[\ln p(\boldsymbol{\mathcal{X}}, \boldsymbol{\Theta})])}{\int \exp(\mathbb{E}_{i\neq j}[\ln p(\boldsymbol{\mathcal{X}}, \boldsymbol{\Theta})])\ d\boldsymbol{\Theta}_j}\ . \tag{5.2.11}$$

For practical realization, it is more convenient to work with the form in (5.2.10), where it can be observed that the optimal solution for a factor $q_j(\boldsymbol{\Theta}_j)$ depends on the joint distribution over all observed and hidden variables by taking the expectation with respect to all other factors $q_i(\boldsymbol{\Theta}_i)$ for $i \neq j$. As matter of fact, the expression, $\mathbb{E}_{i\neq j}[\ln p(\boldsymbol{\mathcal{X}}, \boldsymbol{\Theta})]$ can be simplified into a function of the fixed hyperparameters of the prior distribution over the latent variables and of expectations of latent variables that are not in the current partition, $\boldsymbol{\Theta}_j$. This invariably, points to an interlocked, EM-like iterative evaluation in which the solution of one factor depends on the other. However, with proper choice of the distribution, $q_i(\boldsymbol{\Theta}_i)$ and initialization of parameters and hyperparameters, convergence is guaranteed [53].

5.3 Variational Inference for Univariate Gaussian

In this section, a simple case is considered of the application of variational Bayesian inference technique to learn the statistical properties of a set of univariate, normally distributed spectrum sensing data obtained at a particular sensor. Given that we obtain the data set, $\mathcal{S} = \{x_i\}_{i=1}^N$ under the hypothesis, H_1, where $x_i \in \mathcal{S}, \forall i$ is assumed to be $i.i.d$ Gaussian random variable, the likelihood function of $\mathcal{S}$ is given by

$$p(\mathcal{S}|\mu, \tau) = \big(\frac{\tau}{2\pi}\big)^{N/2} \exp\left\{\frac{-\tau}{2}\sum_{i=1}^{N}(x_i - \mu)^2\right\} \tag{5.3.1}$$

where $\tau = \frac{1}{\sigma^2}$ is known as precision and our desire is to estimate from $\mathcal{S}$, the distribution parameters, μ and τ. The joint probability of the observed

data and parameter can be factorized as

$$p(\mathcal{S}, \mu, \tau) = p(\mathcal{S}|\mu, \tau)p(\mu|\tau)p(\tau) \tag{5.3.2}$$

and the task is to obtain the functional form for each of the factorized probability components. We place conjugate prior distribution on the hidden parameters, μ and τ so that [46], [85]

$$\begin{aligned} p(\tau) &= Gam(\tau|a_0, b_0) \\ &= \frac{1}{\Gamma(a_0)} b_0^{a_0} \tau^{a_0-1} e^{-b_0\tau}, \end{aligned} \tag{5.3.3}$$

$$p(\mu|\tau) = \mathcal{N}(\mu|\mu_0, (\lambda_0\tau)^{-1}), \tag{5.3.4}$$

and

$$p(\mathcal{S}|\mu, \tau) = \prod_{i=1}^{N} \mathcal{N}(x_i|\mu, \tau^{-1}) \tag{5.3.5}$$

where μ_0, λ_0, a_0 and b_0 are hyperparameters with fixed, given values, specifying conjugate priors on the distribution parameters and $\mathcal{N}(x|\mu, \sigma^2) = \frac{1}{\sigma\sqrt{2\pi}} e^{\frac{-(x-\mu)^2}{2\sigma^2}}$. Usually, the hyperparameters are initialized with small, positive numbers to indicate lack of knowledge about the prior distributions of μ and τ. It should be noted from (5.3.3) and (5.3.4) that the mean and the precision are assumed to follow Gaussian and Gamma distribution respectively. This choice of the distributions from the exponential family is very key for the variational Bayesian inference technique to converge to globally optimal solution [82]. Following from the factorized distribution in (5.2.5), the variational distribution that approximates the true distribution over the

unknown parameters can be expressed as

$$q(\mu, \tau) = q(\mu)q(\tau) \tag{5.3.6}$$

By using (5.2.10) and (5.3.2) to (5.3.5), the optimal solution for the mean, μ, can be expressed as

$$\begin{aligned}
\ln q^*(\mu) &= \mathbb{E}_{q(\tau)}[\ln p(\mathcal{S}, \mu, \tau)] + constant \\
&= \mathbb{E}_{q(\tau)}\Bigg[\ln \prod_{i=1}^{N} \mathcal{N}(x_i|\mu, \tau^{-1}) + \ln \mathcal{N}(\mu|\mu_0, (\lambda_0\tau)^{-1}) + \\
&\qquad\qquad \ln \frac{1}{\Gamma(a_0)} b_0^{a_0} \tau^{a_0-1} e^{-b_0\tau} \Bigg] + constant \\
&= \mathbb{E}_{q(\tau)}\Bigg[\ln \Bigg\{ \prod_{i=1}^{N} \Big(\frac{\tau}{2\pi}\Big)^{1/2} \exp\{-\frac{\tau}{2}\big(x_i - \mu\big)^2\} \Bigg\} \\
&\quad + \ln \Bigg\{ \Big(\frac{\lambda_0\tau}{2\pi}\Big)^{1/2} \exp\{-\frac{\lambda_0\tau}{2}\big(\mu - \mu_0\big)^2\} \Bigg\} \Bigg] + constant
\end{aligned} \tag{5.3.7}$$

where the third term has been factored into the constant term since it is independent of μ. Further evaluation of (5.3.7) yields

$$\ln q^*(\mu) = \mathbb{E}_{q(\tau)}\Bigg[-\frac{\tau}{2}\sum_{i=1}^{N}(x_i - \mu)^2 - \frac{\lambda_0\tau}{2}(\mu^2 - 2\mu\mu_0) \Bigg] + constant \tag{5.3.8}$$

where expectation over components whose value does not depend on μ has again been factored into the constant term. We can further re-express (5.3.8)

as

$$\begin{aligned}\ln q^*(\mu) &= -\frac{1}{2}\mathbb{E}_{q(\tau)}[\tau]\left[\sum_{i=1}^{N}(x_i-\mu)^2+\lambda_0(\mu^2-2\mu\mu_0)\right]+constant\\ &= -\frac{1}{2}\mathbb{E}_{q(\tau)}[\tau]\left[\sum_{i=1}^{N}x_i^2-2\mu\sum_{i=1}^{N}x_i+N\mu^2+\lambda_0\mu^2-2\lambda_0\mu_0\mu)\right]+constant\\ &= -\frac{1}{2}\mathbb{E}_{q(\tau)}[\tau]\left[(N+\lambda_0)\mu^2-2(\lambda_0\mu_0+\sum_{i=1}^{N}x_i)\mu\right]+constant\\ &= -\frac{(N+\lambda_0)}{2}\mathbb{E}_{q(\tau)}[\tau]\left[\mu^2-2\frac{(\lambda_0\mu_0+\sum_{i=1}^{N}x_i)}{N+\lambda_0}\mu\right]+constant.\end{aligned} \tag{5.3.9}$$

At this point, if we let $\mu_N = \frac{\lambda_0\mu_0+\sum_{i=1}^{N}x_i}{N+\lambda_0}$ and $\lambda_N = \frac{(N+\lambda_0)}{2}\mathbb{E}_{q(\tau)}[\tau]$, (5.3.9) can be written as [85]

$$\begin{aligned}\ln q^*(\mu) &= -\frac{\lambda_N}{2}\left[\mu^2-2\mu\mu_N\right]+constant\\ &= -\frac{\lambda_N}{2}\left[(\mu-\mu_N)^2-\mu_N^2\right]+constant\\ &= -\frac{\lambda_N}{2}(\mu-\mu_N)^2+constant.\end{aligned} \tag{5.3.10}$$

By taking the exponential of both sides of (5.3.10), it is apparent that $q^*(\mu)$ is a Gaussian distribution which can be expressed as

$$q^*(\mu) = \mathcal{N}(\mu|\mu_N,\lambda_N), \tag{5.3.11}$$

which is functionally dependent on the first moment, $\mathbb{E}_{q(\tau)}[\tau]$. By following similar approach, for the precision, τ, we have

$$\begin{aligned}
\ln q^*(\tau) &= \mathbb{E}_{q(\mu)}[\ln p(\mathcal{S}, \mu, \tau)] + constant \\
&= \mathbb{E}_{q(\mu)}\Bigg[\ln \prod_{i=1}^{N} \mathcal{N}(x_i|\mu, \tau^{-1}) + \\
&\qquad \ln \mathcal{N}(\mu|\mu_0, (\lambda_0\tau)^{-1}) + \ln \frac{1}{\Gamma(a_0)} b_0^{a_0} \tau^{a_0-1} e^{-b_0\tau}\Bigg] + constant \\
&= \mathbb{E}_{q(\mu)}\left[\frac{N}{2}\ln\frac{\tau}{2\pi} - \frac{\tau}{2}\sum_{i=1}^{N}(x_i-\mu)^2 + \frac{1}{2}\ln\frac{\lambda_0\tau}{2\pi} - \frac{\lambda_0\tau}{2}(\mu^2 - 2\mu\mu_0 + \mu_0^2)\right] \\
&\qquad + (a_0-1)\ln\tau - b_0\tau + a_0\ln b_0 + constant \\
&= \mathbb{E}_{q(\mu)}\left[\tau\mu\sum_{i=1}^{N} x_i - \frac{\tau}{2}N\mu^2 - \frac{\lambda_0\tau}{2}\mu^2 + \mu\mu_0\lambda_0\tau\right] - \frac{\tau}{2}\sum_{i=1}^{N} x_i^2 - \frac{\lambda_0\tau\mu_0^2}{2} \\
&\qquad + \frac{N}{2}\ln\frac{\tau}{2\pi} + \frac{1}{2}\ln\frac{\lambda_0\tau}{2\pi} + (a_0-1)\ln\tau - b_0\tau + constant
\end{aligned} \tag{5.3.12}$$

where the terms whose expectation is independent of τ has been factored into the constant term. By re-arranging (5.3.12), we obtain

$$\begin{aligned}
\ln q^*(\tau) &= \left(\tau\sum_{i=1}^{N} x_i + \mu_0\lambda_0\tau\right)\mathbb{E}_{q(\mu)}[\mu] - \left(\frac{\tau}{2}N + \frac{\lambda_0\tau}{2}\right)\mathbb{E}_{q(\mu)}[\mu^2] - \frac{\tau}{2}\sum_{i=1}^{N} x_i^2 - \\
&\qquad \frac{\lambda_0\tau\mu_0^2}{2} + \frac{N}{2}\ln\frac{\tau}{2\pi} + \frac{1}{2}\ln\frac{\lambda_0\tau}{2\pi} + (a_0-1)\ln\tau - b_0\tau + constant \\
&= \tau\Bigg\{\left(\sum_{i=1}^{N} x_i + \mu_0\lambda_0\right)\mathbb{E}_{q(\mu)}[\mu] - \left(\frac{N}{2} + \frac{\lambda_0}{2}\right)\mathbb{E}_{q(\mu)}[\mu^2] - \frac{1}{2}\sum_{i=1}^{N} x_i^2 - \\
&\qquad \frac{\lambda_0\mu_0^2}{2} - b_0\Bigg\} + \left\{\frac{N+1}{2} + (a_0-1)\right\}\ln\tau - \frac{N}{2}\ln 2\pi + \frac{1}{2}(\ln\lambda_0 - \\
&\qquad\qquad \ln 2\pi) + constant \\
&= -\frac{\tau}{2}\Bigg\{-2\left(\sum_{i=1}^{N} x_i + \mu_0\lambda_0\right)\mathbb{E}_{q(\mu)}[\mu] + (N+\lambda_0)\mathbb{E}_{q(\mu)}[\mu^2] + \sum_{i=1}^{N} x_i^2 + \\
&\qquad \lambda_0\mu_0^2 + 2b_0\Bigg\} + \left\{\frac{N+1}{2} + a_0 - 1\right\}\ln\tau + constant
\end{aligned} \tag{5.3.13}$$

If we take the exponential of both sides of (5.3.13) and compare with (5.3.3), it could be observed that (5.3.13) is a Gamma distribution which could be described by [46]

$$q^*(\tau) = Gamma(\tau|a_N, b_N) \tag{5.3.14}$$

where the parameters, a_N and b_N are given by

$$a_N = \frac{N+1}{2} + a_0 \tag{5.3.15}$$

and

$$b_N = \frac{1}{2}\Bigg\{ -2\Bigg(\sum_{i=1}^{N} x_i + \mu_0\lambda_0\Bigg)\mathbb{E}_{q(\mu)}[\mu] + (N+\lambda_0)\mathbb{E}_{q(\mu)}[\mu^2] + \sum_{i=1}^{N} x_i^2 + \lambda_0\mu_0^2 + 2b_0\Bigg\} \tag{5.3.16}$$

respectively. From (5.3.16), it clear that $q^*(\tau)$ is functionally dependent on μ through the first and second moments, $\mathbb{E}_{q(\mu)}[\mu]$ and $\mathbb{E}_{q(\mu)}[\mu^2]$. The first moment of the precision can be extracted from (5.3.14) as [85]

$$\mathbb{E}_{q(\tau)}[\tau] = \frac{a_N}{b_N}. \tag{5.3.17}$$

For simplicity, if we initialize the hyperparameters with zero i.e. if we set $\mu_0 = \lambda_0 = a_0 = b_0 = 0$ and $N \to \infty$, the expectation can be written as [85]

$$\begin{aligned}\mathbb{E}_{q(\tau)}[\tau] &= \frac{N+1}{-2(\sum_{i=1}^{N} x_i)\mathbb{E}_{q(\mu)}[\mu] + N\mathbb{E}_{q(\mu)}[\mu^2] + \sum_{i=1}^{N} x_i^2} \\ &\approx \frac{1}{-2(\frac{1}{N}\sum_{i=1}^{N} x_i)\mathbb{E}_{q(\mu)}[\mu] + \mathbb{E}_{q(\mu)}[\mu^2] + \frac{1}{N}\sum_{i=1}^{N} x_i^2}.\end{aligned} \tag{5.3.18}$$

If we also let the first moment of the mean, $\mathbb{E}_{q(\mu)}[\mu]$ be represented as

$$\begin{aligned}\mathbb{E}_{q(\mu)}[\mu] &= \mu_N \\ &\approx \frac{\sum_{i=1}^{N} x_i}{N} = \bar{x},\end{aligned} \tag{5.3.19}$$

then, (5.3.18) becomes

$$\mathbb{E}_{q(\tau)}[\tau] = \frac{1}{-2\bar{x}\mathbb{E}_{q(\mu)}[\mu] + \mathbb{E}_{q(\mu)}[\mu^2] + \bar{x^2}}. \tag{5.3.20}$$

Further, if we use μ_N and λ_N as previously defined, we can write

$$\mathbb{E}_{q(\mu)}[(\mu - \mu_N)^2] = \frac{1}{\lambda_N} \tag{5.3.21}$$

such that

$$\mathbb{E}_{q(\mu)}[(\mu^2 - 2\mu\mu_N) + \mu_N^2] = \frac{1}{N\mathbb{E}_{q(\tau)}[\tau]} \tag{5.3.22}$$

from where the second moment, $\mathbb{E}_{q(\mu)}[\mu^2]$ can be derived as [85]

$$\begin{aligned}\mathbb{E}_{q(\mu)}[\mu^2] &= 2\mu_N\mathbb{E}_{q(\mu)}[\mu] - \mu_N^2 + \frac{1}{N\mathbb{E}_{q(\tau)}[\tau]} \\ &= \bar{x}^2 + \frac{1}{N\mathbb{E}_{q(\tau)}[\tau]}.\end{aligned} \tag{5.3.23}$$

These moments can now be substituted into (5.3.20) to obtain

$$\mathbb{E}_{q(\tau)}[\tau] = \frac{1}{-\bar{x}^2 + \frac{1}{N\mathbb{E}_{q(\tau)}[\tau]} + \bar{x^2}} \tag{5.3.24}$$

from where the expected value of the precision, $\mathbb{E}_{q(\tau)}[\tau]$ is derived as

$$\begin{aligned}\mathbb{E}_{q(\tau)}[\tau] &= \frac{N-1}{N(\bar{x^2} - \bar{x}^2)} \\ &= \frac{N-1}{\sum_{i=1}^{N}(x_i - \bar{x})^2}.\end{aligned} \tag{5.3.25}$$

It is clearly seen from (5.3.25) that the Bayesian solution yields an unbiased estimate of the sample variance (recall that, $\tau = \frac{1}{\sigma^2}$) as against the biased estimate produced by the maximum likelihood approach. In the following section, an extension of this variational inference technique to multivariate Gaussian is considered to demonstrate its applicability for solving the GMM spectrum sensing problem. In particular, the focus is on scenarios involving multi-antenna SUs and multiple PUs.

5.4 Variational Bayesian Learning for GMM

The problem of detecting spectrum holes under multiple PU conditions is considered. In particular, wideband spectrum sensing problem is considered where the entire band is sub-divided into multiple sub-bands, each sub-band is occupied by individual PU and all sub-bands are being monitored simultaneously. In this case, the task is to determine the actual number of active PUs at any point in time. Let us assume that there are P PUs in the network and that the SU device is equipped with M antennas while operating in the coverage areas of the PUs. When the PUs are transmitting, the received signal vector for the p-th sub-band can be expressed as

$$\mathbf{x}(n) = \boldsymbol{\phi}_p s_p(n) + \boldsymbol{\eta}(n), n = 0, 1, 2 \cdots \tag{5.4.1}$$

where the vector $\boldsymbol{\phi}_p$ represents the channel gain between the p-th PU and all the antennas of the SU and is assumed to be different for each PU. During the sensing interval, the energy of the signal received at the m-th antenna of the SU can be estimated as

$$x_{e_m} = \frac{1}{N_s} \sum_{n=1}^{N_s} |x_m(n)|^2, \tag{5.4.2}$$

where $x_m(n)$ is n-th sample of the signal received at the m-th antenna. The joint probability distribution of the M dimensional energy vector of continuous random variables, $\mathbf{x}_{e_i} = [x_{e_1}, x_{e_2}, \cdots, x_{e_M}]^T$ at the terminal of the SU during the sensing interval, can be treated as a multivariate Gaussian whose PDF can be written as

$$\begin{aligned} f(x_{e_1}, x_{e_2}, \cdots, x_{e_M}) &= \mathcal{N}(\mathbf{x}|\boldsymbol{\mu}, \Sigma) \\ &= \frac{1}{(2\pi)^{M/2}} \frac{1}{|\Sigma|^{1/2}} \exp\big(-\frac{1}{2}(\mathbf{x}-\boldsymbol{\mu})^T \Sigma^{-1}(\mathbf{x}-\boldsymbol{\mu})\big) \end{aligned} \tag{5.4.3}$$

with M dimensional mean vector, $\boldsymbol{\mu}$ and $M \times M$ covariance matrix, Σ whose determinant is $|\Sigma|$.

5.4.1 Spectrum Sensing Data Clustering Based on VBGMM

Based on the premise established above, if we assume that there are N realizations of the observed energy vector, $\mathbf{x}_{e_i}$ comprising of individual energy measurement at the SU antennas under hypotheses H_1 and H_0 for all sub-bands, the data set can be represented as a $M \times N$ matrix, $\boldsymbol{X}$ whose elements are mixture of Gaussians and each column belongs to a particular Gaussian component (cluster). The aim is to blindly determine the number of clusters present in $\boldsymbol{X}$ and also estimate the Gaussian parameters of each cluster for the purpose of classifying new data points. Now, the VBGMM learning framework will be applied by constructing an analytical approximation to the posterior probability of the set of latent variables and parameters, given some observed data, $\boldsymbol{X}$. For simplicity, let $\mathbf{x}_{e_i} = \mathbf{x} \in R^M$ such that $\boldsymbol{X} = \{\mathbf{x}_1, \cdots, \mathbf{x}_N\}$ with corresponding latent variables $K \times N$ matrix, $\boldsymbol{\Theta} = \{\boldsymbol{\theta}_1, \cdots, \boldsymbol{\theta}_N\}$, mixing proportion, $\boldsymbol{\alpha} = \{\alpha_1, \cdots, \alpha_K\}$, means, $\boldsymbol{\mu} = \{\boldsymbol{\mu}_1, \cdots, \boldsymbol{\mu}_K\}$ and covariances, $\boldsymbol{\Sigma} = \{\Sigma_1, \cdots, \Sigma_K\}$, assuming $\boldsymbol{X}$ contains K Gaussian components. The distribution of $\boldsymbol{X}$ takes the

form [46], [86]

$$p(\boldsymbol{X}) = \sum_{k=1}^{K} \alpha_k \mathcal{N}(\boldsymbol{X}|\boldsymbol{\mu}_k, \Sigma_k) \tag{5.4.4}$$

where $0 \leq \alpha_k \leq 1$ and $\sum_{k=1}^{K} \alpha_k = 1$.

In general, the conditional distribution of $\boldsymbol{\Theta}$ given parameter $\boldsymbol{\alpha}$ can be expressed as

$$p(\boldsymbol{\Theta}|\boldsymbol{\alpha}) = \prod_{i=1}^{N} \prod_{k=1}^{K} \alpha_k^{\theta_{ik}} \tag{5.4.5}$$

where for every data point $\mathbf{x}_i$, there is a latent variable θ_i consisting a $1-of-K$ binary vector whose elements are θ_{ik}, $k = 1, \cdots, K$, while the conditional distribution of observed data $\boldsymbol{X}$ given latent variables $\boldsymbol{\Theta}$ and parameters $\boldsymbol{\mu}$ and $\boldsymbol{\Lambda}$ is given as

$$p(\boldsymbol{X}|\boldsymbol{\Theta}, \boldsymbol{\mu}, \boldsymbol{\Lambda}) = \prod_{i=1}^{N} \prod_{k=1}^{K} \mathcal{N}(\mathbf{x}_i|\boldsymbol{\mu}_k, \Lambda_k^{-1})^{\theta_{ik}} \tag{5.4.6}$$

where the precision, $\Lambda_k = \Sigma_k^{-1}$ has been used for mathematical conveniences. Next, appropriate priors have to be chosen for the model parameters $\boldsymbol{\mu}$, $\boldsymbol{\Lambda}$ and $\boldsymbol{\alpha}$ and also distributions have to be carefully assign to these priors. So, for the mixing proportion $\boldsymbol{\alpha}$, the Dirichlet distribution is assigned so that [46]

$$p(\boldsymbol{\alpha}) = Dir(\boldsymbol{\alpha}|\boldsymbol{\psi}) = \frac{\Gamma(\sum_{k=1}^{K} \psi_k)}{\prod_{k=1}^{K} \Gamma(\psi_k)} \prod_{k=1}^{K} \alpha_k^{\psi_k - 1} \tag{5.4.7}$$

where the hyperparameters $\boldsymbol{\psi}$ control the influence of the prior on the posterior distribution and the term $\Gamma(\cdot)$ implies the Gamma function, $\Gamma(z) = \int_0^\infty t^{z-1} \exp(-t) dt$. For the mean and precision of each Gaussian component, a Gaussian-Wishart prior is assigned defined by [46], [82]

$$\begin{aligned} p(\boldsymbol{\mu}, \boldsymbol{\Lambda}) &= p(\boldsymbol{\mu}|\boldsymbol{\Lambda}) p(\boldsymbol{\Lambda}) \\ &= \prod_{k=1}^{K} \mathcal{N}(\boldsymbol{\mu}_k|\boldsymbol{m}_0, (\tau_0 \Lambda_k)^{-1}) \mathcal{W}(\Lambda_k|\boldsymbol{W}_0, \xi_0) \end{aligned} \tag{5.4.8}$$

where

$$\mathcal{W}(\Lambda|\boldsymbol{W},\xi) = \boldsymbol{B}(\boldsymbol{W},\xi)|\Lambda|^{(\frac{\xi-M-1}{2})}\exp\big(-\frac{1}{2}Tr(\boldsymbol{W}^{-1}\Lambda)\big) \tag{5.4.9}$$

$$\boldsymbol{B}(\boldsymbol{W},\xi) = |\boldsymbol{W}|^{-\frac{\xi}{2}}(2^{\frac{\xi M}{2}}\alpha^{\frac{M(M-1)}{4}}\prod_{i=1}^{M}\Gamma(\frac{\xi+1-i}{2}))^{-1} \tag{5.4.10}$$

and $\boldsymbol{m}_0$, τ_0, $\boldsymbol{W}_0$ and ξ_0 are the parameters of the prior. It should be noted, though, that the conjugate prior distribution in (5.4.8) captures models with unknown mean and precision and the choice in both cases is done in such a way that the resulting posterior distributions would have the same functional form as the priors, thereby making the analysis simpler.

By using the priors defined above, the joint probability distribution of the entire model can be written as

$$p(\boldsymbol{X},\boldsymbol{\Theta},\boldsymbol{\alpha},\boldsymbol{\mu},\boldsymbol{\Lambda}) = p(\boldsymbol{X}|\boldsymbol{\Theta},\boldsymbol{\mu},\boldsymbol{\Lambda})p(\boldsymbol{\Theta}|\boldsymbol{\alpha})p(\boldsymbol{\alpha})p(\boldsymbol{\mu}|\boldsymbol{\Lambda})p(\boldsymbol{\Lambda}) \tag{5.4.11}$$

and at this point it is convenient to consider a variational approximation solution to the model for our spectrum sensing problem. To do this, similar to (5.3.6) we will use factorized distribution approach such that the variational distribution of the latent variables and parameters can be factorized as

$$q(\boldsymbol{\Theta},\boldsymbol{\alpha},\boldsymbol{\mu},\boldsymbol{\Lambda}) = q(\boldsymbol{\Theta})q(\boldsymbol{\alpha},\boldsymbol{\mu},\boldsymbol{\Lambda}). \tag{5.4.12}$$

From (5.2.10), the optimal solution for $q(\boldsymbol{\Theta})$ can be obtained as

$$\ln q^*(\boldsymbol{\Theta}) = \mathbb{E}_{\boldsymbol{\alpha},\boldsymbol{\mu},\boldsymbol{\Lambda}}\big[\ln p(\boldsymbol{X},\boldsymbol{\Theta},\boldsymbol{\alpha},\boldsymbol{\mu},\boldsymbol{\Lambda})\big] + constant. \tag{5.4.13}$$

If we let the terms not dependent on $\boldsymbol{\Theta}$ be factored into the constant term,

(5.4.13) can be written as

$$\begin{aligned}
\ln q^*(\boldsymbol{\Theta}) &= \mathbb{E}_{\boldsymbol{\alpha},\boldsymbol{\mu},\boldsymbol{\Lambda}}\big[\ln p(\boldsymbol{X}|\boldsymbol{\Theta},\boldsymbol{\mu},\boldsymbol{\Lambda}) + \ln p(\boldsymbol{\Theta}|\boldsymbol{\alpha})p(\boldsymbol{\alpha})\big] + constant \\
&= \mathbb{E}_{\boldsymbol{\alpha},\boldsymbol{\mu},\boldsymbol{\Lambda}}\big[\sum_{i=1}^{N}\sum_{k=1}^{K}\theta_{ik}\{\ln\mathcal{N}(\mathbf{x}_i|\boldsymbol{\mu}_k,\Lambda_k^{-1}) + \ln\alpha_k\}\big] + constant \\
&= \mathbb{E}_{\boldsymbol{\alpha},\boldsymbol{\mu},\boldsymbol{\Lambda}}\Bigg[\sum_{i=1}^{N}\sum_{k=1}^{K}\theta_{ik}\Bigg\{\frac{1}{2}\ln|\Lambda_k| - \frac{M}{2}\ln 2\alpha - \frac{1}{2}(\mathbf{x}_i-\boldsymbol{\mu}_k)^T\Lambda_k(\mathbf{x}_i-\boldsymbol{\mu}_k) \\
&\qquad\qquad + \ln\alpha_k\Bigg\}\Bigg] + constant \\
&= \sum_{i=1}^{N}\sum_{k=1}^{K}\theta_{ik}\Bigg\{\frac{1}{2}\mathbb{E}_{\boldsymbol{\alpha},\boldsymbol{\mu},\boldsymbol{\Lambda}}[\ln|\Lambda_k|] - \frac{M}{2}\ln 2\alpha - \frac{1}{2}\mathbb{E}_{\boldsymbol{\alpha},\boldsymbol{\mu},\boldsymbol{\Lambda}}[(\mathbf{x}_i-\boldsymbol{\mu}_k)^T \\
&\qquad\qquad \Lambda_k(\mathbf{x}_i-\boldsymbol{\mu}_k)] + \mathbb{E}_{\boldsymbol{\alpha},\boldsymbol{\mu},\boldsymbol{\Lambda}}[\ln\alpha_k]\Bigg\} + constant \\
&= \sum_{i=1}^{N}\sum_{k=1}^{K}\theta_{ik}\Bigg\{\frac{1}{2}\mathbb{E}_{\Lambda_k}[\ln|\Lambda_k|] - \frac{M}{2}\ln 2\alpha - \frac{1}{2}\mathbb{E}_{\boldsymbol{\mu}_k,\boldsymbol{\Lambda}_k}[(\mathbf{x}_i-\boldsymbol{\mu}_k)^T \\
&\qquad\qquad \Lambda_k(\mathbf{x}_i-\boldsymbol{\mu}_k)] + \mathbb{E}_{\alpha_k}[\ln|\alpha_k|] + constant.
\end{aligned} \tag{5.4.14}$$

At this point, if we let

$$\ln\varphi_{ik} = \mathbb{E}_{\alpha_k}[\ln\alpha_k] + \frac{1}{2}\mathbb{E}_{\Lambda_k}[\ln|\Lambda_k|] - \frac{M}{2}\ln(2\alpha) - \frac{1}{2}\mathbb{E}_{\boldsymbol{\mu}_k,\Lambda_k}[(\mathbf{x}_i-\boldsymbol{\mu}_k)^T\Lambda_k(\mathbf{x}_i-\boldsymbol{\mu}_k)], \tag{5.4.15}$$

then, (5.4.14) may be re-written as

$$\ln q^*(\boldsymbol{\Theta}) = \sum_{i=1}^{N}\sum_{k=1}^{K}\theta_{ik}\ln\varphi_{ik} + constant \tag{5.4.16}$$

so that if we take the exponential of both sides,

$$q^*(\boldsymbol{\Theta}) \propto \prod_{i=1}^{N}\prod_{k=1}^{K}\varphi_{ik}^{\theta_{ik}}. \tag{5.4.17}$$

If $r_{ik} = \frac{\varphi_{ik}}{\sum_{j=1}^{K}\varphi_{ij}}$ is the responsibility that cluster k takes for explaining data point $\mathbf{x}_i$ subject to the requirement that the parameters, θ_{ik} sum up to one

over all $k = 1, \cdots, K$, then we can write

$$q^*(\boldsymbol{\Theta}) = \prod_{i=1}^{N} \prod_{k=1}^{K} r_{ik}^{\theta_{ik}} \tag{5.4.18}$$

and

$$q^*(\theta_i) = \prod_{k=1}^{K} r_{ik}^{\theta_{ik}} \tag{5.4.19}$$

and the expectation of $q^*(\theta i)$ can be extracted as [86]

$$\mathbb{E}_{q^*(\theta_{ik})}[\theta_{ik}] = r_{ik}. \tag{5.4.20}$$

By following similar approach, the optimal value of the second term $q(\boldsymbol{\alpha}, \boldsymbol{\mu}, \boldsymbol{\Lambda})$, in (5.4.12) can be derived as

$$\begin{aligned}
q^*(\boldsymbol{\alpha}, \boldsymbol{\mu}, \boldsymbol{\Lambda}) &= \mathbb{E}_{\Theta}\big[\ln p(\boldsymbol{X}, \boldsymbol{\Theta}, \boldsymbol{\alpha}, \boldsymbol{\mu}, \boldsymbol{\Lambda})\big] + constant \\
&= \mathbb{E}_{\Theta}\big[\ln p(\boldsymbol{X}|\boldsymbol{\Theta}, \boldsymbol{\alpha}, \boldsymbol{\mu}, \boldsymbol{\Lambda}) + \ln p(\boldsymbol{\Theta}|\boldsymbol{\alpha})\big] + \ln p(\boldsymbol{\alpha}) + \ln p(\boldsymbol{\mu}|\boldsymbol{\Lambda}) + \\
&\qquad \ln p(\boldsymbol{\Lambda}) + constant \\
&= \mathbb{E}_{\Theta}\big[\sum_{i=1}^{N}\sum_{k=1}^{K} \theta_{ik}\{\ln \mathcal{N}(\mathbf{x}_i|\boldsymbol{\mu}_k, \Lambda_k^{-1}) + \ln \alpha_k\}\big] + \ln p(\boldsymbol{\alpha}) + \ln p(\boldsymbol{\mu}|\boldsymbol{\Lambda}) \\
&\qquad + \ln p(\boldsymbol{\Lambda}) + constant \\
&= \sum_{i=1}^{N}\sum_{k=1}^{K} \mathbb{E}_{\theta_{ik}}[\theta_{ik}] \ln \mathcal{N}(\mathbf{x}_i|\boldsymbol{\mu}_k, \Lambda_k^{-1}) + \sum_{i=1}^{N}\sum_{k=1}^{K} \mathbb{E}_{\theta_{ik}}[\theta_{ik}] \ln \alpha_k + \\
&\ln Dir(\boldsymbol{\alpha}|\psi_0) + \sum_{k=1}^{K} \ln \mathcal{N}(\boldsymbol{\mu}_k|\boldsymbol{m}_0, (\tau_0\Lambda_k)^{-1}) + \sum_{k=1}^{K} \mathcal{W}(\Lambda_k|\boldsymbol{W}_0, \xi_0) \\
&\qquad + constant.
\end{aligned} \tag{5.4.21}$$

However, the variational posterior distribution, $q(\boldsymbol{\alpha}, \boldsymbol{\mu}, \boldsymbol{\Lambda})$, whose optimal value is given in (5.4.21) can also be factorized as

$$q(\boldsymbol{\alpha}, \boldsymbol{\mu}, \boldsymbol{\Lambda}) = q(\boldsymbol{\alpha}) \prod_{k=1}^{K} q(\boldsymbol{\mu}_k, \Lambda_k) \tag{5.4.22}$$

which means that

$$q^*(\boldsymbol{\alpha}, \boldsymbol{\mu}, \boldsymbol{\Lambda}) = \ln q^*(\boldsymbol{\alpha}) + \sum_{k=1}^{K} \ln q^*(\boldsymbol{\mu}_k, \Lambda_k). \tag{5.4.23}$$

Therefore, by comparing (5.4.21) and (5.4.23), and extracting the terms containing $\boldsymbol{\alpha}$, we can write

$$\begin{aligned}
\ln q^*(\boldsymbol{\alpha}) &= \ln Dir(\boldsymbol{\alpha}|\psi_0) + \sum_{i=1}^{N}\sum_{k=1}^{K} \mathbb{E}_{\theta_{ik}}[\theta_{ik}] \ln \alpha_k \\
&= \sum_{k=1}^{K} (\psi_0 - 1) \ln \alpha_k + \sum_{i=1}^{N}\sum_{k=1}^{K} \mathbb{E}_{\theta_{ik}}[\theta_{ik}] \ln \alpha_k + constant \\
&= \sum_{k=1}^{K} \left[(\psi_0 - 1) + \sum_{i=1}^{N} r_{ik} \right] \ln \alpha_k + constant
\end{aligned} \tag{5.4.24}$$

If we take the exponential of both sides of (5.4.24), the optimal value of variational distribution over the mixing ratio can then be written as

$$q^*(\boldsymbol{\alpha}) \propto \prod_{k=1}^{K} \ln \alpha_k^{\psi_0 + \sum_{i=1}^{N} r_{ik} - 1}. \tag{5.4.25}$$

Thus, the optimal solution for $q(\boldsymbol{\alpha})$ is obtained as

$$q^*(\boldsymbol{\alpha}) = Dir(\boldsymbol{\alpha}|\boldsymbol{\psi}) = Dir(\boldsymbol{\alpha}|\psi_1, \psi_2, \cdots, \psi_K) \tag{5.4.26}$$

where each component, $\psi_k \in \boldsymbol{\psi}$ is defined as $\psi_k = \psi_0 + N_k$, where $N_k = \sum_{i=1}^{N} r_{ik}$. The remaining factor in the variational posterior distribution of (5.4.21) is $q(\boldsymbol{\mu}_k, \Lambda_k)$ and its optimal value can be obtained by comparing

(5.4.21) and (5.4.23), and extracting the terms containing $\boldsymbol{\mu}_k$ and Λ_k as

$$
\begin{aligned}
\ln q^*(\boldsymbol{\mu}_k, \Lambda_k) &= \ln \mathcal{N}(\boldsymbol{\mu}_k | \boldsymbol{m}_0, (\tau_0 \Lambda_k)^{-1}) + \\
&\quad \ln \mathcal{W}(\Lambda_k | \boldsymbol{W}_0, \xi_0) + \sum_{i=1}^{N} \mathbb{E}_{\theta_{ik}}[\theta_{ik}] \ln \mathcal{N}(\mathbf{x}_i | \boldsymbol{\mu}_k, \Lambda_k^{-1}) + constant \\
&= -\frac{1}{2}(\boldsymbol{\mu}_k - \boldsymbol{m}_0)^T \tau_0 \Lambda_k (\boldsymbol{\mu}_k - \boldsymbol{m}_0) + \frac{1}{2} \ln |\tau_0 \Lambda_k| - \frac{M}{2} \ln(2\boldsymbol{\alpha}) \\
&\quad + \frac{\xi_0 - M - 1}{2} \ln |\Lambda_k| - \frac{1}{2} Tr(\boldsymbol{W}_0^{-1} \Lambda_k) + \\
&\quad \sum_{i=1}^{N} \mathbb{E}_{\theta_{ik}}[\theta_{ik}] \Big\{ -\frac{1}{2}(\mathbf{x}_i - \boldsymbol{\mu}_k)^T \Lambda_k (\mathbf{x}_i - \boldsymbol{\mu}_k) + \\
&\quad \frac{1}{2} \ln |\Lambda_k| - \frac{M}{2} \ln(2\boldsymbol{\alpha}) \Big\} + constant \\
&= -\frac{\tau_0}{2}(\boldsymbol{\mu}_k - \boldsymbol{m}_0)^T \Lambda_k (\boldsymbol{\mu}_k - \boldsymbol{m}_0) - \\
&\quad \frac{1}{2} \sum_{i=1}^{N} \mathbb{E}_{\theta_{ik}}[\theta_{ik}] (\mathbf{x}_i - \boldsymbol{\mu}_k)^T \Lambda_k (\mathbf{x}_i - \boldsymbol{\mu}_k) + \frac{1}{2} \ln |\Lambda_k| + \\
&\quad \frac{\xi_0 - M - 1}{2} \ln |\Lambda_k| + \frac{1}{2} \sum_{i=1}^{N} \mathbb{E}_{\theta_{ik}}[\theta_{ik}] \ln |\Lambda_k| - \frac{1}{2} Tr(\boldsymbol{W}_0^{-1} \Lambda_k) - \\
&\quad \frac{M}{2} \ln(2\boldsymbol{\alpha}) + \frac{1}{2} \ln |\tau_0| - \frac{M}{2} \mathbb{E}_{\theta_{ik}}[\theta_{ik}] \ln(2\boldsymbol{\alpha}) + constant \\
&= -\frac{\tau_0}{2} \big[\boldsymbol{\mu}_k^T \Lambda_k \boldsymbol{\mu}_k - 2\boldsymbol{\mu}_k^T \Lambda_k \boldsymbol{m}_0 + \boldsymbol{m}_0^T \Lambda_k \boldsymbol{m}_0 \big] - \frac{1}{2} \sum_{i=1}^{N} \mathbb{E}_{\theta_{ik}}[\theta_{ik}] \\
&\quad \big[\mathbf{x}_i^T \Lambda_k \mathbf{x}_i - 2\mathbf{x}_i^T \Lambda_k \boldsymbol{\mu}_k + \boldsymbol{\mu}_k^T \Lambda_k \boldsymbol{\mu}_k \big] + \frac{1}{2} \ln |\Lambda_k| + \frac{\xi_0 - M - 1}{2} \\
&\quad \ln |\Lambda_k| + \frac{1}{2} \sum_{i=1}^{N} \mathbb{E}_{\theta_{ik}}[\theta_{ik}] \ln |\Lambda_k| - \frac{1}{2} Tr(\boldsymbol{W}_0^{-1} \Lambda_k) + constant.
\end{aligned}
\tag{5.4.27}
$$

To simplify (5.4.27), we will factorize the optimal solution for the joint variational posterior, $q^*(\boldsymbol{\mu}_k, \Lambda_k)$ as

$$
q^*(\boldsymbol{\mu}_k, \Lambda_k) = q^*(\boldsymbol{\mu}_k | \Lambda_k) q^*(\Lambda_k) \tag{5.4.28}
$$

and draw comparison between the terms and (5.4.27). If we first deal with

$\ln q^*(\boldsymbol{\mu}_k|\Lambda_k)$ by considering all terms that contain $\boldsymbol{\mu}_k$, we will have

$$
\begin{aligned}
\ln q^*(\boldsymbol{\mu}_k|\Lambda_k) &= -\frac{\tau_0}{2}\Big[\boldsymbol{\mu}_k^T\Lambda_k(\boldsymbol{\mu}_k-\boldsymbol{m}_0)-\boldsymbol{m}_0^T\Lambda_k\boldsymbol{\mu}_k\Big]- \\
&\qquad \frac{1}{2}\sum_{i=1}^{N}\mathbb{E}_{\theta_{ik}}[\theta_{ik}]\Big\{-\boldsymbol{\mu}_k^T\Lambda_k(\mathbf{x}_i-\boldsymbol{\mu}_k)-\mathbf{x}_i^T\Lambda_k\boldsymbol{\mu}_k\Big\}+constant \\
&= -\frac{\beta_0}{2}\Big[\boldsymbol{\mu}_k^T\Lambda_k\boldsymbol{\mu}_k-\boldsymbol{\mu}_k^T\Lambda_k\boldsymbol{m}_0-\boldsymbol{m}_0^T\Lambda_k\boldsymbol{\mu}_k\Big]- \\
&\qquad \frac{1}{2}\sum_{i=1}^{N}\mathbb{E}_{\theta_{ik}}[\theta_{ik}]\Big\{\boldsymbol{\mu}_k^T\Lambda_k\boldsymbol{\mu}_k-\boldsymbol{\mu}_k^T\Lambda_k\mathbf{x}_i-\mathbf{x}_i^T\Lambda_k\boldsymbol{\mu}_k\Big\}+constant \\
&= -\frac{\tau_0}{2}\big[\boldsymbol{\mu}_k^T\Lambda_k\boldsymbol{\mu}_k-2\boldsymbol{\mu}_k^T\Lambda_k\boldsymbol{m}_0\big]- \\
&\qquad \frac{1}{2}\sum_{i=1}^{N}\mathbb{E}_{\theta_{ik}}[\theta_{ik}]\big\{\boldsymbol{\mu}_k^T\Lambda_k\boldsymbol{\mu}_k-2\boldsymbol{\mu}_k^T\Lambda_k\mathbf{x}_i\big\}+constant \\
&= -\frac{1}{2}(\tau_0+\sum_{i=1}^{N}\mathbb{E}_{\theta_{ik}}[\theta_{ik}])\boldsymbol{\mu}_k^T\Lambda_k\boldsymbol{\mu}_k+ \\
&\qquad \boldsymbol{\mu}_k^T\Lambda_k\Big\{\tau_0\boldsymbol{m}_0+\sum_{i=1}^{N}\mathbb{E}_{\theta_{ik}}[\theta_{ik}]\mathbf{x}_i\Big\}+constant \\
&= -\frac{1}{2}(\tau_0+\sum_{i=1}^{N}r_{ik})\boldsymbol{\mu}_k^T\Lambda_k\boldsymbol{\mu}_k+\boldsymbol{\mu}_k^T\Lambda_k\Big\{\tau_0\boldsymbol{m}_0+\sum_{i=1}^{N}r_{ik}\mathbf{x}_i\Big\}+constant \\
&= -\frac{1}{2}(\tau_0+\sum_{i=1}^{N}r_{ik})\Big\{\boldsymbol{\mu}_k^T\Lambda_k\boldsymbol{\mu}_k-2\boldsymbol{\mu}_k^T\Lambda_k\big\{\tau_0\boldsymbol{m}_0+\sum_{i=1}^{N}r_{ik}\mathbf{x}_i\big\} \\
&\qquad (\tau_0+\sum_{i=1}^{N}r_{ik})^{-1}\Big\}+constant \\
&= -\frac{1}{2}(\tau_0+\sum_{i=1}^{N}r_{ik})\big\{(\boldsymbol{\mu}_k-\boldsymbol{m}_k)^T\Lambda_k(\boldsymbol{\mu}_k-\boldsymbol{m}_k)-\boldsymbol{m}_k^T\Lambda_k\boldsymbol{m}_k\big\} \\
&\qquad +constant \\
&= -\frac{1}{2}(\boldsymbol{\mu}_k-\boldsymbol{m}_k)^T(\tau_0+\sum_{i=1}^{N}r_{ik})\Lambda_k(\boldsymbol{\mu}_k-\boldsymbol{m}_k)+ \\
&\qquad \frac{1}{2}\boldsymbol{m}_k^T(\tau_0+\sum_{i=1}^{N}r_{ik})\Lambda_k\boldsymbol{m}_k+constant \\
&= -\frac{1}{2}(\boldsymbol{\mu}_k-\boldsymbol{m}_k)^T\tau_k\Lambda_k(\boldsymbol{\mu}_k-\boldsymbol{m}_k)+constant. \qquad (5.4.29)
\end{aligned}
$$

By taking the exponential of both sides of (5.4.29), we can infer that

$$q^*(\boldsymbol{\mu}_k|\Lambda_k) = \mathcal{N}(\boldsymbol{\mu}_k|\boldsymbol{m}_k, (\tau_k\Lambda_k)^{-1}) \tag{5.4.30}$$

where

$$\tau_k = \tau_0 + N_k \tag{5.4.31}$$

$$\begin{aligned}\boldsymbol{m}_k &= \{\tau_0\boldsymbol{m}_0 + \sum_{i=1}^{N} r_{ik}\mathbf{x}_i\}(\tau_0 + \sum_{i=1}^{N} r_{ik})^{-1} \\ &= \frac{1}{\tau_k}(\tau_0\boldsymbol{m}_0 + N_k\bar{\mathbf{x}}_k)\end{aligned} \tag{5.4.32}$$

and in (5.4.32), $\bar{\mathbf{x}}_k = \frac{1}{N_k}\sum_{i=1}^{N} r_{ik}\mathbf{x}_i$ has been used. Similarly, from (5.4.27) we can extract the terms corresponding to $q^*\Lambda_k$ as

$$\begin{aligned}\ln q^*\Lambda_k &= \ln q^*(\boldsymbol{\mu}_k, \Lambda_k) - \ln q^*(\boldsymbol{\mu}_k|\Lambda_k) \\ &= -\frac{\tau_0}{2}(\boldsymbol{\mu}_k - \boldsymbol{m}_0)^T\Lambda_k(\boldsymbol{\mu}_k - \boldsymbol{m}_0) - \frac{1}{2}\sum_{i=1}^{N}\mathbb{E}_{\theta_{ik}}[\theta_{ik}](\mathbf{x}_i - \boldsymbol{\mu}_k)^T\Lambda_k(\mathbf{x}_i - \boldsymbol{\mu}_k) \\ &\quad + \frac{1}{2}\ln|\Lambda_k| + \frac{\xi_0 - M - 1}{2}\ln|\Lambda_k| + \frac{1}{2}\sum_{i=1}^{N}\mathbb{E}_{\theta_{ik}}[\theta_{ik}]\ln|\Lambda_k| - \frac{1}{2}Tr(\boldsymbol{W}_0^{-1}\Lambda_k) \\ &\quad + \frac{1}{2}(\boldsymbol{\mu}_k - \boldsymbol{m}_k)^T\tau_k\Lambda_k(\boldsymbol{\mu}_k - \boldsymbol{m}_k) - \frac{1}{2}\ln|\Lambda_k| + constant \\ &= -\frac{\tau_0}{2}(\boldsymbol{\mu}_k - \boldsymbol{m}_0)^T\Lambda_k(\boldsymbol{\mu}_k - \boldsymbol{m}_0) - \frac{1}{2}\sum_{i=1}^{N}\mathbb{E}_{\theta_{ik}}[\theta_{ik}](\mathbf{x}_i - \boldsymbol{\mu}_k)^T\Lambda_k(\mathbf{x}_i - \boldsymbol{\mu}_k) \\ &\quad + \frac{1}{2}(\boldsymbol{\mu}_k - \boldsymbol{m}_k)^T\tau_k\Lambda_k(\boldsymbol{\mu}_k - \boldsymbol{m}_k) + \frac{1}{2}\big((\xi_0 - M - 1) + \sum_{i=1}^{N}\mathbb{E}_{\theta_{ik}}[\theta_{ik}]\big)\ln|\Lambda_k| \\ &\quad - \frac{1}{2}Tr(\boldsymbol{W}_0^{-1}\Lambda_k) + constant \\ &= -\frac{1}{2}Tr[\tau_0(\boldsymbol{\mu}_k - \boldsymbol{m}_0)(\boldsymbol{\mu}_k - \boldsymbol{m}_0)^T\Lambda_k] - \frac{1}{2}Tr[\sum_{i=1}^{N}\mathbb{E}_{\theta_{ik}}[\theta_{ik}](\mathbf{x}_i - \boldsymbol{\mu}_k)(\mathbf{x}_i - \boldsymbol{\mu}_k)^T] \\ &\quad + \frac{1}{2}Tr[\tau_k(\boldsymbol{\mu}_k - \boldsymbol{m}_k)(\boldsymbol{\mu}_k - \boldsymbol{m}_k)^T\Lambda_k] + \frac{1}{2}\big(\sum_{i=1}^{N}\mathbb{E}_{\theta_{ik}}[\theta_{ik}] + \xi_0 - M - 1\big)\ln|\Lambda_k| \\ &\quad - \frac{1}{2}Tr(\boldsymbol{W}_0^{-1}\Lambda_k) + constant.\end{aligned} \tag{5.4.33}$$

Further simplification of (5.4.33) leads to

$$\begin{aligned}\ln q^*\Lambda_k = &-\frac{1}{2}Tr[\{\boldsymbol{W}_0^{-1} + \tau_0(\boldsymbol{\mu}_k - \boldsymbol{m}_0)(\boldsymbol{\mu}_k - \boldsymbol{m}_0)^T + \\ &\sum_{i=1}^{N}\mathbb{E}_{\theta_{ik}}[\theta_{ik}](\mathbf{x}_i - \boldsymbol{\mu}_k)(\mathbf{x}_i - \boldsymbol{\mu}_k)^T - \tau_k(\boldsymbol{\mu}_k - \boldsymbol{m}_k)(\boldsymbol{\mu}_k - \boldsymbol{m}_k)^T\}\Lambda_k] + \\ &\frac{1}{2}\big(\sum_{i=1}^{N}\mathbb{E}_{\theta_{ik}}[\theta_{ik}] + \xi_0 - M - 1\big)\ln|\Lambda_k| + constant \\ = &\frac{1}{2}\big(\xi_k - M - 1\big)\ln|\Lambda_k| - \frac{1}{2}Tr[\boldsymbol{W}_k^{-1}\Lambda_k] + constant \end{aligned} \tag{5.4.34}$$

and by taking the exponential of both sides, we readily see that $q^*\Lambda_k$ is Wishart distribution described as

$$q^*\Lambda_k = \mathcal{W}(\Lambda_k|\boldsymbol{W}_k, \xi_k) \tag{5.4.35}$$

where

$$\begin{aligned}\xi_k &= \sum_{i=1}^{N}\mathbb{E}_{\theta_{ik}}[\theta_{ik}] + \xi_0 \\ &= N_k + \xi_0,\ N_k = \sum_{i=1}^{N} r_{ik}\end{aligned} \tag{5.4.36}$$

and

$$\begin{aligned}
\boldsymbol{W}_k^{-1} &= \boldsymbol{W}_0^{-1} + \tau_0(\boldsymbol{\mu}_k - \boldsymbol{m}_0)(\boldsymbol{\mu}_k - \boldsymbol{m}_0)^T + \\
&\qquad \sum_{i=1}^{N} \mathbb{E}_{\theta_{ik}}[\theta_{ik}](\mathbf{x}_i - \boldsymbol{\mu}_k)(\mathbf{x}_i - \boldsymbol{\mu}_k)^T - \tau_k(\boldsymbol{\mu}_k - \boldsymbol{m}_k)(\boldsymbol{\mu}_k - \boldsymbol{m}_k)^T \\
&= \boldsymbol{W}_0^{-1} + \tau_0\boldsymbol{\mu}_k\boldsymbol{\mu}_k^T - \tau_0\boldsymbol{\mu}_k\boldsymbol{m}_0^T - \tau_0\boldsymbol{m}_0\boldsymbol{\mu}_k^T + \tau_0\boldsymbol{m}_0^T\boldsymbol{m}_0 + \\
&\qquad \sum_{i=1}^{N} \mathbb{E}_{\theta_{ik}}[\theta_{ik}](\mathbf{x}_i^T\mathbf{x}_i - \mathbf{x}_i\boldsymbol{\mu}_k^T - \boldsymbol{\mu}_k\mathbf{x}_i^T + \boldsymbol{\mu}_k^T\boldsymbol{\mu}_k) - \\
&\qquad \tau_k\boldsymbol{\mu}_k^T\boldsymbol{\mu}_k + \tau_k\boldsymbol{\mu}_k\boldsymbol{m}_k^T + \tau_k\boldsymbol{m}_k\boldsymbol{\mu}_k^T - \tau_k\boldsymbol{m}_k^T\boldsymbol{m}_k \\
&= \boldsymbol{W}_0^{-1} + (\tau_0 + \sum_{i=1}^{N} \mathbb{E}_{\theta_{ik}}[\theta_{ik}] - \tau_k)\boldsymbol{\mu}_k^T\boldsymbol{\mu}_k + \\
&\qquad \boldsymbol{\mu}_k\bigg(\tau_0\boldsymbol{m}_0^T - \sum_{i=1}^{N} \mathbb{E}_{\theta_{ik}}[\theta_{ik}]\mathbf{x}_i^T + \tau_k\boldsymbol{m}_k^T\bigg) + \\
&\qquad\qquad \boldsymbol{\mu}_k\bigg(-\tau_0\boldsymbol{m}_0^T - \sum_{i=1}^{N} \mathbb{E}_{\theta_{ik}}[\theta_{ik}]\mathbf{x}_i^T + \tau_k\boldsymbol{m}_k^T\bigg) + \\
&\qquad\qquad\qquad \boldsymbol{\mu}_k^T\bigg(-\tau_0\boldsymbol{m}_0 - \sum_{i=1}^{N} \mathbb{E}_{\theta_{ik}}[\theta_{ik}]\mathbf{x}_i + \tau_k\boldsymbol{m}_k\bigg) \\
&\qquad + \tau_0\boldsymbol{m}_0^T\boldsymbol{m}_0 + \sum_{i=1}^{N} \mathbb{E}_{\theta_{ik}}[\theta_{ik}](\mathbf{x}_i^T\mathbf{x}_i) - \tau_k\boldsymbol{m}_k^T\boldsymbol{m}_k. \qquad (5.4.37)
\end{aligned}$$

However, we have that $\tau_0 + \sum_{i=1}^{N} \mathbb{E}_{\theta_{ik}}[\theta_{ik}] - \tau_k = 0$ and $-\tau_0\boldsymbol{m}_0^T - \sum_{i=1}^{N} \mathbb{E}_{\theta_{ik}}[\theta_{ik}]\mathbf{x}_i^T + \tau_k\boldsymbol{m}_k^T$ is zero vector. Therefore, (5.4.37) becomes

$$\boldsymbol{W}_k^{-1} = \boldsymbol{W}_0^{-1} + \tau_0\boldsymbol{m}_0^T\boldsymbol{m}_0 + \sum_{i=1}^{N} r_{ik}(\mathbf{x}_i^T\mathbf{x}_i) - \tau_k\boldsymbol{m}_k^T\boldsymbol{m}_k. \qquad (5.4.38)$$

It should be noted that both N_k and $\bar{\mathbf{x}}_k$ depend on r_{ik} which in turn depends on φ_{ik}. Therefore, it becomes necessary that φ_{ik} be known. Recall from (5.4.15) that φ_{ik} is defined logarithmically by [46], [86]

$$\ln\varphi_{ik} = \mathbb{E}_{\alpha_k}[\ln\alpha_k] + \frac{1}{2}\mathbb{E}_{\Lambda_k}[\ln|\Lambda_k|] - \frac{M}{2}\ln(2\alpha) - \frac{1}{2}\mathbb{E}_{\boldsymbol{\mu}_k,\Lambda_k}[(\mathbf{x}_i - \boldsymbol{\mu}_k)^T\Lambda_k(\mathbf{x}_i - \boldsymbol{\mu}_k)] \qquad (5.4.39)$$

which requires the knowledge of three expectations. Commencing with the

first expectation, $\mathbb{E}_{\alpha_k}[\ln \alpha_k]$, we know from (5.4.35) that $q^*\Lambda_k = \mathcal{W}(\Lambda_k|\boldsymbol{W}_k, \xi_k)$, then we can write that

$$\begin{aligned}\mathbb{E}_{\Lambda_k}[\ln|\Lambda_k|] &= \sum_{m=1}^{M} \digamma(\frac{\xi_k + 1 - m}{2}) + M\ln 2 + \ln|\boldsymbol{W}_k| \\ &\equiv \ln\tilde{\Lambda}_k \end{aligned} \tag{5.4.40}$$

where M is the dimensionality of each data point in $\boldsymbol{X}$ (number of SU's antennas) and $\digamma(y)$ is the digamma function $\equiv \frac{d}{dy}\ln\Gamma(y)$.

Similarly, the second expectation in (5.4.39) can be derived by employing the trace trick expressed as [86]

$$\begin{aligned}\bar{q}^T V \bar{q} &= Tr(\bar{q}^T V \bar{q}) \\ &= Tr(V\bar{q}\bar{q}^T) \end{aligned} \tag{5.4.41}$$

and

$$\begin{aligned}\mathbb{E}[\bar{q}^T V \bar{q}] &= \mathbb{E}[Tr(V\bar{q}\bar{q}^T)] \\ &= Tr(V\mathbb{E}[\bar{q}\bar{q}^T]). \end{aligned} \tag{5.4.42}$$

Using (5.4.41) and (5.4.42),

$$\begin{aligned}&\mathbb{E}_{\boldsymbol{\mu}_k,\Lambda_k}[(\mathbf{x}_i - \boldsymbol{\mu}_k)^T \cdot \\ &\Lambda_k(\mathbf{x}_i - \boldsymbol{\mu}_k)] = \int\int (\mathbf{x}_i - \boldsymbol{\mu}_k)^T \Lambda_k (\mathbf{x}_i - \boldsymbol{\mu}_k) q^*(\boldsymbol{\mu}_k|\Lambda_k) q^*(\Lambda_k) d\boldsymbol{\mu}_k d\Lambda_k \\ &= \int\int Tr[(\mathbf{x}_i - \boldsymbol{\mu}_k)^T \Lambda_k (\mathbf{x}_i - \boldsymbol{\mu}_k)] q^*(\boldsymbol{\mu}_k|\Lambda_k) q^*(\Lambda_k) d\boldsymbol{\mu}_k d\Lambda_k \\ &= \int\int Tr[\Lambda_k (\mathbf{x}_i - \boldsymbol{\mu}_k)(\mathbf{x}_i - \boldsymbol{\mu}_k)^T] q^*(\boldsymbol{\mu}_k|\Lambda_k) q^*(\Lambda_k) d\boldsymbol{\mu}_k d\Lambda_k \\ &= Tr\left[\Lambda_k \int \left\{ \int (\mathbf{x}_i - \boldsymbol{\mu}_k)(\mathbf{x}_i - \boldsymbol{\mu}_k)^T q^*(\boldsymbol{\mu}_k|\Lambda_k) \right\} d\boldsymbol{\mu}_k d\Lambda_k \right]. \end{aligned} \tag{5.4.43}$$

By using the trace trick, (5.4.43) can also be re-expressed as

$$\mathbb{E}_{\boldsymbol{\mu}_k,\Lambda_k}[(\mathbf{x}_i-\boldsymbol{\mu}_k)^T\Lambda_k(\mathbf{x}_i-\boldsymbol{\mu}_k)] = Tr\{\mathbb{E}_{\Lambda_k}[\Lambda_k\mathbb{E}_{\boldsymbol{\mu}_k|\Lambda_k}[(\mathbf{x}_i-\boldsymbol{\mu}_k)(\mathbf{x}_i-\boldsymbol{\mu}_k)^T]]\}. \tag{5.4.44}$$

Now in (5.4.43), we first deal with the inner expectation with respect to $\boldsymbol{\mu}_k|\Lambda_k$ which can be expressed as

$$\begin{aligned}\int (\mathbf{x}_i-\boldsymbol{\mu}_k)(\mathbf{x}_i-\boldsymbol{\mu}_k)^T\cdot & \\ q^*(\boldsymbol{\mu}_k|\Lambda_k)d\boldsymbol{\mu}_k &= \int (\mathbf{x}_i-\boldsymbol{\mu}_k)(\mathbf{x}_i-\boldsymbol{\mu}_k)^T\mathcal{N}(\boldsymbol{\mu}_k|\boldsymbol{m}_k,(\tau_k\Lambda_k)^{-1})d\boldsymbol{\mu}_k \\ &= \int [\mathbf{x}_i\mathbf{x}_i^T-\mathbf{x}_i\boldsymbol{\mu}_k^T-\boldsymbol{\mu}_k\mathbf{x}_i^T+\boldsymbol{\mu}_k\boldsymbol{\mu}_k^T] \\ &\qquad \mathcal{N}(\boldsymbol{\mu}_k|\boldsymbol{m}_k,(\tau_k\Lambda_k)^{-1})d\boldsymbol{\mu}_k \\ &= \mathbf{x}_i\mathbf{x}_i^T-\mathbf{x}_i\boldsymbol{m}_k^T-\boldsymbol{m}_k\mathbf{x}_i^T+\boldsymbol{m}_k\boldsymbol{m}_k^T+(\tau_k\Lambda_k)^{-1} \\ &= (\mathbf{x}_i-\boldsymbol{m}_k)(\mathbf{x}_i-\boldsymbol{m}_k)^T+(\tau_k\Lambda_k)^{-1}. \end{aligned} \tag{5.4.45}$$

It should be noted here that $\mathbb{E}_{\boldsymbol{\mu}_k|\Lambda_k}[\boldsymbol{\mu}_k]=\boldsymbol{m}_k$ and $\mathbb{E}_{\boldsymbol{\mu}_k|\Lambda_k}[\boldsymbol{\mu}_k\boldsymbol{\mu}_k^T]=\boldsymbol{m}_k\boldsymbol{m}_k^T+(\tau_k\Lambda_k)^{-1}$. Next, we substitute (5.4.45) into (5.4.44) and evaluate the outer expectation on the R.H.S with respect to Λ_k to obtain

$$\begin{aligned}\mathbb{E}_{\boldsymbol{\mu}_k,\Lambda_k}[(\mathbf{x}_i-\boldsymbol{\mu}_k)^T\Lambda_k(\mathbf{x}_i-\boldsymbol{\mu}_k)] &= Tr\{\mathbb{E}_{\Lambda_k}[\Lambda_k(\mathbf{x}_i-\boldsymbol{m}_k)(\mathbf{x}_i-\boldsymbol{m}_k)^T+\tau_k^{-1}I]\} \\ &= Tr\{(\mathbf{x}_i-\boldsymbol{m}_k)\mathbb{E}_{\Lambda_k}[\Lambda_k](\mathbf{x}_i-\boldsymbol{m}_k)^T+\tau_k^{-1}I\} \\ &= (\mathbf{x}_i-\boldsymbol{m}_k)^T\mathbb{E}_{\Lambda_k}[\Lambda_k](\mathbf{x}_i-\boldsymbol{m}_k)+M\tau_k^{-1} \\ &= \xi_k(\mathbf{x}_i-\boldsymbol{m}_k)^T\boldsymbol{W}_k(\mathbf{x}_i-\boldsymbol{m}_k)+M\tau_k^{-1}. \end{aligned} \tag{5.4.46}$$

Now, we consider the remaining expectation term in (5.4.39), i.e. $\mathbb{E}[\ln|\boldsymbol{\alpha}_k|]$,

which can be calculated as

$$\begin{aligned}\mathbb{E}_{\alpha_k}[\ln|\boldsymbol{\alpha}_k|] &= \digamma(\psi_k) - \digamma(\hat{\psi}_k) \\ &\equiv \ln\tilde{\alpha}_k \end{aligned} \tag{5.4.47}$$

where $\hat{\psi} = \sum_k \psi_k$. At this point, if we substitute (5.4.40), (5.4.46) and (5.4.47) into (5.4.39), we obtain the expression for φ_{ik} as

$$\begin{aligned}\ln\varphi_{ik} &= \mathbb{E}_{\alpha_k}[\ln\alpha_k] + \frac{1}{2}\mathbb{E}_{\Lambda_k}[\ln|\Lambda_k|] - \frac{M}{2}\ln(2\alpha) - \frac{1}{2}\mathbb{E}_{\boldsymbol{\mu}_k,\Lambda_k}[(\mathbf{x}_i-\boldsymbol{\mu}_k)^T\Lambda_k(\mathbf{x}_i-\boldsymbol{\mu}_k)] \\ &= \ln\tilde{\alpha}_k + \frac{1}{2}\ln\tilde{\Lambda}_k - \frac{M}{2}\ln(2\alpha) - \frac{1}{2}[\xi_k(\mathbf{x}_i-\boldsymbol{m}_k)^T\boldsymbol{W}_k(\mathbf{x}_i-\boldsymbol{m}_k) + M\tau_k^{-1}]\end{aligned} \tag{5.4.48}$$

and if we take the exponential of both sides, we will have

$$\varphi_{ik} = \frac{\tilde{\alpha}_k\tilde{\Lambda}_k^{1/2}}{(2\alpha)^{-M/2}}\exp\left\{-\frac{M}{2\tau_k} - \frac{\xi_k}{2}(\mathbf{x}_i-\boldsymbol{m}_k)^T\boldsymbol{W}_k(\mathbf{x}_i-\boldsymbol{m}_k)\right\}. \tag{5.4.49}$$

Thus, the responsibilities, r_{ik} can be written as

$$r_{ik} \propto \tilde{\alpha}_k\tilde{\Lambda}_k^{1/2} exp\big\{-\frac{M}{2\tau_k} - \frac{\xi_k}{2}(\mathbf{x}_i-\boldsymbol{m}_k)^T\boldsymbol{W}_k(\mathbf{x}_i-\boldsymbol{m}_k)\big\}. \tag{5.4.50}$$

From the foregoing, it can be observed that similar to the univariate Gaussian case, the optimization of the variational posterior distribution that solves our GMM problem is an iterative process that involves alternating between two steps. These are the VB E-step (Expectation-step) where the initial values of all the parameters, ψ_0, τ_0, $\boldsymbol{m}_0$, $\boldsymbol{W}_0$ and ξ_0 are used to compute the initial responsibilities, r_{ik}, $\forall\ i,k$ via the expectations in (5.4.40) to (5.4.46) and (5.4.47) and the VB M-step (Maximization-step) where the values of r_{ik} are used to re-compute the variational distribution over the parameters using (5.4.26) and (5.4.28) via the Gaussian-Wishart distribution given by (5.4.30) and (5.4.35) which are in turn used to recompute the re-

sponsibilities, r_{ik}, until the algorithm converges and optimal solutions, $q^*(\boldsymbol{\alpha})$ and $q^*(\boldsymbol{\mu}_k, \Lambda_k)$ are obtained.

At this point, it should be noted that the value of K used to initialize the VBGMM algorithm is usually far greater than the true number of components present. Hence, upon convergence, there will be components such that the expected values of the mixing components can not be numerically distinguishable from their prior values (i.e. do not grow). These components essentially takes no responsibility for explaining the data points which means that they are irrelevant, and thus are deleted.

To classify new data point, $\mathbf{x}^{new}$, a rule is proposed that is based on the likelihood function as

$$\frac{\alpha_k^*.\ \mathcal{N}(\mathbf{x}^{new}|\boldsymbol{\mu}_k^*, (\Lambda_k^*)^{-1})}{\alpha_{l,\forall l\neq k}^*.\ \mathcal{N}(\mathbf{x}^{new}|\boldsymbol{\mu}_{l,\forall l\neq k}^*, (\Lambda_{l,\forall l\neq k}^*)^{-1})} > \pi_{th} \tag{5.4.51}$$

where π_{th} is the threshold for trading-off misclassification errors and $\mathbf{x}^{new}$ belongs to cluster $k \iff$ (5.4.51) is true. The algorithm for the implementation of the proposed VBGMM scheme is shown in Algorithm 5.1.

Algorithm 5.1: VBGMM Based Spectrum Sensing Algorithm

1. Generate the $N \times D$ data matrix $\boldsymbol{X}$ of the energy samples from all sub-bands over a fixed sensing interval using (5.4.2).
2. Initialize the parameters ψ_0, τ_0, $\boldsymbol{m}_0$, $\boldsymbol{W}_0$ and ξ_0.
3. ***for*** $n = 1, \cdots, N$ ***do***

   for $k = 1, \cdots, K$ ***do***

   Compute the initial responsibilities, r_{nk} using (5.4.50)

   end for

   for $k = 1, \cdots, K$ ***do***

   Normalize the responsibilities.

   end for

   end for
4. ***repeat***

   for $k = 1, \cdots, K$ ***do***

   Use the result in step (3) to compute N_k, $\bar{\mathbf{x}}_k$, ψ_k, τ_k, $\boldsymbol{m}_k$, $\boldsymbol{W}_k^{-1}$ and ξ_k.

   end for

   Recompute responsibilities, r_{nk} $\forall$ n, k using step (3)

   until convergence
5. Delete irrelevant clusters.
6. Use the optimal results from step (4) to classify each new data point, $\mathbf{x}^{new}$ using (5.4.51) to decide the corresponding PU's status, H_0 or H_1.

5.5 Simulation Results and Discussion

For investigation purpose cases of SU assumed to be equipped with $M = 2$ and 3 antennas are considered and the PU's transmitted signal is assumed as BPSK with unity power. The noise is complex additive white Gaussian with variance, σ_η^2. Furthermore, the noise and signals are assumed to be uncorrelated and the antennas of the SU are assumed to be spatially sepa-

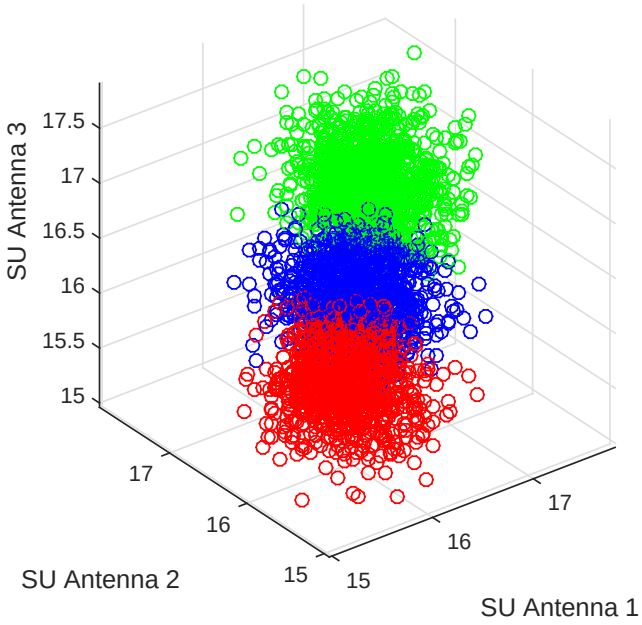

Figure 5.1. Constellation plot of three Gaussian components blindly identified, number of PUs, $P = 2$, number of samples, $N_s = 3000$, the number of antennas, $M = 3$, SNR = -12dB.

rated from each other while the SU is located within the PU detection area. The channel gain is assumed to be approximately constant during the period of training and testing. All results are averaged over 1000 Monte Carlo realizations where for each realization, random noise and BPSK signals were generated. There were 3000 realizations of M dimensional data points i.e. $N = 3000$, out of which 1200 were used for training and the rest for testing purpose. Furthermore, the system's performance was evaluated using Pd, Pfa, ROC and clustering accuracy as metrics, over different SNR range.

Figure 5.1 shows the constellation plot of three Gaussian components blindly identified by the proposed VBGMM scheme. Two PUs are considered transmitting with a specific power such that their SNR as received at the SU is 0 dB and -2 dB respectively. Two sets of data streams representing the PUs' signals generated with $N_s = 3000$ under H_1 and a set of data stream corresponding to H_0, were fed to the classifier. The SU is assumed

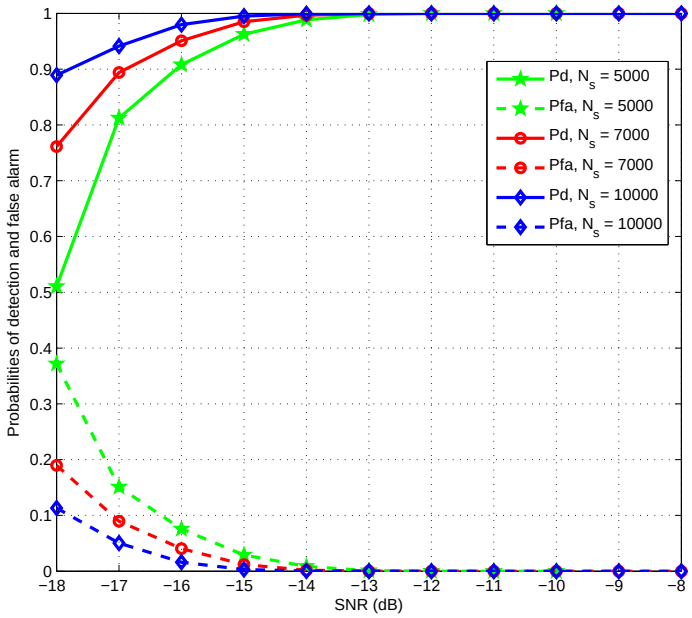

Figure 5.2. Probabilities of detection and false alarm versus SNR with N_s = 5000, 7000, 10000, $P = 1$, $M = 3$.

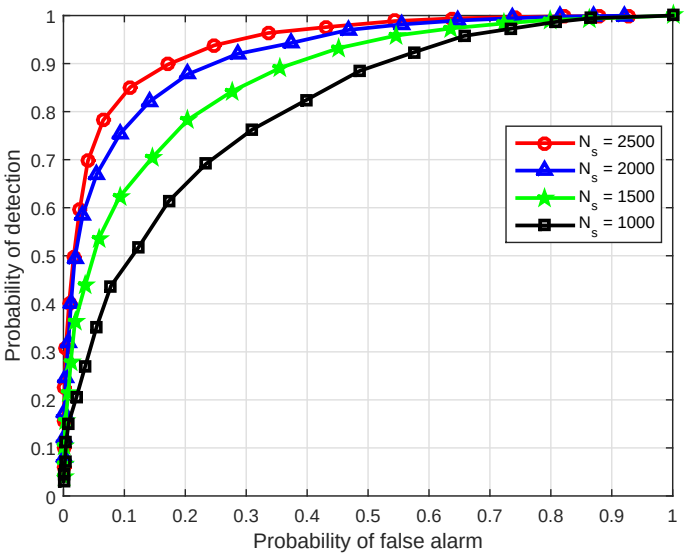

Figure 5.3. ROC curves showing the performance of VBGMM algorithm, at SNR = -15 dB, N_s = 1000, 1500, 2000 and 2500, $P = 1$, $M = 2$.

to be operating at the SNR = -12 dB. Although the number of components (i.e. number of PUs) was unknown to the classifier, it is of interest that the correct number of Gaussian components was detected and the clusters were separated as shown, even when there is an overlapping. Figure 5.2 shows the plot of clustering accuracy against SNR where the performance of the scheme was evaluated under multiple PUs detection. It can be seen that as expected, clustering accuracy improves as N_s is increased and an accuracy of about 93% is achievable at -15dB when N_s is 5000.

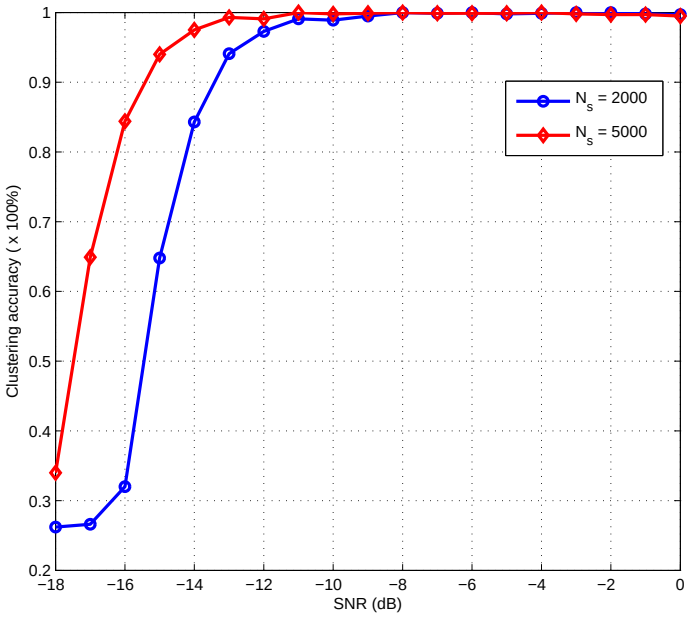

Figure 5.4. Clustering accuracy versus SNR, $P = 2$, $M = 3$, $N_s = 2000$ and 5000.

In Figure 5.3, the ROC performance of the proposed scheme is shown at SNR = -15 dB using different N_s. It can be observed that the performance of the scheme is improved as more samples of PU's signals are obtained for the feature realization. It can be seen that at Pfa of 0.1, Pd rises from about 0.5 to about 0.83 as N_s is increased from 1000 to 2500. Figure 5.4, show the plots of Pd and Pfa against SNR for N_s = 5000, 7000 and 10000. Here, the Pd is seen to improve as N_s in increased from 5000 to 10000. Furthermore,

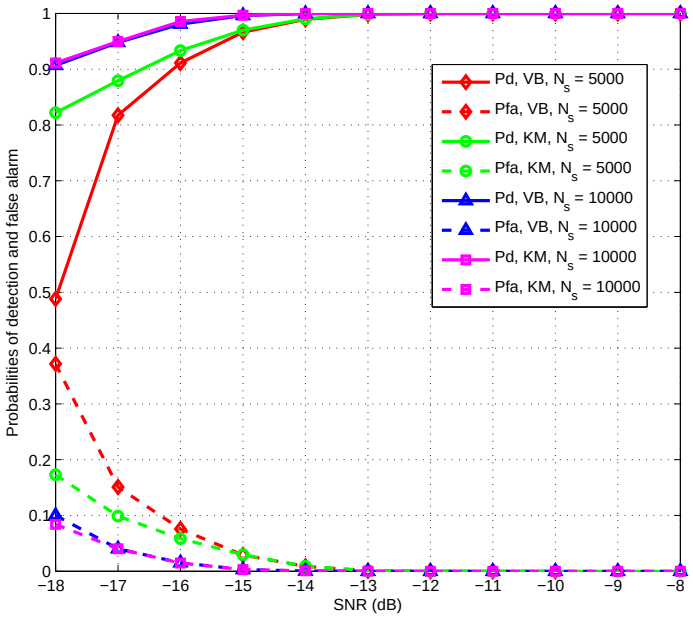

Figure 5.5. Probabilities of detection and false alarm versus SNR with different N_s, $P = 1$, $M = 3$, showing comparison between VB and K-means Clustering.

at SNR of -15 dB for all cases considered, $Pd \geq 90\%$ and at -18 dB, Pd of 90% can be seen to be achievable when $N_s = 10000$. Similarly, the Pfa falls below 10% for all cases at -15 dB and drops from 28% to 10% as N_s goes from 5000 to 10000 at SNR = -18 dB. It can be further observed that the miss-detection probability (1-Pd) equals Pfa at SNR = -18 dB when N_s = 10000, affording us the possibility of designing the learning machine for a given false alarm requirement.

In Figure 5.5, the investigation is concluded by considering how the proposed VB-based scheme compares with the K-means classifier using Pd and Pfa metrics over an SNR range of -8 dB to -18 dB. It can be seen that when $N_s = 5000$, the K-means scheme outperforms the VB scheme between -15 dB and -18 dB. However, as N_s is increased to 10000, the performance of the VB scheme closely matches that of K-means, despite the fact that K-means method requires a prior knowledge of the exact number of clusters,

over the entire range of SNR considered. In general, the proposed technique is found to exhibit a robust behavior and lends itself readily for autonomous, blind spectrum sensing application in cognitive radio networks.

5.6 Summary

In this chapter, a novel fully Bayesian parametric variational inference technique was proposed for autonomous spectrum sensing in cognitive radio networks. The underpinning theories are discussed in detail. The scheme does not suffer from over-fitting problem, it avoids the singularity problem of EM algorithm and yields globally optimal solution. Simulation results show that with few cooperating secondary devices, the scheme offers overall correct detection rate of 90% and above with the false alarm rate kept at 10% when the number of collected signal samples approaches 10000. An attractive feature of the proposed VB algorithm is that it does not require a priori knowledge of the exact number of PUs unlike in supervised and semi-supervised learning algorithms. In Chapter 6 which is the last contribution chapter, a novel preprocessing technique for enhancing the detection accuracy of classification algorithms in multi-antenna systems will be presented.

Chapter 6

BEAMFORMER-AIDED SVM ALGORITHMS FOR SPATIO-TEMPORAL SPECTRUM SENSING IN COGNITIVE RADIO NETWORKS

6.1 Introduction

The accuracy of classification algorithms in general depends on the quality of the features that are used for training and prediction [87]. In this chapter, a novel, beamformer aided feature realization strategy is proposed for enhancing the capability of the learning algorithms. Without loss of generality, the aim is to address the problem of spatio-temporal spectrum sensing in multi-antenna CR systems using SVM algorithms. For completeness, under single PU scenario, the performance of the proposed feature and binary SVM for solving the temporal spectrum sensing problem is re-evaluated. However,

under multiple PUs scenario, the ECOC based multi-class SVM algorithms is re-visited and the performance is re-evaluated. In addition, a multiple independent model (MIM) alternative is provided for solving the multi-class spectrum sensing problem. The performance of the proposed beamformer aided detectors are quantified in terms of Pd, Pfa, ROC, area under ROC curves (AuC) and overall classification accuracy.

6.2 System Model and Assumptions

A scenario similar to the one described in sub-section (3.6.4) is adopted where the SUs are multi-antenna devices equipped with M antennas and operating in the coverage areas of P PU transmitters. The PUs, however in this case might be high power macro cell base stations while the SU might be a low power micro cell base station (SBS) located at the cell edge of multiple macrocells. This offers the possibility of frequency re-use within nearby cells and with appropriate transmission strategies such as beamforming and user location based power allocation, can result in more efficient utilization of spectrum resources. Under this scenario, as shown earlier in this thesis, the ensuing spatio-temporal spectrum sensing problem can be formulated as a multiple hypothesis testing problem where there are multiple classes and ecah class comprises of one or more states. A more compact form of the multi-class sensing problem now presented.

First, a class in the classification problem is defined as the number of active PUs in the network at any given point in time. Hence, the set of all possible classes can be defined as

$$\mathcal{P} = \{C_1, C_2, \cdots, C_P\} = \{C_i\}_{i=1}^{P}. \tag{6.2.1}$$

Within each class, there is a set of possible states. Each state indicates the various, different combinations of PUs that are active. For example, for class

3, i.e. for C_3, three PUs are active. Hence, out of P possible PUs, there are $C(P,3)$ combinations that are referred to as states where $\mathrm{C}(P,i) = \binom{P}{i} = \frac{P!}{(P-i)!\,i!}$. In general, for the i-th class, we will have $Q(i) = \mathrm{C}(P,i)$ possible states which is written as

$$C_i = \{\mathcal{S}_1^i, \mathcal{S}_2^i, \cdots, \mathcal{S}_{Q(i)}^i\} = \{\mathcal{S}_q^i\}_{q=1}^{Q(i)} \tag{6.2.2}$$

where $\mathcal{S}_q^i$ is a particular selection of PUs in class C_i. The spectrum sensing problem is therefore formulated as determining not only the availability of spectrum hole but also the state of the network, i.e. to determine which primary user(s) are active. Hence, the received signal model under this scenario is writen as a multiple hypothesis testing of the form

$$H_0 : \mathbf{y}(n) = \boldsymbol{\eta}(n) \tag{6.2.3}$$

$$H_{i,q} : \mathbf{y}(n) = \sum_{p \in \mathcal{S}_q^i} \bar{\boldsymbol{\phi}}_p s_p(n) + \boldsymbol{\eta}(n), \forall \mathcal{S}_q^i \in C_i, \forall C_i \in \mathcal{P} \tag{6.2.4}$$

where H_0 implies that *all* PUs are inactive and $H_{i,q}$, means that i number of PUs corresponding to the q-th state are active. Therefore, the alternative hypothesis for H_0 is

$$H_1 = \bigcup_{\substack{i=\{1,\cdots,P\} \\ q=\{1,\cdots,Q(i)\}}} H_{i,q}. \tag{6.2.5}$$

Furthermore, $\mathbf{y}(n) = [y_1(n), y_2(n), \cdots, y_M(n)]^T$ is the vector of instantaneous signal received at the SU over bandwidth ω of interest within which the PUs operate, $\bar{\boldsymbol{\phi}}_p = [\bar{\phi}_{1,p}, \bar{\phi}_{2,p}, \cdots, \bar{\phi}_{M,p}]^T$ is the vector of channel coefficients between the p-th PU and the SU. The remaining parameters in (6.2.4) are $s_p(n)$ which is the instantaneous PU signal, assumed to be BPSK modulated with variance, $\mathbb{E}|s_p(n)|^2 = \sigma_{s_p}^2$, and $\boldsymbol{\eta}(n) = [\eta_1(n), \eta_2(n), \cdots, \eta_M(n)]^T$, which is the vector of noise, $\eta_m(n)$, assumed to be an $i.i.d$ circularly symmetric complex zero-mean Gaussian with variance, $\mathbb{E}|\eta_m(n)|^2 = \sigma_\eta^2$.

Under H_0, all PUs are inactive and it corresponds to the null hypothesis. On the other hand, H_1 corresponds to *composite* alternative hypothesis where at any given time, *at least one* PU is active during the sensing interval. It is apparent that this composite hypothesis intuitively embeds P classes of alternative hypothesis each of which may comprise of one or more possible network states. The goal is to learn the peculiar attributes that uniquely characterize each state under H_1, and to use this knowledge to discriminate them.

6.3 Beamformer Design for Feature Vectors Realization

In this section, a beamforming technique is presented for enhancing the receive SNR and hence, the quality of received PU(s) signals used for realizing the feature vectors of the spectrum sensing scheme. Let us assume that the M antennas of the SU are identical and equally spaced so that they form a uniform linear array (ULA). Let $s_m(n)$ denote the discrete time PU's signal arriving at the m-th antenna of the array at an angle of arrival (AOA), θ, assumed to be uniformly distributed within the interval $[\theta_{min}, \theta_{max}]$. The total azimuth coverage of the array is restricted to 180° so that the array scans the entire range, $\Theta \in [-90°, 90°]$ for θ [88]. In this beamformer design, the entire range of the ULA's azimuth coverage, Θ is partitioned into K = 9 sectors denoted as $\{\bar{\theta}_k\}_{k=1}^{K}$, where each sector $\bar{\theta}_k$ has a width of 20° within which we assume the AOA of the PU signals, θ lies. For example, $\bar{\theta}_1 \in [-90, -70)$, $\bar{\theta}_2 \in [-70, -50)$, and so on. The overall goal is to design a unique beamformer for each sector $\bar{\theta}_k \in \Theta$ such that for every beamformer, the array gain is maximized within $\bar{\theta}_k$ and minimized elsewhere, that is, throughout the remaining sectors of the azimuth angles, $\bar{\theta}_j \in \Theta \setminus \bar{\theta}_k$.

Let the sector of interest $\bar{\theta}_k$ be further represented as a set of $\bar{K}$, fine angular sub-partitions described by $\{\tilde{\theta}_{\bar{k}}\}_{\bar{k}=1}^{\bar{K}}$. Additionally, let the *desired*

beampattern for the sector be represented by $\phi(\bar{\theta}_k)$ and the array response vector associated with AOA, θ be written as $\mathbf{a}(\theta) = [1 \ \mathrm{e}^{-j\theta} \ \cdots \ \mathrm{e}^{-j(M-1)\theta}]^T$, $\theta = (\frac{2\pi d}{\lambda}) \sin\phi$, where ϕ is the actual angle of incidence of the plane wave relative to the array broadside, $d = \frac{\lambda}{2}$ is the antenna spacing, λ is the wavelength of the impinging PU signal transmitted at the carrier frequency. If the required beamformer to obtain the beampattern, $\phi(\bar{\theta}_k)$ is denoted by $\mathbf{w}_{\bar{\theta}_k}$, the goal is to determine a rank one matrix, $\mathbf{R} = \mathbf{w}_{\bar{\theta}_k}\mathbf{w}_{\bar{\theta}_k}^H$ that minimizes the difference between the desired beampattern, $\phi(\bar{\theta}_k)$ and the *actual* receive beampattern, $\mathbf{a}^*(\bar{\theta}_k)\mathbf{R}\mathbf{a}(\bar{\theta}_k)$ in the least squares sense. The operation, $(\cdot)^*$ denotes the conjugate transpose. Hence, the beampattern matching problem can be formulated mathematically as an optimization problem of the form

$$\begin{aligned} &\underset{\tilde{\alpha},\mathbf{R}}{\text{minimize}} \quad t \\ \text{subject to} \ &\sum_{\bar{k}=1}^{\bar{K}} \left[\tilde{\alpha}\phi(\tilde{\theta}_{\bar{k}}) - \mathbf{a}^*(\tilde{\theta}_{\bar{k}})\mathbf{R}\mathbf{a}(\tilde{\theta}_{\bar{k}})\right]^2 < t, \\ &\mathbf{R} \succeq 0, \ rank(\mathbf{R}) = 1 \end{aligned} \tag{6.3.1}$$

where $\tilde{\alpha}$ is a scaling factor whose optimal value can be obtained jointly as part of the solution of the optimization problem. However, due to the matrix rank constraint in (6.3.1) the problem is rendered non-convex. So, the equality restriction imposed on $\mathbf{R}$ is relaxed and (6.3.1) is recast into a semi-definite optimization problem which can be solved with the aid of semi-definite programming algorithm to obtain optimal $\mathbf{R}$ ($\mathbf{R}_{\bar{\theta}_k}^{opt}$) [89]. The desired beamformer weights, $\mathbf{w}_{\bar{\theta}_k}$ can be extracted from $\mathbf{R}_{\bar{\theta}_k}^{opt}$. Ideally, the rank of $\mathbf{R}_{\bar{\theta}_k}^{opt}$ should be one and if this is the case, $\mathbf{w}_{\bar{\theta}_k}$ can be obtained as the eigenvector of $\mathbf{R}_{\bar{\theta}_k}^{opt}$ which corresponds to the principal eigenvalue multiplied by the square root of the principal eigenvalue. On the other hand, if the rank of $\mathbf{R}_{\bar{\theta}_k}^{opt}$ is greater than one, to derive $\mathbf{w}_{\bar{\theta}_k}$ we have to resort to randomization technique.

6.4 Beamformer-Aided Energy Feature Vectors for Training and Prediction

In this section, the applicability of the designed beamformers is demonstrated. Without loss of generality, two practical cognitive radio deployment scenarios are considered and the algorithms for deriving our training and prediction energy features using the beamformers are described. The scenarios considered are that the PU(s) signals are received by the SU via (a) clear line-of-sight and (b) strong multipath components (overlapping and non-overlapping cases).

6.4.1 Reception of PU Signals with Clear Line-of-Sight

Here, spectrum sensing scenarios where a clear line-of-sight (LOS) can be established between the PU(s) and SU is considered. Typically, this kind of scenario occurs when the PU antenna is located at a high altitude such as a base station tower and LOS can be established up to the vicinity of the SU. Although there may be presence of local scatterers, it is possible for the multipath signals to arrive at the SU within close range of angles that fall within one sector, $\bar{\theta}_k$ as described in section 6.3. To perform spectrum sensing, the implementation of the SVM based learning is considered as a two-phase process. The first phase is termed the *qualification* phase during which the SU tries to *learn* the range of azimuth angles or direction of arrival (DOA) of the impinging PU signals with the aid of beamformers. The main objective is to identify the sole beamformer under single PU case or set of beamformers in the case of multiple PUs whose output is/are capable of providing the required, high quality training energy features and where future test energy samples can also be derived. The qualification process is implemented using the following procedure. Let the discrete time signal

received at the M-element array of the SU receiver be represented as

$$\mathbf{y}(n) = \begin{cases} \mathbf{a}(\theta)s(n) + \boldsymbol{\eta}(n), & \text{if } P = 1 \\ \sum_{i=1}^{P} \mathbf{a}(\theta_i)s_i(n) + \boldsymbol{\eta}(n), & \text{if } P > 1 \end{cases} \tag{6.4.1}$$

where $\mathbf{y}(n) \in \mathbb{C}^M$. If the beamformer designed for the k^{th} sector is $\mathbf{w}_{\bar{\theta}_k}$, the beamformer output can be expressed as

$$x_k(n) = \mathbf{w}_{\bar{\theta}_k}^H \mathbf{y}(n). \tag{6.4.2}$$

Suppose we collect N samples of $x_k(n)$, the qualifying energy feature is computed from the beamformer output as

$$\vartheta_k = \frac{1}{N} \sum_{n=1}^{N} |x_k(n)|^2. \tag{6.4.3}$$

If the vector of energy samples computed for the set of all beamformers is denoted as $\boldsymbol{\vartheta} \triangleq [\vartheta_1, \vartheta_2, \cdots, \vartheta_K]$, where $\boldsymbol{\vartheta} \in R^K$, ($K$ is the number of sectors in Θ), the desire is to determine the set of qualified beamformer(s) which would produce the *actual* SVM's feature vector. To accomplish this objective, the decision threshold, ζ_1 defined for a target false alarm probability, $\bar{P}_{fa}$ as [67]

$$\zeta_1 = \sigma_{s_p}^2 \gamma^{-1} \left(1 + \sqrt{\frac{2}{N}} Q^{-1}(\bar{P}_{fa}) \right) \tag{6.4.4}$$

is applied where $\gamma = \frac{\sigma_{sp}^2}{\sigma_{\eta}^2}$ is the receive SNR of the PU(s) signal measured at the SU under hypothesis $H_{i,q}$ that corresponds to the state, $\mathcal{S}_{Q(P)}^P$ (i.e. when all PUs are active) and Q^{-1} denotes the inverse Q-function,

$$Q(x) = \frac{1}{2\pi} \int_x^{+\infty} \exp\left(-t^2/2\right) dt. \tag{6.4.5}$$

By applying (6.4.4), the dimension of the SVM feature vector, $\bar{S} \ll K$ given by $card(\boldsymbol{\vartheta})$ such that $\vartheta_k > \zeta_1$, $\forall k \in K$ can be determined. In addition, since

$\bar{S} \ll M$ it follows that after the qualification phase, we will have succeeded in significantly reducing the dimension of the feature vector in the input space and thereby reduce the computational complexity of the sensing algorithm compared to the non beamformer based alternative. Furthermore, under multiple PUs, by correctly identifying the PU(s) responsible for the energy sample at each qualified beamformer, ϑ_k, $\forall k \in \bar{S}$, it will be possible to use independent binary SVM classifier to monitor the activities of individual PU without recourse to multi-class learning algorithms. In the following subsection, the process for associating the energy samples with their respective sources will be discussed. Meanwhile, having identified the DOA of the PU's signal via the qualified beamformers set, during the second phase of the learning process which is referred to as the *training* phase, the SU derives the required training energy features from the qualified beamformers set *only* while other beamformers' output are simply ignored.

6.4.2 Reception of PU Signals via Strong Multipath Components

In certain practical sensing scenarios, the presence of heavily built structures may result in the PU(s) signals arriving the SU receiver via multiple strong paths. Under this scenario, it is possible that reflections from multiple sources arrive at the SU receiver within a range of azimuth angles that are covered by the same sector, $\bar{\theta}_k$. This is treated as a case of overlapping reflections. On the other hand, the reflections may be received by the SU at widely separated AOAs corresponding to different sectors, thus, considered as a non overlapping case. To take advantage of multipath propagation to improve sensing performance, using the beamformers to aid the SVM classifier is considered. During the $qualification$ phase, as in the LOS case, the beamformers are used to determine the number of significant PU's signal components at the SU and their DOAs. Under single PU, the task is essentially to determine the actual beamformers set whose output are suf-

ficient to provide the required training energy features and could also be used for predicting the PU's status. However, under multiple PUs scenarios, in addition to determining the qualified beamformers set, we also need to know the particular beamformer(s) to which respective PU signal is associated, thereby identifying the sources responsible for the signals received at each beamformer. This will enable us to employ multiple, independent SVM models (MIMSVM) to simultaneously monitor the activities of all PUs as a viable alternative to multi-class SVM (MSVM) algorithms.

In general, let the set of qualified beamformers be represented by $\mathcal{B} = \{b_1, b_2, \cdots, b_{\bar{S}}\} \in \{\mathbf{w}_{\bar{\theta}_1}, \mathbf{w}_{\bar{\theta}_2}, \cdots, \mathbf{w}_{\bar{\theta}_K}\}$. Further, let the corresponding sequences of samples of PU signal derived at these beamformers output be described as $\mathbf{X} = [\mathbf{x}_1, \mathbf{x}_2, \cdots, \mathbf{x}_{\bar{S}}]$ where $\mathbf{x}_{\bar{s}} \triangleq [x_{\bar{s}}(1), x_{\bar{s}}(2), \cdots, x_{\bar{s}}(N)]^T$, N is the number of samples, $\forall \bar{s} \in \bar{S}$. To solve the beamformer association problem, it is assumed that at least one of the multipaths is from the LOS indicating the known direction of the PUs. The beamformer corresponding to the LOS signal of the i-th PU (PU_i) is denoted as b^i_{ref}, where $b^i_{ref} \in \mathcal{B}$. However, we need to associate the other mutipaths to each of the PU. This is performed by determining the cross correlation of the known beamformer's output to other beamformers' output and comparing it to a threshold, ζ_2. The cross correlation between the sequences derived at the output of any two beamformers, $\mathbf{x}_i$ and $\mathbf{x}_j$ is computed for various delays as

$$\begin{aligned} R_{\mathbf{x}_i\mathbf{x}_j}(\tau) &= \mathbb{E}[x_i(n)x_j^*(n+\tau)] \\ &= \frac{1}{N}\sum_{n=1}^{N}[x_i(n)x_j^*(n+\tau)], n = 1, \cdots, N. \end{aligned} \tag{6.4.6}$$

The test statistic for comparison is therefore derived as

$$\mho_d = \sum_{\tau=-\tau_d}^{\tau_d} |R_{\mathbf{x}_{ref}\mathbf{x}_{\bar{s}}}(\tau)|^2, \tag{6.4.7}$$

where $R_{\mathbf{x}_{ref}\mathbf{x}_{\bar{s}}}(\tau)$ denotes the τ-lag cross correlation between $\mathbf{x}_{ref}$ and $\mathbf{x}_{\bar{s}}$ and $\mho_d$ is the sum of square of the magnitude of cross correlation returns over the search interval, $[-\tau_d, \tau_d]$. The search interval must be carefully chosen to capture the likely delay, τ', between $\mathbf{x}_{ref}$ and the reflected version which may be present in $\mathbf{x}_{\bar{s}}$. It should be noted here, that the exact amount of the delay, τ', may *not* be known a priori, so τ_d should be sufficiently large. To determine the presence of $\mathbf{x}_{ref}$ in $\mathbf{x}_{\bar{s}}$, $\mho_d$ is compared to ζ_2 defined by

$$\zeta_2 = \tilde{\varrho}|R_{\mathbf{x}_{ref}\mathbf{x}_{ref}}(0)|^2 \tag{6.4.8}$$

where $\tilde{\varrho}$ is an appropriate scalar. If $\mho_d \geq \zeta_2$, we conclude that $\mathbf{x}_{ref}$ is present in $\mathbf{x}_{\bar{s}}$ and vice versa. In the following sub-sections, the performance of the proposed beamformer aided SVM algorithm to solve the temporal spectrum sensing problem is investigate under single and multiple PU scenarios respectively.

6.4.3 Spectrum Sensing Using Beamformer-derived Features and Binary SVM Classifier Under Single PU Condition

Under single PU scenario, our beamforming based spectrum sensing problem can be formulated as a binary hypothesis testing problem of the form

$$x_k(n) = \mathbf{w}_{\theta_k}^H \mathbf{y}(n) \tag{6.4.9}$$

where $\mathbf{y}(n) = \boldsymbol{\eta}(n)$ under H_0 and $\mathbf{y}(n) = \mathbf{a}(\theta_k)s(n) + \boldsymbol{\eta}(n)$ under H_1, $\forall k \in \mathcal{B}$ and $x_k(n)$ is the instantaneous signal at the output of the k-th beamformer. Without loss of generality, if we assume non-overlapping multipath scenario and collect D independent energy vectors, each comprising energy samples realized according to (6.4.3) for training purpose. Let $\mathcal{S} = \{(\boldsymbol{\vartheta}_1, \bar{l}_1), (\boldsymbol{\vartheta}_2, \bar{l}_2), \cdots, (\boldsymbol{\vartheta}_D, \bar{l}_D)\}$ represent the training data set where

$\boldsymbol{\vartheta}_i \in \mathcal{R}^{\bar{S}}$ is an $\bar{S}$-dimensional feature vector and $\bar{l}_i \in \{-1, 1\}$ is the corresponding class label. Following from sub-section (3.6.12), the classification task is solved by using the soft margin SVM which can be formulated as an optimization problem. The PU's status, H_0 or H_1 is determined in terms of the class of a new observed data vector, $\boldsymbol{\vartheta}^{new}$, as

$$\bar{l}(\boldsymbol{\vartheta}^{new}) = sgn\left(\sum_{i=1}^{N_s} \bar{l}_i \alpha_i \beta(\boldsymbol{\vartheta}^{new}, \boldsymbol{\vartheta}_i) + b\right) \tag{6.4.10}$$

where N_s is the number of support vectors. In Algorithm 7.1, a summary of the proposed beamformer-aided spectrum sensing technique under single PU scenarios is presented.

Algorithm 7.1: Beamformer Aided SVM Algorithm for Spectrum Sensing Under Single PU Scenarios

Learning stage:
- *Qualification phase*
  - *i* Load pre-designed beamformer's weight, $\mathbf{w}_{\bar{\theta}_k}$, $\forall k \in K$.
  - *ii*. Scan entire look directions, Θ, and compute *qualifying* energy set, $\boldsymbol{\vartheta} \in R^K$, under H_1 using (6.4.3).
  - *iii*. Apply threshold, ζ_1 in (6.4.4) to $\boldsymbol{\vartheta}$ in (*ii*) to determine qualified beamformer set, $\mathcal{B}$.
- *Training phase*
  - *iv*. Compute D *training* energy vectors, $\boldsymbol{\vartheta} \in R^{\bar{S}}$, from the output of set $\mathcal{B}$ in (*iii*) under H_0 and H_1 using (6.4.3).
  - *v*. Generate SVM decision model in (6.4.10) from the set in (*iv*).

Prediction stage:
- *vi*. Obtain test energy samples during *prediction* interval.
- *vii*. Classify each new test sample in (*vi*) using (*v*) to decide the corresponding PU's status, H_0 or H_1.
- *viii*. Repeat steps (*vi*) and (*vii*).

6.4.4 ECOC Based Beamformer Aided Multiclass SVM for Spectrum Sensing Under Multiple PUs Scenarios

The application of the proposed beamformer aided ECOC MSVM algorithm is described by considering a scenario with two PUs operating under LOS condition. For example, let us assume that the signals from PU_1 and PU_2

are received by the SU at AOAs corresponding to $\theta_1 \in \bar{\theta}_3$ and $\theta_2 \in \bar{\theta}_6$ respectively, in this case, the multiple hypotheses problem defined in (6.2.3) and (6.2.4) translates to four hypotheses testing problem. If we let the indexes, i and q in $H_{i,q}$ indicate the class and state respectively, these hypotheses can be written as

$$H_0 : \mathbf{x}(n) = [\mathbf{w}_{\bar{\theta}_3}^H \boldsymbol{\eta}(n) \;\; \mathbf{w}_{\bar{\theta}_6}^H \boldsymbol{\eta}(n)]^T \tag{6.4.11a}$$

$$H_{1,1} : \mathbf{x}(n) = [\mathbf{w}_{\bar{\theta}_3}^H \mathbf{y}_1(n) \;\; \mathbf{w}_{\bar{\theta}_6}^H \boldsymbol{\eta}(n)]^T,$$

$$\mathbf{y}_1(n) = \mathbf{a}(\theta_1)s_1(n) + \boldsymbol{\eta}(n) \tag{6.4.11b}$$

$$H_{1,2} : \mathbf{x}(n) = [\mathbf{w}_{\bar{\theta}_3}^H \boldsymbol{\eta}(n) \;\; \mathbf{w}_{\bar{\theta}_6}^H \mathbf{y}_2(n)]^T,$$

$$\mathbf{y}_2(n) = \mathbf{a}(\theta_2)s_2(n) + \boldsymbol{\eta}(n) \tag{6.4.11c}$$

$$H_2 : \mathbf{x}(n) = [\mathbf{w}_{\bar{\theta}_3}^H \mathbf{y}_1(n) \;\; \mathbf{w}_{\bar{\theta}_6}^H \mathbf{y}_2(n)]^T,$$

$$\mathbf{y}_1(n) = \mathbf{a}(\theta_1)s_1(n) + \boldsymbol{\eta}(n),$$

$$\mathbf{y}_2(n) = \mathbf{a}(\theta_2)s_2(n) + \boldsymbol{\eta}(n). \tag{6.4.11d}$$

where $\mathbf{x}(n)$ is the instantaneous received signal vector derived at the output of $\mathcal{B}$. Under this operating condition, it is assumed that only one of the four states in (6.4.11) can exist during any sensing duration and the goal is to declare spatial spectrum hole in the operating environment of any inactive PU(s). To address this multi-class signal detection problem, the peculiar attribute(s) of each state is to be learnt using the beamformer aided features and the MSVM techniques described in section (3.6.5). A summary of the procedure for solving the multiple PUs sensing problem using beamformer derived feature based ECOC multi-class algorithm is presented in Algorithm 7.2. An alternative approach based on the described MIMSVM method is also presented in Algorithm 7.3.

Algorithm 7.2: Beamformer Aided ECOC MSVM Algorithm for Spectrum Sensing Under Multiple PU Scenarios

Learning stage:

Qualification phase

i Load pre-designed beamformer's weight, $\mathbf{w}_{\bar{\theta}_k}$, $\forall k \in K$.

ii. Scan entire look directions, Θ, and compute *qualifying* energy set, $\boldsymbol{\vartheta} \in R^K$, under $\mathcal{S}^P_{Q(P)}$ using (6.4.3).

iii. Apply the threshold, ζ_1 in (6.4.4) to $\boldsymbol{\vartheta}$ in (*ii*) to determine qualified beamformers set, $\mathcal{B}$.

Training phase

iv. Obtain D set of *training* energy vector, $\boldsymbol{\vartheta} \in R^{\bar{S}}$ from the output of $\mathcal{B}$ in (*iii*) under H_0 and $H_{i,q}$, i.e. $\forall \mathcal{S}^i_q \in \mathcal{C}_i, \forall \mathcal{C}_i \in \mathcal{P}$ using (6.4.3).

v. Generate J decision models in (3.6.38) or (3.6.41) from the set in (*iv*).

Prediction stage:

vi. Obtain test energy samples during *prediction* interval using (6.4.3).

vii. Classify each new data point in (*vi*) using (*v*) to decide the corresponding system state, H_0 or $H_{i,q}$.

viii. Repeat steps (*vi*) and (*vii*).

6.5 Numerical Results and Discussion

The performance of the proposed beamformer-aided SVM algorithms is evaluated for single and multiple PUs' scenarios. The CSVM algorithm was applied under the single PU considerations while the MSVM and MIMSVM algorithms were implemented under the multiple PU scenarios. The results are quantified in terms of Pd, Pfa, ROC, area under ROC curve (AuC) and overall classification accuracy (CA_{ovr}).

6.5.1 Single PU Scenario

Under this scenario, the aim is simply to detect the presence or absence of the PU. For the purpose of simulation, under H_1, it is assumed that the signal of the PU is $BPSK$ modulated. It is further considered that during the sensing interval, the transmission is multipath propagated and received at the SU via two strong components at AOAs, $\theta_1 \in [-45°, -35°]$ and $\theta_2 \in$

Algorithm 7.3: Beamformer Aided MIMSVM Algorithm for Spectrum Sensing Under Multiple PU Scenarios

Learning stage:

Qualification phase

i Load pre-designed beamformer's weight, $\mathbf{w}_{\bar{\theta}_k}$, $\forall k \in K$.

ii. Scan entire look directions, Θ, and compute *qualifying* energy set, $\boldsymbol{\vartheta} \in R^K$, under $\mathcal{S}^P_{Q(P)}$ using (6.4.3).

iii. Apply the threshold, ζ_1 in (6.4.4) to $\boldsymbol{\vartheta}$ in (*ii*) to determine qualified beamformers set, $\mathcal{B}$.

iv **for** $i = 1$ to P, **do**

v. Perform source search by computing $\mho_d$ in (6.4.7) for every beamformer pair $\{b^i_{ref}, b_{\bar{s}}\}, \forall b_{\bar{s}} \in \mathcal{B}$, $b^i_{ref} \neq b_{\bar{s}}$.

vi. Associate $\{b^i_{ref}, b_{\bar{s}}\} \subset \mathcal{B}$ with PU_i if $\mho_d(b^i_{ref}, b_{\bar{s}}) \geq \zeta_2$ in (6.4.8).

vii. **end for**

Training phase

viii. **for** $i = 1$ to P, **do**

ix. Obtain D set of *training* energy vectors from the output of the beamformer set in (*vi*) under H_0 and H_1 using (6.4.3).

x. Generate independent SVM decision model in (6.8.10) from the training set in (*ix*)

xi. **end for**

Prediction stage:

xii $\forall i \in P$, **do repeat**

xiii. Obtain test samples during *prediction* interval using (6.4.3).

xiv. Classify each new data point in (*xiii*) using corresponding decision model in (*x*) and decide the PUs' state, H_0 or H_1.

$[15°, 20°]$ corresponding to reception at two different sectorial partitions, $\bar{\theta}_3$ and $\bar{\theta}_6$ in Θ. The delay between the arrival of the multipath components is assumed to be 5 symbols and the total received power is normalized to unity. It is further assumed that the noise is circularly symmetric complex additive white Gaussian with power, η_n^2. The PU's signal and the noise are assumed to be uncorrelated. To investigate the performance of the resulting two-dimensional, beamformer derived feature vector, the target false alarm probability, $\bar{P}_{fa}$ was set to 0.01 and $\gamma = 0$ dB, the CSVM is applied with linear kernel and the box constraint, Γ is 0.9. Some 2000 set of energy vectors were generated through random realizations of the channels, out of which

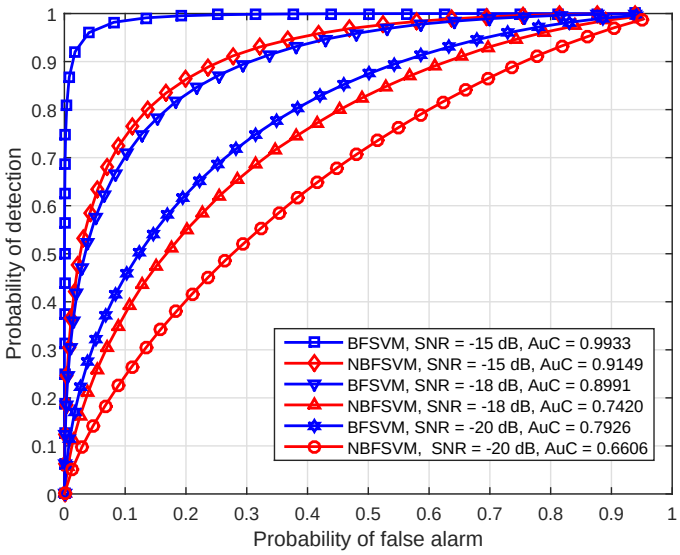

Figure 6.1. ROC performance comparison between beamformer based and non-beamformer based SVM schemes under different SNR, number of PU, $P = 1$ and number of samples, $Ns = 500$.

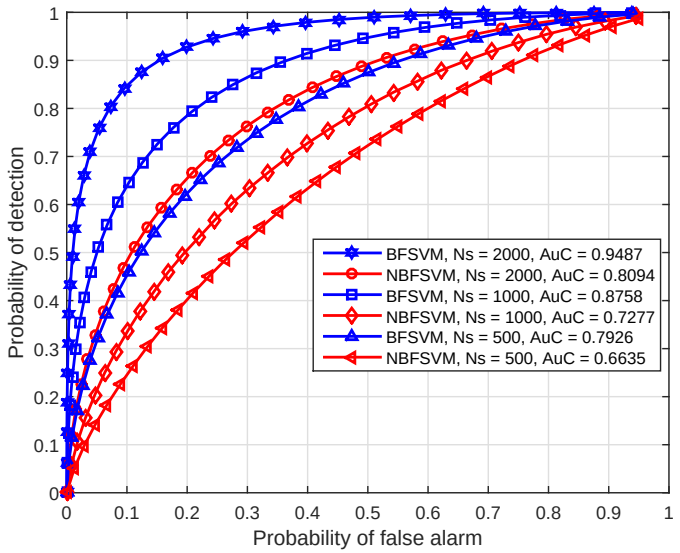

Figure 6.2. ROC performance comparison between beamformer based and non-beamformer based SVM schemes with different number of samples Ns, and SNR = -20 dB.

400 were used for training and the rest for testing purpose. The number of antennas, M at the SU is assumed to be 8 with spacing $d = 0.5\lambda$.

Figure 6.1 shows the performance of the proposed beamformer based

SVM binary classifier (BFSVM) in terms of the ROC curves for fixed number of received signal samples, $Ns = 500$ when the SNR = -15 dB, -18 dB and -20 dB in comparison with the alternative in which the use of beamformers is not considered, that is, the non-beamformer based scheme (NBFSVM). As expected, the BFSVM scheme takes advantage of the beamforming array gain of $10\log_{10} M$ dB and thus exhibits significant performance improvement compared to the NBFSVM scheme. Specifically, at $Pfa = 0.1$, the Pd achieved by the BFSVM scheme is about 0.99 whereas the NBFSVM achieves about 0.74 when SNR is -15 dB. In terms of AuC, the BFSVM scheme yields 0.9933 while NBFSVM offers 0.9149 at SNR of -15 dB. Similar trend can be observed through all cases of SNR considered. The proposed BFSVM scheme consistently outperforms the NBFSVM scheme which demonstrates the potential of the beamformer derived features to enhance the capability of the SVM binary classifier. It is strikingly interesting to note that the dimension of the feature vector of the BFSVM scheme in the input space is far less than that of the NBFSVM scheme which indicates that the proposed scheme offers significant reduction in implementation complexity.

In Figure 6.2, the effect of varying the number of PU signal samples, Ns is shown on the performance of the proposed scheme where the SNR is kept at -20 dB. As seen, when Ns is increased from 500 to 2000 and Pfa is 0.1, about 40% improvement in performance is observed for the BFSVM scheme, where Pd is increased from 0.45 to 0.85. On the other hand, the NBFSVM method yields only about 24% improvement, i.e. Pd is increased from 0.25 to 0.49. Furthermore, given the same Pfa and where $Ns = 2000$, the proposed scheme attains the Pd of 0.85 against 0.49 yielded by the NBFSVM alternative. Similarly, from the AuC perspective, an increase from 0.7926 to 0.9487 and from 0.6635 to 0.8094 is observed for the BFSVM and NBFSVM respectively for fixed SNR of -20 dB as Ns is increased.

The investigation on the single PU scenario is concluded in Figure 6.3

where the impact of receive SNR on Pd and Pfa is evaluated and both metrics are compared under the BFSVM and NBFSVM schemes. As expected, the performance of both schemes improves as SNR is increased. However, the proposed BFSVM scheme outperforms the NBFSVM scheme as seen for example at SNR of -20 dB where the BFSVM scheme attains Pd of about 0.88 when $Ns = 2000$ and $Pfa \approx 0.1$. On the other hand, the NBFSVM only attains Pd of about 0.72 and Pfa of about 0.28. Furthermore, as Ns is increased from 500 to 2000 and at SNR of -20 dB, Pd rises in the case of BFSVM scheme from 0.7 to 0.88 (about 18% gain) while Pfa reduces from 0.28 to 0.12 (about 16% drop) whereas, for the NBFSVM, rise in Pd is from 0.6 to about 0.72 (12 % gain) and Pfa reduces from 0.39 to 0.28 (about 11% drop). The performance of the proposed BFSVM scheme at Ns equals 500 almost matches that of the NBFSVM scheme at Ns equals 2000 indicating some savings in sensing time for the same performance level. From the foregoing, it is evident that the proposed beamformer based scheme exhibits a superior performance in terms of improving the usage of the radio spectrum resources and reduced implementation complexity in comparison with the non beamformer based alternative.

6.5.2 Multiple PUs Scenario

The performance of the beamformer-aided scheme is investigated using the ECOC MSVM and MIMSVM algorithms with energy features and the results are quantified in terms of CA_{ovr}. A network comprising two PUs operating in the frequency band of interest and transmitting with a specific power such that the SNR at the receiver is 0 dB and -2 dB respectively is considered. The channel coefficients have also been normalized to one. Further, two scenarios are considered for the angle of arrival signals. In the first scenario, the signal from PU1 is received from two paths, the first one arrives with an AOA, $\theta_1 \in [-45°, -35°] \in \bar{\theta}_3$ and the second path comes with an AOA,

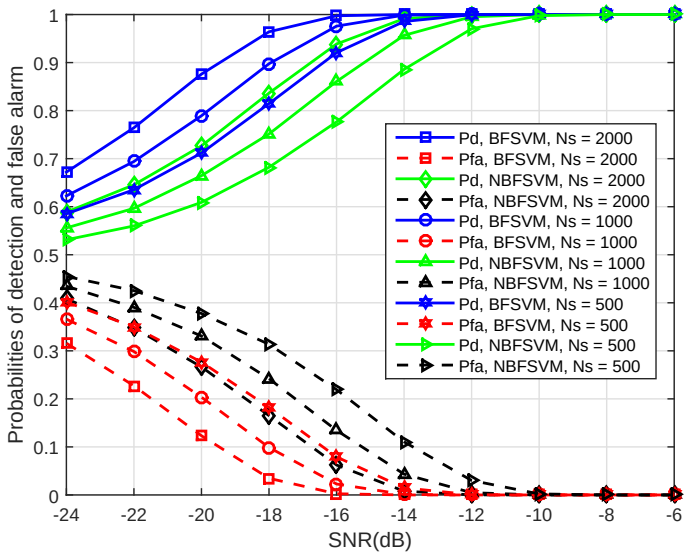

Figure 6.3. Performance comparison between beamformer based and non-beamformer based SVM schemes showing probabilities of detection and false alarm versus SNR, with different sample number, Ns.

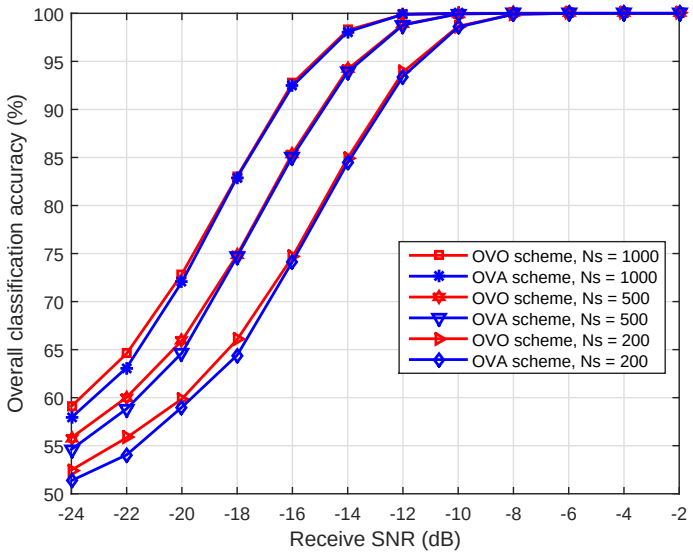

Figure 6.4. Performance comparison between OVO and OVA ECOC MSVM schemes under non-overlapping transmission scenario with different number of samples Ns, and number of PU, $P = 2$.

$\theta_2 \in [15°, 20°] \in \bar{\theta}_6$. Similarly, the two multipath components of PU2 arrive at angles $\theta_3 \in [-20°, -15°] \in \bar{\theta}_4$ and $\theta_4 \in [40°, 45°] \in \bar{\theta}_7$ respectively. In the second scenario, a situation is considered where the multipath components

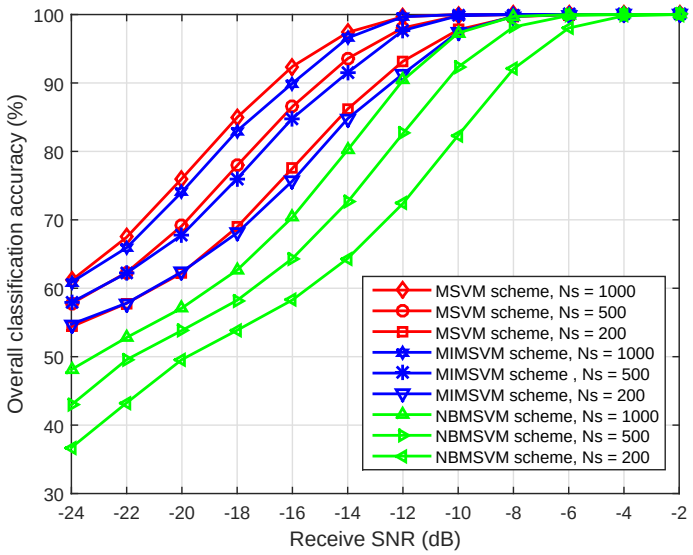

Figure 6.5. Performance comparison of OVO MSVM, MIMSVM and OVO NBMSVM schemes under LOS transmission scenario with different number of samples Ns, and number of PU, $P = 2$.

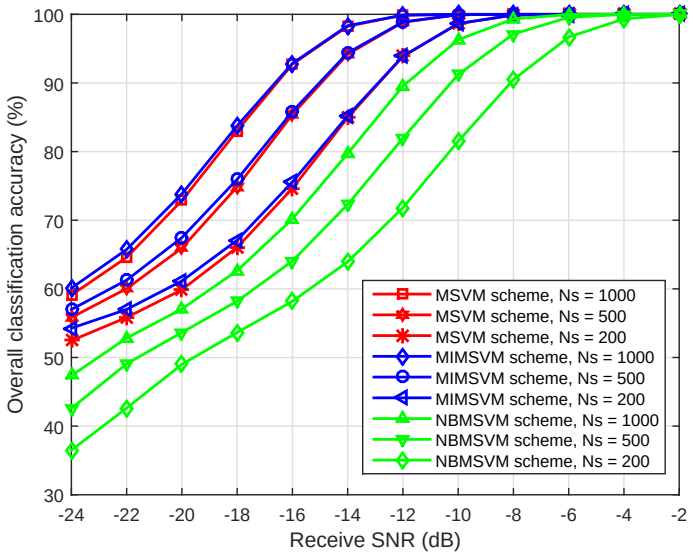

Figure 6.6. Performance comparison of OVO-MSVM, MIMSVM and OVO-NBMSVM schemes under non-overlapping reflection scenario with different number of samples Ns, and number of PU, $P = 2$.

of the first PU arrive with AOAs, $\theta_1 \in [-45°, -35°] \in \bar{\theta}_3$ and $\theta_2 \in [15°, 20°] \in \bar{\theta}_6$. However, for the second PU, they arrive at $\theta_3 \in [15°, 20°] \in \bar{\theta}_6$ and $\theta_4 \in [40°, 45°] \in \bar{\theta}_7$. It means that the beamformer corresponding to $\bar{\theta}_6$

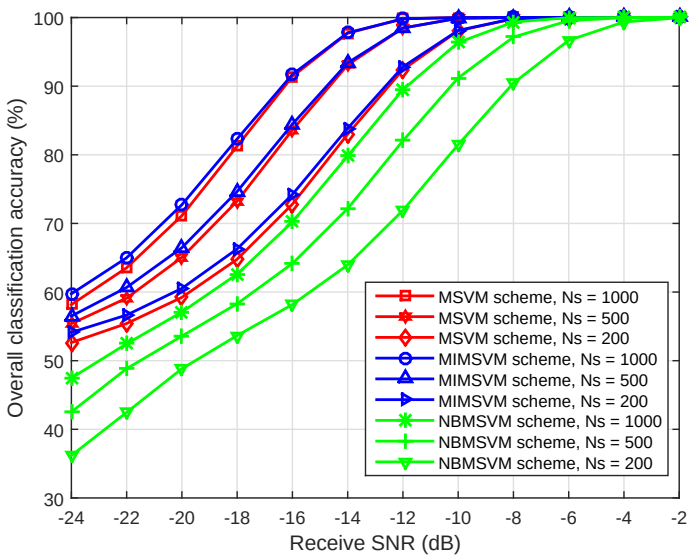

Figure 6.7. Performance comparison of OVO MSVM, MIMSVM and OVO NBMSVM schemes under overlapping reflection scenario with different number of samples Ns, and number of PU, $P = 2$.

picks up signals from both PUs. This scenario is called the overlapping multipath case. Hence, the first scenario is non overlapping. For each PU, the multipath components received via the two distinct paths are assumed to arrive the receiver with a delay of 5 symbols.

Furthermore, by cross-validation the SVM box constraint parameter, Γ is 1 and Gaussian kernel scaling factor, σ is 10. However, when implementing the OVA scheme, the corresponding values for box constraint parameters, Γ^+ and Γ^- are obtained as the ratio of the pair of classes as discussed in section V-B. Some 2000 set of energy vectors were generated through random channel realization, out of which 400 were used for training and the rest were used for testing. In Figure 6.4, the suitability of the OVO and OVA coding techniques was investigated by evaluating their performance in terms of CA_{ovr} at different receive SNR using the ECOC MSVM algorithm. The performance evaluation under the non-overlapping transmission scenario indicates that for both schemes, the CA_{ovr} improves as the SNR is increased. For example, when Ns is 1000, CA_{ovr} increases from about

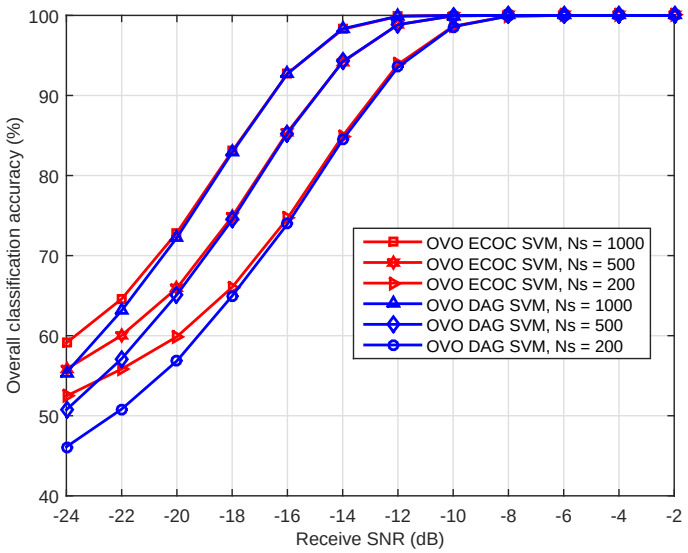

Figure 6.8. Performance comparison between OVO ECOC and DAG based MSVM under non-overlapping reflection scenario with different number of samples Ns, and number of PU, $P = 2$.

58% to 100% as SNR is raised from -24 dB to -8 dB. Similar trend can be observed for various Ns values. The OVO scheme appeared to slightly outperform the OVA scheme especially in the very low SNR regime. At any rate, in deciding which coding scheme to use, the system's complexity in terms of the number of classifiers required to be constructed by each method, the memory requirement and the training as well as testing time should be considered. In Figure 6.5, under the LOS transmission scenario, the performance of our beamformer aided MIMSVM and ECOC MSVM algorithms were investigated over a range of SNR and these were compared with the non beamformer based alternative (NBMSVM). As seen, the beamformer aided schemes significantly outperform the NBMSVM. For instance, when $Ns = 1000$, for the beamformer aided schemes, CA_{ovr} improves from about 60% to 100% when the SNR is increased from -24 dB to -12 dB, whereas for the NBMSVM scheme, CA_{ovr} only increased from about 48% to 90% for the same SNR increment. In addition, the OVO ECOC MSVM is seen to slightly outperform its MIMSVM counterpart over a considerable

portion of the SNR range and for all cases of Ns.

In Figure 6.6 and Figure 6.7, the performance of the MIMSVM, ECOC MSVM and NBMSVM schemes were examined under non-overlapping and overlapping transmission scenarios. Both results show that the performance of the three schemes is similar to that seen for the LOS scenario where CA_{ovr} is observed to improve as the receive SNR is increased. It could however be noticed in these two cases, that in addition to offering far less computational complexity, the MIMSVM slightly outperforms the OVO based ECOC MSVM scheme especially in the very low SNR regime. This may largely be due to the fact that the MIMSVM scheme benefits from increase in the dimension of its feature space under these two scenarios. Furthermore, it can be seen that both the MIMSVM and ECOC MSVM schemes perform equally well and consistently outperform the NBMSVM under the cognitive radio deployment scenarios described in section 6.4, thereby further lending credence to the robustness of the proposed beamformer based learning approach. Next, in Figure 6.8 the comparison between the OVO ECOC MSVM and the DAG SVM methods is shown. It is observable here that the ECOC MSVM performs better than the DAGSVM in the low SNR regime. This can be seen for instance at the SNR of -24 dB where as Ns is increased from 200 to 1000, we see that the CA_{ovr} rises from about 52% to 60% for the ECOC MSVM whereas in the case of DAGSVM, the rise in CA_{ov} is approximately from 46% to 55%.

Finally, to conclude the investigation under the multiple PU case, the comparison between the SVM and kNN classification techniques is shown in Figure 6.9 where both non-parametic methods are considered under beamformer based multiclass OVO ECOC scheme over a range of SNR and different Ns. As seen, the SVM consistently outperforms the kNN. In summary, all simulation results indicate that the proposed, beamformer aided scheme offers significant advantage for SVM classifier in solving spectrum

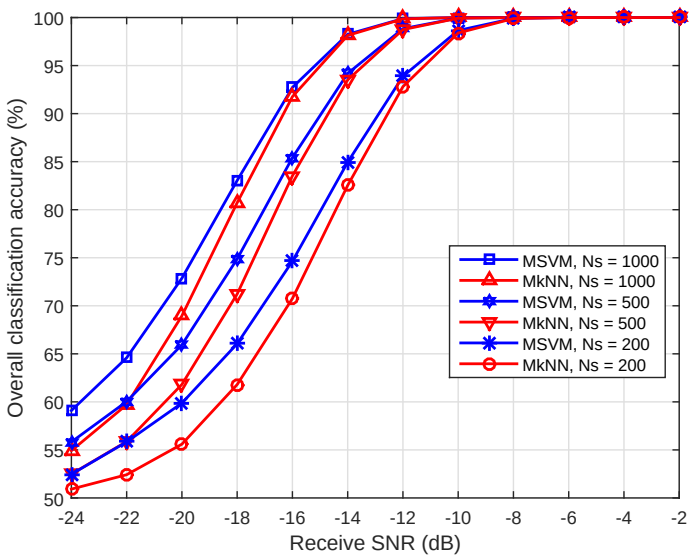

Figure 6.9. Performance comparison of OVO based MSVM and MkNN techniques with different number of samples Ns, number of neighbor = 5, and number of PU, $P = 2$.

sensing problem given both single and multiple primary user scenarios in multi-antenna CR networks.

6.6 Summary

In this chapter, beamformer aided SVM is proposed for spectrum sensing in multi-antenna cognitive radio networks. In particular, new algorithms have been developed for multiple hypothesis testing facilitating joint spatio-temporal spectrum sensing. Using the energy features and the ECOC technique, the key performance metrics of the classifiers were evaluated which demonstrate the superiority of the proposed methods over previously proposed alternatives. In the next chapter, the contributions of this thesis and the conclusions that can be drawn from them is summarized. Research direction for possible future work is also included.

Chapter 7

CONCLUSIONS AND FUTURE WORK

This chapter summarizes the contributions of this thesis and the conclusions that can be drawn from them. In addition, it includes a discussion on research direction for possible future work.

7.1 Conclusions

The focus of this thesis has been on the development of machine learning algorithms for spectrum sensing within the context of cognitive radio wireless networks. In particular, supervised, semi-supervised and unsupervised learning algorithms have been proposed and investigated for interweave spectrum sharing. Furthermore, novel eigenvalue based features have been proposed and shown to possess the capability to improve the performance of SVM classifiers for spectrum sensing under multi-antenna consideration. In addition, novel beamformer based pre-processing technique has been developed for improving the quality of the features and enhancing the performance of the learning algorithms. For the investigation, probability of detection, probability of false alarm, receiver operating characteristics (ROC) curves and area under ROC curves have been used to evaluate the performance of the proposed schemes. Considering the chapters in detail:

In Chapter 1, the current command and control approach to frequency

allocation was described. The spectrum scarcity and under-utilization problems was also introduced. Furthermore, a general description of CR technology and various paradigms as viable solutions to spectrum scarcity problem were discussed. In addition, the role of spectrum sensing in the successful implementation of CR systems was highlighted. This is followed by rationale behind the choice of machine learning techniques for the schemes proposed in this thesis was provided. The chapter is concluded with an outline of the thesis structure and brief discussion of contributions made.

In Chapter 2, an overview of the various local spectrum sensing methodologies in CR networks that are of interest to the thesis was presented. In particular, we reviewed blind and semi blind methods suitable for both single and multi-antenna conditions. These include methods such as matched filtering, cyclostationary detection, energy detection and hybrid schemes. Cooperative sensing methods which enables multiple SUs take advantage of spatial diversity for improving detection performance and containing the effects of channel imperfections is also briefly described.

In Chapter 3, various supervised classification algorithms were proposed and investigated for spectrum sensing application in CR networks. Multi-antenna CR networks was considered and a novel, eigenvalue based feature which has the capability to enhance the performance of SVM algorithms was proposed. Furthermore, spectrum sensing under multiple PU scenarios was given attention and a new re-formulation of the sensing task as a multiple hypothesis problem comprising multiple classes where each class embeds one or more states was presented. Generalized expressions for the various possible states was also provided. In addition, the ECOC based multi-class SVM algorithms for solving the ensuing multiple class signal detection problem was investigated using two different coding strategies. Finally, simulation studies was included which lends credence to the robustness of the proposed sensing schemes.

In Chapter 4, scenarios where the secondary network has only partial knowledge about the PU's network was considered. Two semi-supervised parametric classifier that are based on the K-means and the EM algorithms were proposed for spectrum sensing purpose. Furthermore, it was recognized that the performance of the classifiers can degrade severely when they are deployed for sensing under slowly fading channel resulting when mobile SUs operate in the presence of scatterers. To address this problem, a Kalman filter based channel estimation strategy was proposed for tracking the fading channel and updating the decision boundary of the classifiers in real time. Simulation studies was presented which confirmed that the proposed scheme offers significant gain in performance.

In Chapter 5, the unsupervised classification algorithms based on the soft assignment, variational Bayesian learning framework was presented. Unlike the supervised and semi-supervised methods, the technique does not require any prior knowledge about the number of active PUs operating in the network and can successfully estimate this and other statistical parameters that are required for decision making. The proposed inference algorithm is thus blind in nature and lends itself readily for autonomous spectrum sensing application making it useful when an SU finds itself in alien RF environment. Simulation studies reveals that with few cooperating secondary devices, an overall correct detection rate of about 90% and above can be achieved, with the false alarm rate kept at 10% when the number of collected signal samples approaches 10000.

In Chapter 6, a novel beamforming based pre-processing technique for feature realization was presented for enhancing the performance of classification algorithms under multi-antenna consideration. Furthermore, new algorithms were developed for multiple hypothesis testing facilitating joint spatio-temporal spectrum sensing. Using energy features and the error correcting output codes technique, the key performance metrics of the classifiers

were evaluated which demonstrate the superiority of the proposed methods in comparison with previously proposed alternatives.

In summary, in this thesis, firstly the practicality of adopting and applying machine learning algorithms for spectrum sensing purpose in CR networks was clearly demonstrated. Particularly, supervised, semi-supervised and unsupervised classification based sensing algorithms were developed. The proposed schemes are blind in the sense that the exact knowledge of the PU signal, noise or the channel gain is not required. Secondly, the problem of spectrum sensing under time varying channel condition occasioned by the mobility of SUs in the presence of scatterers was considered and a Kalman filter estimation based technique was proposed for channel tracking and for updating the decision boundary in real time towards enhancing the classifiers performance. Finally, a novel feature realization strategy was proposed for improving the performance of learning algorithms deployed for spectrum sensing application in CR networks.

7.2 Future Work

The research presented in this thesis could be extended in several directions.

Firstly, the cooperating sensing problem in Chapter 3 can be extended by considering the application of game theoretic techniques such as the overlapping coalitional game [90]. In this case, the SUs may first be clustered based on certain criteria so that instead of having all SUs send their sensing results to the SBS, only cluster heads do. Under this situation, it is possible to have one or more SUs located in overlapping regions of multiple clusters and SUs have to decide where to report. In addition, we have assumed that the reporting channel between the SUs and SBS is error free. In practical CR deployment, such channels may exhibit some imperfections. The impacts of this imperfection on the overall system performance should be analyzed and

ways of mitigating these effects be investigated.

Secondly, in Chapter 4, tracking PU-SU channel gain under Rayleigh distributed, flat fading environment was assumed and considered. A wider class of fading channel conditions could also be considered, which could be modeled by for example the Nakagami-m distribution [91]. It is of interest to know that this fading distribution has gained much attention lately owing to the fact that the Nakagami-m distribution gives a better model for land-mobile and indoor mobile multi-path propagation environments as well as scintillating ionospheric radio links [92]. Furthermore, the ideas presented in Chapter 4 and Chapter 5 could be combined by considering the use of multi-target tracking methods such as the probability hypothesis density (PHD) filter [93] to simultaneously track the activities of multiple PUs under SUs' mobility scenarios.

Another possible research problem is how to ensure cooperation among SUs. In this work and almost all the related works on cooperative spectrum sensing, it is assumed that the SUs are trustworthy and well-behaved, which may not always be the case in reality. There may exist some dishonest users, even malicious ones in the system, corrupting or disrupting the normal operation of the CRN [94], [95]. Consequently, the system's performance can be compromised. Thus, this security issue needs to be considered for emerging CRNs and a possible way of addressing this is to use mechanism design [96] which is an important concept in game theory.

Finally, the solutions presented in this thesis are for interweave approach to dynamic spectrum access, the other two methods, namely; underlay and overlay approaches briefly described at the outset could also be considered.

References

[1] A. F. Molisch, *Wireless Communications, Second edition.* 2011.

[2] F. Melgani and L. Bruzzone, "Classification of hyperspectral remote sensing images with support vector machines," *Geosci. Remote Sens. IEEE Trans.*, vol. 42, no. 8, pp. 1778–1790, 2004.

[3] A. Goldsmith, S. Jafar, I. Maric, and S. Srinivasa, "Breaking spectrum gridlock with cognitive radios: an information theoretic perspective," *Proceedings of the IEEE*, vol. 97, pp. 894–914, May 2009.

[4] T. Yucek and H. Arslan, "A survey of spectrum sensing algorithms for cognitive radio applications," *IEEE Commun. Surv. Tutorials*, vol. 11, no. 1, pp. 116–130, 2009.

[5] L. Khaled and Z. Wei, "Cooperative communications for cognitive radio networks," *Proceedings of the IEEE*, vol. 97, pp. 878–893, May 2009.

[6] Z. Guodong, M. Jun, G. Li, W. Tao, K. Young, A. Soong, and Y. Chenyang, "Spatial spectrum holes for cognitive radio with relay-assisted directional transmission," *Wireless Communications, IEEE Transactions on*, vol. 8, pp. 5270–5279, Oct. 2009.

[7] J. Mitola and J. Maguire, G.Q., "Cognitive radio: making software radios more personal," *Personal Communications, IEEE*, vol. 6, pp. 13–18, Aug 1999.

[8] S. Haykin, "Cognitive Radio : Brain-empowered wireless communications," *IEEE J. Sel. Areas Commun.*, vol. 23, no. 2, pp. 201–220, 2005.

[9] Y. C. Liang, A. T. Hoang, and H. H. Chen, "Cognitive radio on tv bands: a new approach to provide wireless connectivity for rural areas," *Wireless Communications, IEEE*, vol. 15, pp. 16–22, June 2008.

[10] Z. Quan, S. Cui, and A. Sayed, "Optimal linear cooperation for spectrum sensing in cognitive radio networks," *Selected Topics in Signal Processing, IEEE Journal of*, vol. 2, pp. 28–40, Feb 2008.

[11] I. Akyildiz, L. Won-Yeol, M. C. Vuran, and S. Mohanty, "A survey on spectrum management in cognitive radio networks," *Communications Magazine, IEEE*, vol. 46, pp. 40–48, Apr. 2008.

[12] C. Cordeiro, K. Challapali, D. Birru, and N. Shankar, "Ieee 802.22: An introduction to the first wireless standard based on cognitive radios," *J. Commun.*, vol. 1, pp. 38–47, Apr. 2006.

[13] C. Stevenson, "Reply to comments on ieee 802.18." `http://ieee802.org/18/`. Accessed October 30, 2012.

[14] W. Su, J. Matyjas, and S. Batalama, "Active cooperation between primary users and cognitive radio users in cognitive ad-hoc networks," in *Acoustics speech and sig. proc. (ICASSP), IEEE Int. Conf. on*, pp. 3174–3177, Mar. 2010.

[15] N. Andrew, "Introduction to machine learning." `http://online.stanford.edu/course/machine-learning-1/`. Accessed October 10, 2015.

[16] R. S. Sutton and A. Barto, *Reinforcement learning: an introduction*. 1998.

[17] R. Duda, P. Hart, and D. Stork, *Pattern classification*. 2000.

[18] Q. Liang, M. Liu, and D. Yuan, "Channel estimation for opportunistic spectrum access: Uniform and random sensing," *Mobile computing, IEEE Transactions on*, vol. 11, pp. 1304–1316, Aug 2012.

[19] L. Lu, X. Zhou, U. Onunkwo, and G. Li, "Ten years of research in spectrum sensing and sharing in cognitive radio," *EURASIP Journ. on Wireless Comm. and Networking*, vol. 28, pp. 1–16, Jan. 2012.

[20] S. Dhope and D. Simunic, "Spectrum sensing algorithm for cognitive radio networks for dynamic spectrum access for ieee 802.11 af standard," *Int. Jour. of research and reviews in wireless sensor networks*, vol. 2, pp. 28–40, Mar 2012.

[21] I. F. Akyildiz, B. F. Lo, and R. Balakrishnan, "Cooperative spectrum sensing in cognitive radio networks: A survey," *Phys. Commun.*, vol. 4, pp. 40–62, Mar. 2011.

[22] S. Kay, *Fundamentals of statistical signal processing, Vol. II: detection theory.* 1998.

[23] A. Ghasemi and E. S. Sousa, "Impact of user collaboration on the performance of sensing based opportunistic spectrum access," in *Proc. IEEE Veh. Tech. Conf.*, (Montreal, Que. Canada, Sept. 25-28), pp. 1–6, 2006.

[24] R. Suresh and M. Suganthi, "Review of energy detection for spectrum sensing in various channels and its performance for cognitive radio applications," *American Journal of Engineering and Applied Sciences*, vol. 5, pp. 151–156, Feb. 2012.

[25] D. Cabric, S. M. Mishra, and R. Brodersen, "Implementation issues in spectrum sensing for cognitive radios," in *38th Conference on signals, systems and computers*, (Asilomar, USA, Nov. 7-10), pp. 772–776, 2004.

[26] B. Zhiqiang, W. Bin, H. Pin-han, and L. Xiang, "Adaptive threshold control for energy detection based spectrum sensing in cognitive radio networks," in *Global Tel. Conf. (GLOBECOM),IEEE*, (Houston, TX, USA, Dec. 5-9), pp. 1–5, Dec 2011.

[27] M. Jun and L. Ye, "Soft combination and detection for cooperative spectrum sensing in cognitive radio networks," in *Global Tel. Conf.,(GLOBECOM). IEEE*, (Washington, DC, USA, Nov. 26-30), pp. 3139–3143, Nov 2007.

[28] F. Digham, M. Alouini, and M. K. Simon, "On the energy detection of unknown signals over fading channels," in *IEEE Int. Conf. on Commun. (ICC)*, (Anchorage, Alaska, USA, May 11-15), pp. 3575–3579, 2003.

[29] L. Zhang, J. Huang, and T. C., "Novel energy detection scheme in cognitive radio," in *Sig. Proc., Comm. and Comp. (ICSPCC), 2011 IEEE International Conference on*, pp. 1–4, Sept 2011.

[30] H. Urkowitz, "Energy detection of unknown deterministic signals," *Proc. IEEE*, vol. 55, no. 4, pp. 523–531, 1967.

[31] R. Tandra and A. Sahai, "Snr walls for signal detection," *Selected Topics in Signal Processing, IEEE Journal of*, vol. 2, pp. 4–17, Feb 2008.

[32] Y. Zeng and Y. C. Liang, "Eigenvalue-based spectrum sensing algorithms for cognitive radio," *Commun. IEEE Trans.*, vol. 57, no. 6, pp. 1784–1793, 2009.

[33] K. Hassan, R. Gautier, I. Dayoub, E. Radoi, and M. Berbineau, "Non-parametric multiple-antenna blind spectrum sensing by predicted eigenvalue threshold," in *Comm. (ICC), IEEE Int. Conf. on*, pp. 1634–1629, June 2012.

[34] Y. Zeng and Y. Liang, "Spectrum sensing algorithms for cognitive radio

based on statistical covariances," *Vehicular Technology, IEEE Transactions on*, vol. 58, pp. 1804–1815, May 2009.

[35] T. Zhi and G. Giannakis, "A wavelet approach to wideband spectrum sensing for cognitive radios," in *Cognitive Radio Oriented Wireless Networks and Communications, 2006. 1st International Conference on*, pp. 1–5, June 2006.

[36] S. Mallat and W. Hwang, "Singularity detection and processing with wavelets," *Info. Theory, IEEE Trans.*, vol. 38, no. 3, pp. 617–643, 1992.

[37] T. Bogale and L. Vandendorpe, "Moment based spectrum sensing algorithm for cognitive radio networks with noise variance uncertainty," in *Information Sciences and Systems (CISS), 47th Annual Conference on*, pp. 1–5, March 2013.

[38] C. Tao, T. Jia, G. Feifei, and C. Tellambura, "Moment-based parameter estimation and blind spectrum sensing for quadrature amplitude modulation," *Commun., IEEE Transactions on*, vol. 59, pp. 613–623, February 2011.

[39] S. Chunyi, Y. Alemseged, H. Tran, G. Villardi, S. Chen, S. Filin, and H. Harada, "Adaptive two thresholds based energy detection for cooperative spectrum sensing," in *Consumer Communications and Networking Conference (CCNC), 7th IEEE*, pp. 1–6, Jan 2010.

[40] S. Maleki, A. Pandharipande, and G. Leus, "Two-stage spectrum sensing for cognitive radios," in *Acoustics Speech and Sig. Proc. (ICASSP), IEEE Int. Conf. on*, pp. 2946–2949, March 2010.

[41] D. Cabric and R. Tkachenko, "Experimental study of spectrum sensing based on energy detection and network cooperation," in *First international workshop on technology and policy for accessing spectrum (TAPAS)*, (Boston, Massachusetts, USA, Nov.), March 2006.

[42] G. Ganesan and Y. Li, "Cooperative spectrum sensing in cognitive radio networks," in *new frontiers in dynamic spectrum access networks, (DySPAN) First IEEE International symposium on*, (Baltimore, MD, USA, Nov. 8-11,), pp. 137–143,, Nov 2005.

[43] O. Chapelle, B. Schlkopf, and A. Zien, *Semi-supervised learning*. The MIT Press, 1st ed., 2010.

[44] P. Tan, M. Steinbach, and V. Kumar, *Introduction to data mining, (First Edition)*. Boston, MA, USA: Addison-Wesley Longman Publishing Co., Inc., 2005.

[45] S. S. Haykin, *Neural networks and learning machines*, vol. 3. Pearson Education Upper Saddle River, 2009.

[46] C. Bishop, *Pattern recognition and machine learning*. 2006.

[47] C. Manning, R. Prabhakar, and S. Hinrich, *Introduction to Information Retrieval*. Cambridge University Press, 2008.

[48] D. Lowd and P. Domingos, "Naive bayes models for probability estimation," in *22nd Int. Conf. on Machine Learning*, (Bonn, Germany, Aug. 7-11), pp. 529–536, ACM Press, 2005.

[49] T. Hastie, R. Tibshirani, and J. Friedman, *The elements of statistical learning*. New York, NY, USA: Springer New York Inc., 2001.

[50] S. Mika, G. Ratsch, J. Weston, B. Scholkopf, and K. Muller, "Fisher discriminant analysis with kernels," in *Neural Networks for Sig. Proc. IX, Proc. of the IEEE Sig. Proc. Soc. Workshop.*, (Madison, WI, USA, Aug. 23-25), pp. 41–48, 1999.

[51] G. J. McLachlan, *Discriminant Analysis and Statistical Pattern Recognition*. Hoboken, NJ, USA: John Wiley and Sons Inc., 1992.

[52] R. Batuwita and V. Palade, "Class imbalance learning methods for support vectors machines," in *H. He and Y. Ma (Eds.), Imbalanced Learning: Foundations, Algorithms, and Applications, Wiley*, pp. 83–96.

[53] S. Boyd and L. Vandenberghe, *Convex Optimization*. 2004.

[54] D. Jonsson, "Some limit theorems for the eigenvalues of a sample covariance matrix," *J. Multivar. Anal.*, vol. 38, pp. 1–38, 1982.

[55] L. Wei and O. Tirkkonen, "Spectrum sensing in the presence of multiple primary users," *Commun. IEEE Trans.*, vol. 60, no. 5, pp. 1268–1277, 2012.

[56] G. Strang, *Linear algebra and its applications*. 1988.

[57] C. Cortes and V. Vapnik, "Support vector networks," *Mach. Learn.*, vol. 20, pp. 273–297, 1995.

[58] M. Davenport, R. Baraniuk, and C. Scott, "Tuning support vector machines for minimax and Neyman-Pearson classification," *Pattern Analysis and Machine Intell. IEEE Trans.*, vol. 32, no. 10, pp. 1888–1898, 2010.

[59] C. Burges, "A tutorial on support vector machines for pattern recognition," *Data Mining and Knowledge Discovery*, vol. 2, no. 2, pp. 121–167, 1998.

[60] X. Lin, J. Andrews, and A. Ghosh, "Spectrum sharing for device-to-device communication in cellular networks," *Wireless Commun. IEEE Trans.*, vol. 13, no. 12, pp. 6727–6740, 2014.

[61] S. Kim, E. DallAnese, and G. Giannakis, "Cooperative spectrum sensing for cognitive radios using kriged Kalman filtering," *IEE Jour. Sel. Top. Signal Process.*, vol. 5, no. 1, pp. 24–36, 2011.

[62] C. Hsu and C. Lin, "A comparison of methods for multiclass support vector machines," *Neural Networks, IEEE Trans.*, vol. 13, no. 2, pp. 415–425, 2002.

[63] E. Allwein, R. Schapire, and Y. Singer, "Reducing multiclass to binary: A unifying approach for margin classifiers," *J. Mach. Learn.*, vol. 1, pp. 113–141, 2001.

[64] T. Dietterich and G. Bakiri, "Solving multiclass learning problems via error-correcting output codes," *Jour. Artif. Intell. Res.*, vol. 2, 1995.

[65] S. Escalera, O. Pujol, and P. Radeva, "Separability of ternary codes for sparse designs of error-correcting output codes," *Pattern Recognit. Lett.*, vol. 30, pp. 285–297, Feb 2009.

[66] W. Max and K. Kenichi, "Bayesian k-means as a "maximization-expectation" algorithm," in *Proc. of the Sixth SIAM Int. Conf. on data mining*, (Bethesda, MD, USA, Apr. 20-22), pp. 474–478, 2006.

[67] Y. Liang and Y. Zeng, "Sensing-throughput tradeoff for cognitive radio networks," *IEEE Trans. Wirel. Commun.*, vol. 7, no. 4, pp. 1326–1337, 2008.

[68] F. Lindsten, H. Ohlsson, and L. Ljung, "Just relax and come clustering! a convexification of k-means clustering," (Department of Electrical Engineering, Linkoping University, Linkoping, Sweden), 2011.

[69] D. Reynolds, "Gaussian mixture models," *Encyclopedia of Biometric Recognition. Springer*, Feb. 2008.

[70] K. M. Thilina, N. Saquib, and E. Hossain, "Machine learning techniques for cooperative spectrum sensing in cognitive radio networks," *IEEE Jour. Sel. Areas Commun.*, vol. 31, no. 11, pp. 2209–2221, 2013.

[71] A. P. Dempster, N. M. Laird, and D. B. Rubin, "Maximum likelihood from incomplete data via the expectation maximization algorithm," *Journal of the Royal Statistical Society, Series B*, vol. 39, no. 1, pp. 1–38, 1977.

[72] K. Sankar and M. Pabitra, *Pattern recognition algorithms for data mining.* Chapman and Hall/CRC, 2004.

[73] C. Biao, J. Ruixiang, T. Kasetkasem, and P. Varshney, "Fusion of decisions transmitted over fading channels in wireless sensor networks," in *Conf. rec. thirty-sixth Asilomar conf. signals, syst. comput.*, (Pacific Grove, CA, USA, Nov. 3-6), pp. 1184–1188, 2002.

[74] T. Wang, L. Song, Z. Han, and W. Saad, "Overlapping coalitional games for collaborative sensing in cognitive radio networks," in *IEEE Wirel. Commun. Netw. Conf.*, (Shanghai, China, Apr. 7-10), pp. 4118–4123, 2013.

[75] Y. Kondareddy and P. Agrawal, "Enforcing cooperative spectrum sensing in cognitive radio networks," in *IEEE Glob. Telecommun. Conf.*, (Houston, USA, Dec. 5-9), pp. 1–6, 2011.

[76] Y. Liu, P. Ning, and H. Dai, "Authenticating primary users' signals in cognitive radio networks via integrated cryptographic and wireless link signatures," in *IEEE Symp. Secur. Priv.*, (Oakland, CA, USA, May 16-19), pp. 286–301, 2010.

[77] R. Gerzaguet and L. Ros, "Self-adaptive stochastic Rayleigh flat fading channel estimation," in *18th Int. Conf. Digit. Signal Process.*, (Fira, Greece, Jul. 1-3), pp. 1–6, 2013.

[78] L. Ros, E. P. Simon, and H. Shu, "Third-order complex amplitudes tracking loop for slow flat fading channel online estimation," *IET Commun.*, vol. 8, pp. 360–371, Jan. 2014.

[79] K. Baddour and N. Beaulieu, "Autoregressive modeling for fading channel simulation," *IEEE Trans. Wirel. Commun.*, vol. 4, no. 4, pp. 1650–1662, 2005.

[80] P. Dent, G. Bottomley, and T. Croft, "Jakes fading model revisited," *Electron. Lett.*, vol. 29, no. 13, 1993.

[81] T. Clancy, A. Khawar, and T. Newman, "Robust signal classification using unsupervised learning," *Wireless Communications, IEEE Transactions on*, vol. 10, pp. 1289–1299, April 2011.

[82] N. Nasios and A. Bors, "Variational learning for gaussian mixture models," *Systems, Man, and Cybernetics, Part B: Cybernetics, IEEE Transactions on*, vol. 36, pp. 849–862, Aug 2006.

[83] D. Tzikas, C. Likas, and N. Galatsanos, "The variational approximation for bayesian inference," *Signal Processing Magazine, IEEE*, vol. 25, pp. 131–146, Nov. 2008.

[84] A. Hagai, "A variational bayesian framework for graphical models," in *In Advances in Neural Information Processing Systems*, pp. 209–215, MIT Press, 2000.

[85] K. Kittipat, "Some examples of variational inference." `https://dl.dropboxusercontent.com/u/14115372/variational_apprx_inference/variationalExampleBishop.pdf/`. Accessed September 21, 2015.

[86] K. Kittipat, "Derivation of variational bayesian for gaussian mixture model." `https://dl.dropboxusercontent.com/u/14115372/variational_apprx_inference/VBGMM_derivation.pdf/`. Accessed September 21, 2015.

[87] M. Pal and G. Foody, "Evaluation of svm, rvm and smlr for accurate image classification with limited ground data," *Selected Topics in Applied Earth Observations and Remote Sensing, IEEE Journal of*, vol. 5, pp. 1344–1355, Oct 2012.

[88] P. Stoica and R. Moses, *Spectral Analysis of Signals*. 2005.

[89] A. Deligiannis, J. A. Chambers, and S. Lambotharan, "Transmit beamforming design for two-dimensional phased-MIMO radar with fully-overlapped subarrays," in *Sensor Sig. Proc. for Defence Conf.*, (Edinburgh, Sept. 8-9), pp. 1–6, 2014.

[90] Z. Zengfeng, S. Lingyang, H. Zhu, and W. Saad, "Coalitional games with overlapping coalitions for interference management in small cell networks," *Wireless Communications, IEEE Transactions on*, vol. 13, pp. 2659–2669, May 2014.

[91] M. Nakagami, "The m-distribution, a general formula of intensity distribution of rapid fading," in *Hoffman, W. C. Statistical methods of radio wave propagation, Oxford, England, 1960.*

[92] M. Simon, J. Omura, and B. K. Levitt, *Spread spectrum communication handbook, revised edition.* 1994.

[93] T. Xu, C. Xin, M. McDonald, R. Mahler, R. Tharmarasa, and T. Kirubarajan, "A multiple-detection probability hypothesis density filter," *Sig. Proc., IEEE Transactions on*, vol. 63, pp. 2007–2019, Apr. 2015.

[94] W. Wenkai, L. Husheng, S. Yan, and H. Zhu, "Catchit: Detect malicious nodes in collaborative spectrum sensing," in *Global Tel. Conf., (GLOBECOM) IEEE*, pp. 1–6, Nov 2009.

[95] D. Lingjie, A. Min, H. Jianwei, and K. Shin, "Attack prevention for collaborative spectrum sensing in cognitive radio networks," *Selected Areas in Communications, IEEE Journal on*, vol. 30, pp. 1658–1665, Oct. 2012.

[96] A. Panoui, S. Lambotharan, and R. C. W. Phan, "Vickrey-clarke-groves for privacy-preserving collaborative classification," in *Computer Science and Information Systems (FedCSIS), Federated Conference on*, pp. 123–128, Sept 2013.